To the Graduate Council:

I am submitting herewith a dissertation written by Lamartine Nogueira Frutuoso Guimaraes entitled "Non-Linear Dynamics of a Once-Through Steam Generator." I have examined the final copy of this dissertation for form and content and recommend that it be accepted in partial fulfillment of the requirements for the degree of Doctor of Philosophy, with a major in Nuclear Engineering.

R. B. Perez, Major Professor

We have read this dissertation
and recommend its acceptance:

Belle R Upadhyaya

Paul N. Stevens

Accepted for the Council:

Associate Vice Chancellor and
Dean of The Graduate School

Non-Linear Dynamics of a Once-Through Steam Generator

A Dissertation
Presented for the Doctor of Philosophy
Degree
The University of Tennessee, Knoxville

Lamartine Guimaraes

August 1992

This dissertation is dedicated to Regina for all the strength she gave me throughout all the period of this work.

"Pure logical thinking cannot yield us any knowledge of the empirical world; all knowledge of reality starts from experience and ends in it. Propositions arrived at by purely logical means are completely empty of reality."

Albert Einstein

"Never utter these words:
'I do not know this, therefore it is false.'
One must study to know;
know to understand;
understand to judge.

Apothegm of Narada

ACKNOWLEDGMENTS

The author expresses his gratitude to his academic advisor Dr. Rafael B. Perez for his invaluable support, encouragement, technical advice, and friendship throughout the entire period of this research.

The members of the doctoral committee, Professors Dr. Paul Stevens, Dr. Belle Upadhyaya and Professor of Electrical Engineering Dr. J. Reece Roth are sincerely acknowledged for their constructive criticism and technical advice.

The ideas developed within this dissertation would undoubtedly not exist without the participation of Mr. Ned E. Clapp, Dr. J. March-Leuba, Dr. C. March-Leuba, and Mr. T. Wilson. Their motivative approach and ingenious comments are very much appreciated.

The author express his gratitude to the "Coordenacao de Aperfeicoamento de Pessoal de Nivel Superior - CAPES" for partially providing the financial support for the realization of the author's PhD program.

The author is most grateful to the Nuclear Engineering department head Dr. Thomas W. Kerlin for providing the academic advice which have made the completion of this work possible.

This work was partially sponsored by the Instrumentation and Controls Division, Oak Ridge National Laboratory, under the Advanced Controls Program. The author is very thankful to the former program manager Mr. J. D. White and the program manager Dr. Ray Brittain for their continued support throughout the completion of this work.

The author also appreciates the help received from Ms. D. J. Nypaver, Dr. D. Ugolini, Mr. M. A. Abdalla, Dr. R. C. (John) Berkan, Mr. M. Naghedolfeizi, Dr. V. Protopopescus, and Mr. T. Sofu for their helpful discussion and encouragement.

ABSTRACT

This dissertation presents a new analytical model for the Once-Through Steam Generator (OTSG) which is a component responsible for the primary coolant heat removal and the generation and supply of superheated steam to the turbine of the Pressurized Water Reactor (PWR) manufactured by Babcock & Wilcox (B&W) Co. This new analytical model provides the explanation of the oscillatory phenomenon observed in all PWRs manufactured by B&W that uses the OTSG as part of the steam supply system. It was found that the oscillatory behavior is related to the friction pressure drop caused by the reduction in flow area due to the presence of the metal tube holders. The linear analysis performed has shown a pair of complex conjugate eigenvalues with real negative parts, indicating that the OTSG is stable for small perturbations. The global stability was investigated by the construction of the bifurcation diagram whereby the amplitude of the pressure oscillation was plotted against the friction corrector factor. The bifurcation diagram indicates that the limit cycle is stable within the range of physical values of the friction corrector factor. Power spectral density of the plant data revealed two marked features: a resonance at the frequency of oscillation of the limit cycle and a broadband region preceding the location of the resonance peak. The present model does not reproduce the broadband region. A detailed simulation study of the modulation of the amplitude of a limit cycle both with band limited white noise and chaotic noise has shown that the broadband generated by band limited white noise exhibits a power-law dependence on the frequency whereas the chaotic broadband decreases exponentially with frequency. The broadband obtained in the power spectral density of power plant data presented the latter behavior leading to the conclusion that the OTSG limit cycle is modulated by a chaotic component. Furthermore, the calculation of the Lyapunov exponents using the plant data results in positive values reinforcing the above conclusion. It is also demonstrated in this work that undersampling effects seriously hinder the chaotic signatures. This study has shown that the best criterion to determine the chaotic signature in experimental time series is the frequency dependence of the broadband structure in the signal power spectral density. The originality of this work is two fold. First is the model development that leads to the identification of the causative mechanism for the observed OTSG limit cycle.

Second is the novel use of otherwise well established tests in the simulation studies of degraded signals for the identification of chaotic components. The recommendations for future work are the extension of the model to allow for motion of all nodal boundaries rather than just the uppermost nodal limits, study of the interaction between the two steam generators in the plant, study of the dependency of the OTSG model eigenvalues with reactor power, and availability of better quality plant data is stressed.

Contents

List of Tables

List of Figures

Symbols

A_p is the total primary flow area (ft^2)

A_w is the total cross-sectional metal area (ft^2)

A_s is secondary flow area (ft^2)

A_{dc} is the downcomer flow area (ft^2)

α_{dc} is the percent in volume occupied by the gas in the downcomer

α is the void fraction as function of height and time

c_{pp} is the heat capacity of the primary liquid ($\frac{BTU}{lbF}$)

c_{pw} is the metal heat capacity ($\frac{BTU}{lbF}$)

C_{bp} is the friction coefficient of the bled port

c_{st} is an adjustable steam flow constant

D_{eqs} equivalent diameter on the superheated region (ft)

D_{edc} is the equivalent diameter of the downcomer (ft)

D_{eqb} is the equivalent diameter of the boiling region (ft)

Δ_i is the length of the node i (ft)

Δ_b is $L_b - z_I$ (ft)

ΔP_{ext} pressure drop set externally by the feedwater pump (psi)

f_s superheated steam friction factor

f_b boiling friction factor

f_l downcomer friction factor

f_{crd} frictional corrector factor to take into account the tube supports

G is the mass flux as a function of height and time ($\frac{lb}{ft^2{}_s}$)

g is the gravitational constant ($\frac{ft}{s^2}$)

h_{pw} is the heat transfer coefficient between primary and metal ($\frac{BTU}{ft^2{}_sF}$)

h_{ws} is heat transfer coefficient between metal and the superheated secondary side ($\frac{BTU}{ft^2 sF}$)

h_{wb} is the heat transfer coefficient between the metal and the boiling secondary side ($\frac{BTU}{ft^2 sF}$)

h_{si} is the enthalpy of the superheated steam, node i, $i = 1,2$ ($\frac{BTU}{lb}$)

h_g is the enthalpy of the saturated steam ($\frac{BTU}{lb}$)

h_f is the enthalpy of the saturated liquid ($\frac{BTU}{lb}$)

h_{fw} is the enthalpy of the feedwater ($\frac{BTU}{lb}$)

h_{bp} is the enthalpy of the bled superheated steam ($\frac{BTU}{lb}$)

h_c is the enthalpy of the condensing steam ($\frac{BTU}{lb}$)

kor is the friction coefficient of the orifice at the bottom of the downcomer ($\frac{s^2 psi ft}{lb}$)

k_{sba} pressure dependent parameter for slip ratio calculation

K_{tb} friction coefficient for the friction losses between the OTSG and the turbine ($\frac{s^2 psi}{ft^3 lb}$)

kc is the proportional gain

L_{ba} water level in tube region for the OTSG A (ft)

L_{bb} water level in tube region for the OTSG B (ft)

L_t is the total tube length (ft)

L_b is the position of the moving boundary (ft)

L_{si} is the length of the superheated region, node i, $i = 1,2$ (ft)

L_{bp} is the height of the bleeding port (ft)

L_{dc} is the height of the water column at the bottom of the downcomer (ft)

N is the total number of tubes

P_{sa} superheated steam pressure at OTSG A (psi)

P_{sb} superheated steam pressure at OTSG B (psi)

P_{sha} turbine header steam pressure A (psi)

P_{shb} turbine header steam pressure B (psi)

P_s is the pressure at the superheated region, node 1 (psi)

P_{s2} is the pressure between nodes 1 and 2 (psi)

P_{ss} is the pressure between the boiling and superheated region (psi)

P_{db} is the pressure at the bottom of the downcomer (psi)

P_{dc} is the pressure at the top of the downcomer (psi)
P_{tb} is the model turbine header steam pressure (psi)
P_{set} is the set value for the model turbine header steam pressure (psi)
Pow reactor thermal power (%)
Q' is the volumetric heat rate ($\frac{BTU}{ft^3 s}$)
r_i is the tube internal radius (ft)
r_o is the outside diameter of the tube (ft)
ρ_p is the density of primary water ($\frac{lb}{ft^3}$)
ρ_w is metal density ($\frac{lb}{ft^3}$)
ρ_{si} is the density of the superheated steam, node i, $i = 1, 2$ ($\frac{lb}{ft^3}$)
r_{ba} pressure dependent parameter for slip ratio calculation ($\frac{lb}{ft^3}$)
ρ_f is the density of saturated liquid ($\frac{lb}{ft^3}$)
ρ_g is the density of saturated gas ($\frac{lb}{ft^3}$)
R is the Martinelli-Nelson corrector factor
s_i is the slip ratio
s is equal to $\frac{P_{set}}{925.}$
ti is the integral time constant (s)
T_{p0a} hot leg temperature for the OTSG A (F)
T_{p0b} hot leg temperature for the OTSG B (F)
T_{pi} is the primary temperature on node i, $i = 1, 2, 3, 4$ (F)
T_{wi} is the metal temperature on node i, $i = 1, 2, 3, 4$ (F)
T_{p0} is primary inlet temperature (F)
T_{sat} is the saturation temperature on the boiling region (F)
T_{si} is the temperature of the superheated region, node i, $i = 1, 2$ (F)
τ_s is a time constant (s)
V_{dc} is the downcomer volume (ft^3)
v_{ss} is half of the volume of the superheated region (ft^3)
W_{fwa} feedwater flow rate for the OTSG A ($\frac{lb}{s}$)
W_{fwb} feedwater flow rate for the OTSG B ($\frac{lb}{s}$)
W_{pin} is the primary inlet flow ($\frac{lb}{s}$)
W_{21} is the steam flow going from region 2 to region 1 ($\frac{lb}{s}$)
W_b is the steam mass flow rate leaving the boiling region ($\frac{lb}{s}$)

W_{bp} is the bleeding mass flow rate ($\frac{lb}{s}$)
W_s is the superheated mass flow rate leaving the OTSG ($\frac{lb}{s}$)
W_{fw} is the inlet feedwater mass flow rate ($\frac{lb}{s}$)
W_{db} is the liquid mass flow rate leaving the downcomer ($\frac{lb}{s}$)
W_c is the steam condensation flow rate ($\frac{lb}{s}$)
W_{s0} is the average value of the flow obtained from plant data ($\frac{lb}{s}$)
x is equal to $\frac{P_{tb}}{925.}$
x_i is the quality which is a function of the void fraction
z_I is the fixed upper boundary of the node immediately before the last node (ft)
z_i is the boundary of node i (ft)
BLN ... band limited white noise
OTSG ... Once-Through Steam Generator
OTSGA ... power plant OTSG A
OTSGB ... power palnt OTSG B
PSD ... power spectral density

Chapter 1

Introduction

In a recent Electric Power Research Institute (EPRI) sponsored workshop on Applications of Chaos [1] the following introductory remark was made

> Although chaos has been an exciting topic recently, its discussions have been mostly confined to a relatively small group of academic people and research scientists concerned with identifying and describing chaotic phenomena. Practical applications of these ideas in engineering, biology, ecology, physiology, and other technical fields have not yet been widely perceived or appreciated by "practitioners" in these technical areas. There seems to be a need to fill this gap by focusing on aspects of "chaos theory" with clear and direct applicability, i.e., identifying how chaos "science" can lead to chaos "technology".

Filling the gap between nonlinear science and technological application is likely to occur, in the words of J. Dorning [2],

> ... when the nonlinear scientist explores technological applications finding both particular motivation and new needs and ideas that embody both basic research problems and rich intellectual content, and when engineers and scientists oriented toward applied technologies probe into nonlinear science to gain understanding and techniques which they then might generalize and use in practical applications.

This dissertation describes the probing efforts of an engineer into nonlinear science. Thus it combines the practical aspects of developing a model for a Once-Through Steam Generator (OTSG) with an effort to understand and implement the tools of nonlinear science for the analysis of engineering systems.

The choice of the OTSG system for this study was made on the grounds of its relevance as a part of the nuclear steam supply system, and that its behavior is dominated by the intricacies of two-phase flow dynamics, known to be closely related to chaotic phenomena ([3],[4]).

The OTSG system is the supplier of superheated steam in the Pressurized Water Reactor (PWR) built by the Babcock and Wilcox (B&W) Company. The pressure on the secondary side of those steam generators enters into an oscillation with a frequency of around 0.2 Hz for a particular set of operating conditions. The oscillatory behavior of the pressure signal propagates throughout the balance of plant and to the reactor core, thus generating an unwanted reactor power oscillation.

In the context of the above scenario, this dissertation addresses the following issues: (a) identification of the causative mechanism for the appearance of the observed oscillatory behavior, (b) study of the stability (both in the small and globally) of the oscillation, and (c) identification of chaotic signatures in the plant signals.

1.1 Background Information

Nonlinear models of the OTSG system have been previously developed by Chen [5] and by B&W [6]. Although there are some differences between the algorithms used, both models treat the boiling region as a single lump. This approximation precludes the description of the density waves which characterize the propagation of two-phase fluids along heated channels. As a result, neither of the two models predict the observed oscillatory regime of the system.

Since the jargon and tools of "chaos" theory are not yet widely used in the field of nuclear engineering, a few general remarks may be found useful.

The definition of chaos given by The Merriam-Webster dictionary is " the confused unorganized state existing before the creation of distinct forms" or "complete disorder", also synonym to confusion. This definition associates the idea of chaos with a high state of entropy, disorganization and unpredictability. A better definition of chaos, at least from the engineering viewpoint, is that of an erratic motion of the state variables that appears random but that in fact exhibits an underlying ordered structure.

The phenomena that are said to be chaotic present very particular conditions [7]: (a) sensitive dependence on initial conditions, (b) periodic input of one frequency leads to randomlike output with a broadband spectrum of frequencies, and (c) loss of information about the initial conditions. Sensitive dependence on initial conditions means that two sets of very close initial conditions will generate two completely different trajectories in phase space.

There are many examples of physical systems exhibiting chaotic behavior: cardiac oscillations [8], pendulum movement [9], non-linear electric circuits [7], magnetomechanical devices [7], dynamical behavior of plasma [10], the leaky faucet [11], weather prediction [12], turbulent flow ([13],[14]), Boiling Water Reactor (BWR) dynamics ([15],[16]), and two-phase flow dynamics ([3],[4]).

Several models of dynamic systems relevant to the field of nuclear engineering have been considered previously. A reduced model of a Boiling Water Reactor (BWR) [15], which contained five coupled nonlinear first order differential equations, has been found to exhibit chaotic behavior after going through a cascade of pitchfork bifurcations [17], as the overall fuel-to-coolant heat transfer coefficient was varied.

Rizwan-uddin and Dorning ([3],[4]) have worked with a model of a vertical channel where liquid water enters in a subcooled state, is heated to boiling condition, and a mixture of water and steam exits at the top of the channel. This model uses a nodal approach to deal with the spatial effects in the boiling channel. They have shown that under certain conditions of frequency and amplitude, simple input modulation functions can force the system into chaos.

Franceschini [18] has analyzed a system of seven ordinary differential equations that are a truncation of the Navier-Stokes equations for an incompressible fluid. In one of the equations of the set, an additive parameter related to the Reynolds number, was varied and a period-doubling pitchfork bifurcation of the system solution was observed, characterizing the system as en route to chaotic behavior.

The common feature of those studies is the appearance of a limit cycle which under certain conditions, either the change of a system parameter or the use of an external input, becomes unstable and ends up as a chaotic aperiodic motion. Clearly the study of this behavior in the nuclear engineering field, is of substantial relevance for its implications in establishing a suitable environment for the safe operation of nuclear power plants.

1.2 Original Contributions

The original work in this dissertation can be classified into two categories: model development and implementation of a battery of tests for chaotic signature identification in experimental time series. The first category includes the development of a nodal method with a time-varying node limit which has led to the identification of the causative mechanism for the observed limit cycle oscillations. None of the previous models for the Once-Through Steam Generator could account for the oscillatory behavior of the plant. In the second category one must stress the novel use, of otherwise well established tests, in simulation studies of degraded signals to implement an algorithm for the identification of chaotic signals.

1.3 Organization of this Dissertation

This dissertation has been divided in six chapters including the Introduction, plus two appendixes.

Chapter 2 presents a general description of the physical process occurring in the OTSG, a description of the available plant data obtained in the oscillatory regime, a full description of the mathematical development of the new OTSG model, a validation and stability analysis of this model in the non-oscillatory regime, and a comparison with the two OTSG's previous models.

A comparison of the frequency domain analysis of the OTSG model and of the plant data is presented in Chapter 3.

Chapter 4 introduces several concepts associated with the study of chaotic behavior, and presents some examples and applications of this study to chaotic systems such as the Rossler and Lorenz.

Chapter 5 deals with the application of the study in Chapter 4 to the search for a chaotic signature in the plant data.

Chapter 6 presents the conclusions, originality and recommendations for future work.

Appendix A includes a copy of the OTSG model computer program developed and Appendix B gives a brief summary of the Rossler and Lorenz differential equations used to generate chaotic time series throughout this work.

Chapter 2

The Once-Through Steam Generator Simulation

2.1 Introduction

The pressurized water reactors (PWR) manufactured by Babcock and Wilcox Company (B & W) uses a Once-Through Steam Generator (OTSG) as part of the nuclear steam supply system. There are two OTSGs per power plant. The OTSG exchanges heat from the primary to secondary water circuit, and supplies superheated steam to the turbine. Figure 2.1, reproduced from reference [19], gives a good visual description of the OTSG.

A description of the physical process occurring in the OTSG, based on Figure 2.1, is given as follows. The primary water coming from the hot leg enters at the top of the steam generator (1), travels straight through metal tubes (9) and exits at the bottom of the steam generator (2), returning to the reactor vessel through the cold leg. As the primary water travels down the metal tubes it transfers heat to the secondary water. The secondary water, coming from the feedwater supply system, is pumped into an annular region of the steam generator called the downcomer. The feedwater is mixed with steam coming from the tube region through the bleed port (6), and deposits at the bottom of the downcomer (7). This mixing raises the temperature of the feedwater from the subcooled to the saturation condition. The saturated water at the bottom of the downcomer is forced into the bottom of the

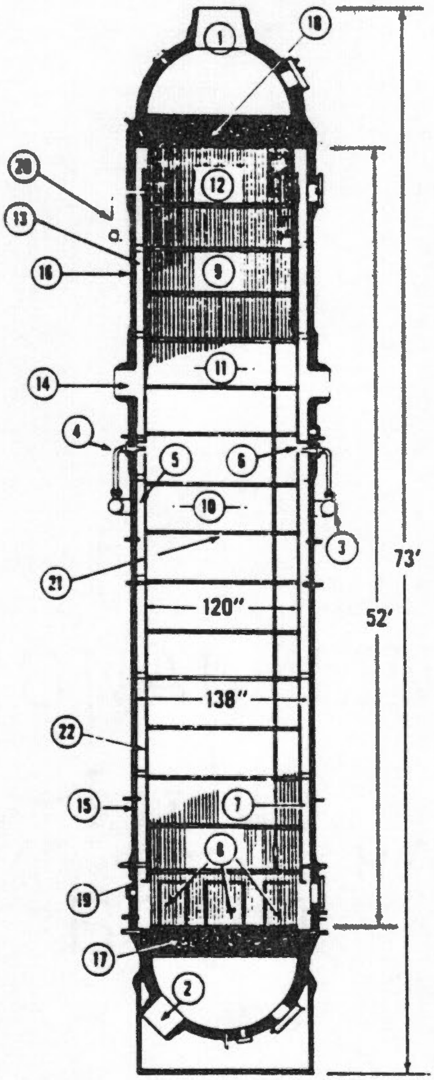

Fig. 2 - Nuclear OTSG (once-through steam generator). 1, primary inlet nozzle; 2, primary outlet nozzle (2); 3, feedwater header; 4, feedwater spray nozzles (32); 5, feedwater heating chamber; 6, « Bleed » steam port; 7, saturated feedwater; 8, ports; 9, generating tubes (15,500); 10, departure from nucleate boiling; 11, 100% quality; 12, superheated steam; 13, steam annulus; 14, steam outlet nozzles (2); 15, lower shell; 16, upper shell; 17, lower tube sheet; 18, upper tube sheet; 19, adjustable orifice; 20, auxiliary feedwater inlet; 21, tube support plates (15); 22, cylindrical baffle.

Figure 2.1: A pictorial representation of the Once-Through Steam Generator.

tube region (8). As the saturated water enters the tube region it begins to boil and flows upwards. The boiling process continues until it reaches a quality of one. The saturated steam is heated to superheated condition and then leaves the OTSG through the steam outlet nozzles (14).

2.2 Available Power Plant Information

A reactor power oscillation has been reported in the B&W power plants using OTSG as part of the nuclear steam supply system [20], when the reactor operates at partial power levels between 50% and 80%. The mechanism causing this oscillation was believed to be located in the OTSG. A characteristic behavior of this oscillation is that the amplitude of the oscillation would reach a maximum and then decrease as power was increased. In the case of the steam pressure of the OTSG, the maximum amplitude observed was $16psi$. The point in power where the maximum is reached varies from plant to plant. The oscillation poses an unnecessary difficulty in maintaining steady state operation at partial power levels. One of the many mechanisms considered as possible causes for OTSG tube leakage was the long term accumulation of cyclic thermal gradients associated with the oscillation of the liquid level within the tube bundle region. Several unsuccessful attempts were made to re-tune the integral control system to reduce the oscillation. A recommendation was made to increase the downcomer ΔP in order to reduce or eliminate the oscillation. The recommendation was implemented as follows. The OTSG was built with an adjustable cross section flow area orifice located at the bottom of the downcomer, which can be seen in Figure 2.1, ball number 19. The OTSG comes from the factory with this orifice adjusted to 50% open. After installation at the power plant, this orifice is set to 25% open for the power plant operation. The decision was made to fully close the orifice. It is necessary to emphasize that even with the orifice fully closed, there is still a uniform annular gap that allows the flow of water from the downcomer to the tube bundle region.

Steam pressure measurements after the closing of the orifice indicated the disappearance of the oscillation. Although, a fluctuation in the feedwater flow with a period of 20 seconds has been observed. This fluctuation was attributed to noise in the feedwater flow of both secondary loops of the power plant. Even though the oscillation on the OTSG had been eliminated, the mechanism by which the oscillation occurs has not yet been identified.

2.3 The Once-Through Steam Generator Data Available

A set of plant data was obtained [21] from the Arkansas Power & Light Company at one of the power conditions for which the oscillation occurs. The signals made available for the present study are:

P_{sa} superheated steam pressure at OTSG A;
P_{sb} superheated steam pressure at OTSG B;
P_{sha} turbine header steam pressure A;
P_{shb} turbine header steam pressure B;
W_{fwa} feedwater flow rate for the OTSG A;
W_{fwb} feedwater flow rate for the OTSG B;
T_{p0a} hot leg temperature for the OTSG A;
T_{p0b} hot leg temperature for the OTSG B;
L_{ba} water level in tube region for the OTSG A;
L_{bb} water level in tube region for the OTSG B; and
Pow reactor thermal power.

These signals were taken at a sampling rate of one second and are 600 seconds long.

The P_{sa}, W_{fwa}, T_{p0a}, Pow, and L_{ba} signals were averaged in order to provide input and validation information for the model. The resulting average values are: 901 psi, 830.95 lb/s, 592.12 F, 0.614 %, and 16.1 ft respectively.

A visual inspection of the signals revealed that P_{sa}, P_{sb}, P_{sha}, W_{fwa}, W_{fwb}, T_{p0b}, and Pow had a good distribution around the mean value and could be used for the frequency domain analysis of the oscillation, whereas the signals P_{shb}, T_{p0a}, L_{ba}, and L_{bb} exhibited a bad distribution around the mean value and were declared unsuitable for the frequency domain analysis of the oscillation.

2.4 A Mathematical Model For the Once-Through Steam Generator

This section deals with the development of a model for the OTSG. The set of equations described here were programmed using the Advanced Continuous Simulation Language (ACSL) [22]. An effort was made to make the programs self-explanatory. Copies of the programs developed are given in the Appendix A, which also includes the pertinent parameters used in the present model. A set of water property functions have to be provided by the user. In the particular case of this work, Garland water property functions [23] were used. Figure 2.2 shows the nodalization used to model the OTSG.

2.4.1 The Primary and Metal Side Model Description

Although the primary and the metal side analytical descriptions were developed by Chen [5], his final results are repeated here for completeness.

The Primary Side Equations

The primary side is divided into four nodes and incorporates the moving boundary effect. The nodes are numbered from 1 to 4, from top to bottom as depicted in Figure 2.2. An energy balance is used to obtain the temperature of each node. The equations below summarize the primary description.

$$\dot{T}_{p1} = a_5 \frac{T_{p0} - T_{p1}}{L_t - L_b} - a_4(T_{p1} - T_{w1}) \tag{2.1}$$

$$\dot{T}_{p2} = a_5 \frac{T_{p1} - T_{p2}}{L_t - L_b} - a_4(T_{p2} - T_{w2}) \tag{2.2}$$

$$\dot{T}_{p3} = a_5 \frac{T_{p2} - T_{p3}}{L_b} - a_4(T_{p3} - T_{w3}) \tag{2.3}$$

$$\dot{T}_{p4} = a_5 \frac{T_{p3} - T_{p4}}{L_b} - a_4(T_{p4} - T_{w4}) \tag{2.4}$$

Where:

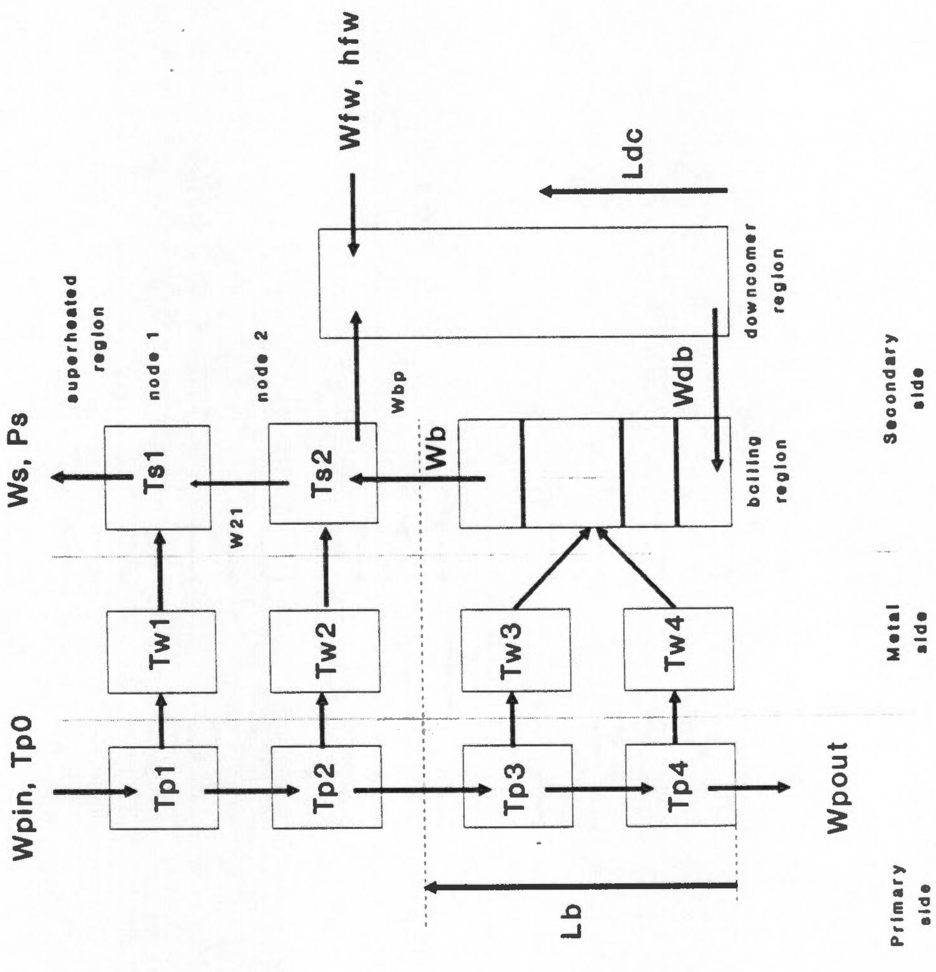

Figure 2.2: Graphical illustration of the nodalization used for the OTSG model.

T_{pi} is the primary temperature on node i, $i = 1,2,3,4$;
T_{wi} is the metal temperature on node i, $i = 1,2,3,4$;
T_{p0} is primary inlet temperature;
L_t is the total tube length; and
L_b is the position of the moving boundary.

The coefficients a_4 and a_5 are given by:

$$a_4 = \frac{h_{pw} r_i \pi N}{\frac{\rho_p A_p c_{pp}}{2.}} \tag{2.5}$$

$$a_5 = \frac{W_{pin} c_{pp}}{\frac{\rho_p A_p c_{pp}}{2.}} \tag{2.6}$$

Where:

h_{pw} is the heat transfer coefficient between primary and metal;
r_i is the tube internal radius;
N is the total number of tubes;
ρ_p is the density of primary water;
A_p is the total primary flow area;
c_{pp} is the heat capacity of the primary liquid; and
W_{pin} is the primary inlet flow.

The material properties such as density and heat capacity as well as the heat transfer coefficient between the primary liquid and the metal tubes are considered to be constant.

The Metal Side Equations

The metal side is divided into four nodes and incorporates the moving boundary effect. The nodes are numbered from 1 to 4, from top to bottom as shown in Figure 2.2. The metal side description requires only an energy balance. The equations below summarize the metal description.

$$\dot{T}_{w1} = -\dot{L}_b \frac{T_{w2} - T_{w1}}{2.(L_T - L_b)} + a_6(T_{p1} - T_{w1}) - a_7(T_{w1} - T_{s1}) \tag{2.7}$$

$$\dot{T}_{w2} = -\dot{L}_b \frac{2.T_{w3} - T_{w2} - T_{w1}}{2.(L_T - L_b)} + a_6(T_{p2} - T_{w2}) - a_7(T_{w2} - T_{s2}) \tag{2.8}$$

$$\dot{T}_{w3} = -\dot{L}_b \frac{T_{w4} + T_{w3} - 2.T_{w2}}{2.L_b} + a_6(T_{p3} - T_{w3}) - a_8(T_{w3} - T_{sat}) \tag{2.9}$$

$$\dot{T}_{w4} = -\dot{L}_b \frac{T_{w4} - T_{w3}}{2.L_b} + a_6(T_{p4} - T_{w4}) - a_8(T_{w4} - T_{sat}) \tag{2.10}$$

Where:

T_{si} is the temperature of the superheated gas on the secondary side, node i, $i = 1, 2$; and
T_{sat} is the saturation temperature on the boiling region.

The coefficients a_6, a_7, and a_8 are given by:

$$a_6 = \frac{h_{pw} r_i \pi N}{\frac{\rho_w A_w c_{pw}}{2.}} \tag{2.11}$$

$$a_7 = \frac{h_{ws} r_o \pi N}{\frac{\rho_w A_w c_{pw}}{2.}} \tag{2.12}$$

$$a_8 = \frac{h_{wb} r_o \pi N}{\frac{\rho_w A_w c_{pw}}{2.}} \tag{2.13}$$

Where:

ρ_w is metal density;
A_w is the total cross-sectional metal area;
c_{pw} is the metal heat capacity;
h_{ws} is heat transfer coefficient between metal and the superheated secondary side;
r_o is the outside diameter of the tube; and
h_{wb} is the heat transfer coefficient between the metal and the boiling secondary side.

The material properties of the metal are considered to be constants. The heat transfer coefficients between the metal and the secondary are considered to be dependent only on the power load.

2.4.2 The Secondary Side Description

This portion of the OTSG model was substantially changed from previous works. The secondary side was divided into three distinct physical regions: the superheated region, the boiling region, and the downcomer region.

The superheated region is represented by two nodes as shown in Figure 2.2. Node 1 is the upper or exit node. Node 2 is the lower or nearest to the boiling region. Temperature of the steam on both nodes and pressure at the upper node were chosen as the state variables.

For this model, the downcomer bleed flow is extracted from the second node of the superheated region, as shown in Figure 2.2. This was done because the moving boundary is always below the bleeding port position for the conditions of interest.

The boiling region is represented by more than one node. All the nodes have fixed boundaries, except the node close to the superheated region where the moving boundary calculation has been introduced.

Two different physical descriptions are used for the downcomer. In the first description the downcomer it is represented as an accumulation tank, whereas in the second one separation of phases (water/steam) in the downcomer is taken into account. The justification for this is to evaluate how different downcomer physical interpretations changes the coupling among the downcomer, the boiling, and the superheated regions. Both representations assume that the feedwater enters at the subcooled state, mixes with the bleed superheated steam, and deposits in the bottom of the downcomer as a saturated liquid. The downcomer is assumed to be in saturation condition and in thermal equilibrium with the boiling region for both cases.

The downcomer considered as an accumulation tank uses mass and energy balances for the mixture. The use of this description requires that the pressure at the top of the downcomer ,P_{dc}, be considered equal to the pressure at the upper node of the superheated region, P_s, plus an external Δ P caused by the feedwater pump.

The downcomer considering the separation of phases consists of writing mass and energy balances for steam and water independently. The basic difference is that the pressure at the top of the downcomer, P_{dc}, is calculated by solving a differential equation. All the water properties necessary for the downcomer calculation are now given as a function of this pressure. This method allows for a calculation of the steam condensation flow rate, W_c, and the amount of enthalpy delivered to the feedwater, h_c.

2.4.3 The Superheated Region

The mass balance for the superheated region, nodes 1 and 2 (see Figure 2.2) are given respectively by the equations:

$$\frac{d(\rho_{s1} L_{s1} A_s)}{dt} = W_{21} - W_s \tag{2.14}$$

$$\frac{d(\rho_{s2} L_{s2} A_s)}{dt} = W_b - W_{bp} - W_{21} \tag{2.15}$$

Where:

ρ_{si} is the density of the superheated steam, node i, $i = 1, 2$;
L_{si} is the length of the superheated region, node i, $i = 1, 2$;
A_s is secondary flow area;
W_{21} is the steam flow going from region 2 to region 1;
W_b is the steam mass flow rate leaving the boiling region;
W_{bp} is the bleeding mass flow rate; and
W_s is the superheated mass flow rate leaving the OTSG.

The energy balance for the superheated region, nodes 1 and 2 are given respectively by the equations:

$$\frac{d(\rho_{s1} L_{s1} A_s h_{s1})}{dt} = W_{21} h_{s2} - W_s h_{s1} + 10.^6 A_s L_{s1} \dot{P}_s + Q_{s1} \tag{2.16}$$

$$\frac{d(\rho_{s2} L_{s2} A_s h_{s2})}{dt} = W_b h_g - (W_{bp} + W_{21}) h_{s2} + 10.^6 A_s L_{s2} \dot{P}_s + Q_{s2} \tag{2.17}$$

Where:

h_{si} is the enthalpy of the superheated steam, node i, $i = 1, 2$;
h_g is the enthalpy of the saturated steam; and
P_s is the pressure at the superheated region, node 1.

The heat rate delivered from the metal to the superheated region node 1, Q_{s1}, and node 2, Q_{s2}, are respectively defined by:

$$Q_{s1} = 2.\pi R_o N h_{ws} L_{s1}(T_{w1} - T_{s1}) \tag{2.18}$$

$$Q_{s2} = 2.\pi R_o N h_{ws} L_{s2}(T_{w2} - T_{s2}) \tag{2.19}$$

Where T_{si} is the temperature of the superheated region, node i, $i = 1, 2$.

The momentum balance in the superheated region is used to calculate the pressure P_{s2}, between nodes 1 and 2, and the pressure P_{ss}, at the interface between boiling and superheated regions. The momentum balance considers the gravitation and the friction pressure drop. The acceleration pressure drop is considered negligible because there is only single phase flow in this region. The equations for the pressure drop are

$$P_{s2} = P_s + 10.^{-6}(\rho_{s1} L_{s1} g + r_s f_s \frac{W_s^2 L_{s1}}{2.D_{eqs} \rho_{s1} A_s^2}) \tag{2.20}$$

$$P_{ss} = P_{s2} + 10.^{-6}(\rho_{s2} L_{s2} g + r_s f_s \frac{W_{21}^2 L_{s2}}{2.D_{eqs} \rho_{s2} A_s^2}) \tag{2.21}$$

Where:

P_{s2} is the pressure between nodes 1 and 2;
P_{ss} is the pressure between the boiling and superheated region;
g is the gravitational constant;
r_s frictional corrector factor to take into account the tube supports;
f_s single phase friction factor; and
D_{eqs} equivalent diameter on the superheated region.

The length of the nodes in the superheated region, L_{si}, is given as a function of the total tube height, L_t, and the moving boundary height, L_b, by:

$$L_{si} = \frac{L_t - L_b}{2} \tag{2.22}$$

The time derivative of the length of the superheated nodes, L_{si}, is written as:

$$\dot{L}_{si} = -\frac{\dot{L}_b}{2} \tag{2.23}$$

The time derivative of the enthalpy and the density are calculated as functions of the time derivatives of pressure and temperature.

$$\dot{h}_{s1} = \frac{\partial h_{s1}}{\partial P}\dot{P}_s + \frac{\partial h_{s1}}{\partial T}\dot{T}_{s1} \tag{2.24}$$

$$\dot{h}_{s2} = \frac{\partial h_{s2}}{\partial P}\dot{P}_s + \frac{\partial h_{s2}}{\partial T}\dot{T}_{s2} \tag{2.25}$$

$$\dot{\rho}_{s1} = \frac{\partial \rho_{s1}}{\partial P}\dot{P}_s + \frac{\partial \rho_{s1}}{\partial T}\dot{T}_{s1} \tag{2.26}$$

$$\dot{\rho}_{s2} = \frac{\partial \rho_{s2}}{\partial P}\dot{P}_s + \frac{\partial \rho_{s2}}{\partial T}\dot{T}_{s2} \tag{2.27}$$

After some algebraic manipulations one obtains the temperature and pressure equations used to model the superheated region.

$$\dot{T}_{s1} = \frac{W_{21}(h_{s2} - h_{s1})}{cf_{ss5}} + \frac{cf_{ss6}}{cf_{ss5}}\dot{P}_s + \frac{Q_{s1}}{cf_{ss5}} \tag{2.28}$$

$$\dot{T}_{s2} = \frac{W_b(h_g - h_{s2})}{cf_{ss1}} + \frac{cf_{ss2}}{cf_{ss1}}\dot{P}_s + \frac{Q_{s2}}{cf_{ss1}} \tag{2.29}$$

$$\dot{P}_s = \frac{cf_{ss3}cf_{ss8}W_b - cf_{ss8}W_{bp} - W_s - cf_{ss10} + cf_{ss11}\dot{L}_b}{cf_{ss9}} \tag{2.30}$$

The energy balance for node 2 as given by equation 2.17 provides a relationship for calculating the steam flow from node 2 to 1, W_{21}.

$$W_{21} = W_b - W_{bp} - v_{ss}(\frac{\partial \rho_{s2}}{\partial P}\dot{P}_s + \frac{\partial \rho_{s2}}{\partial T}\dot{T}_{s2}) + \frac{A_s\rho_{s2}\dot{L}_b}{2} \tag{2.31}$$

Where v_{ss} is half of the volume of the superheated region, and is defined by:

$$v_{ss} = \frac{(L_t - L_b)As}{2} \tag{2.32}$$

The factors cf_{ss1}, cf_{ss2}, cf_{ss3}, cf_{ss4}, cf_{ss5}, cf_{ss6}, cf_{ss7}, cf_{ss8}, cf_{ss9}, cf_{ss10}, and cf_{ss11} are defined by:

$$cf_{ss1} = v_{ss}\rho_{s2}\frac{\partial h_{s2}}{\partial T} \tag{2.33}$$

$$cf_{ss2} = v_{ss}(10^6 - \rho_{s2}\frac{\partial h_{s2}}{\partial P}) \tag{2.34}$$

$$cf_{ss3} = 1. - \frac{v_{ss}\frac{\partial \rho_{s2}}{\partial T}(h_g - h_{s2})}{cf_{ss1}} \tag{2.35}$$

$$cf_{ss4} = v_{ss}(\frac{\partial \rho_{s2}}{\partial P} + \frac{\frac{\partial \rho_{s2}}{\partial T}cf_{ss2}}{cf_{ss1}}) \tag{2.36}$$

$$cf_{ss5} = v_{ss}\rho_{s1}\frac{\partial h_{s1}}{\partial T} \tag{2.37}$$

$$cf_{ss6} = v_{ss}(10^6 - \rho_{s1}\frac{\partial h_{s1}}{\partial P}) \tag{2.38}$$

$$cf_{ss7} = v_{ss}(\frac{\partial \rho_{s1}}{\partial P} + \frac{\frac{\partial \rho_{s1}}{\partial T}cf_{ss6}}{cf_{ss5}}) \tag{2.39}$$

$$cf_{ss8} = 1. - \frac{v_{ss}\frac{\partial \rho_{s1}}{\partial T}(h_{s2} - h_{s1})}{cf_{ss5}} \tag{2.40}$$

$$cf_{ss9} = cf_{ss7} + cf_{ss4}cf_{ss8} \tag{2.41}$$

$$cf_{ss10} = v_{ss}(\frac{cf_{ss8}\frac{\partial \rho_{s2}}{\partial T}Q_{s2}}{cf_{ss1}} + \frac{\frac{\partial \rho_{s1}}{\partial T}Q_{s1}}{cf_{ss5}}) \tag{2.42}$$

$$cf_{ss11} = \frac{A_s(\rho_{s1} + cf_{ss8}\rho_{s2})}{2} \tag{2.43}$$

2.4.4 The Boiling Region

The boiling region is modelled as a vertical one-dimensional channel and is divided into a series of nodes to represent the spacial dependence. The differential mass balance for the two phase flow is given by:

$$\frac{\partial((1.-\alpha)\rho_f+\alpha\rho_g)}{\partial t}+\frac{\partial G}{\partial z}=0. \tag{2.44}$$

Where:

α is the void fraction as function of height and time; and
G is the mass flux as a function of height and time.

The differential energy balance for the two phase flow is given by:

$$\frac{\partial((1.-\alpha)\rho_f h_f+\alpha\rho_g h_g)}{\partial t}+\frac{\partial((1.-x)h_f G+x h_g G)}{\partial z}=Q' \tag{2.45}$$

Where:

x is the quality which is a function of the void fraction; and
Q' is the volumetric heat rate.

The differential momentum balance for the two phase flow is given by:

$$\begin{aligned}\frac{\partial p}{\partial z}=10.^{-6}(& -\frac{\partial G}{\partial t}-\frac{1}{2}\frac{\partial(\frac{(1.-x)^2G^2}{(1.-\alpha)\rho_f}+\frac{x^2G^2}{\alpha\rho_g})}{\partial z} \\ & -((1.-\alpha)\rho_f+\alpha\rho_g)g-f_{crd}f_bR\frac{G^2}{2.\rho_f D_{eqb}})\end{aligned} \tag{2.46}$$

Where:

f_{crd} correctional friction coefficient to take into account the metal tube holders restriction;
f_b is the friction factor;
R is the Martinelli-Nelson corrector factor; and
D_{eqb} is the equivalent diameter of the boiling region.

To obtain the nodal equations for the boiling region, an integration over the height is performed. This integration is performed using one of the two integral operators op1 and op2:

$$op1=\frac{1.}{\Delta_i}\int_{z_{i-1}}^{z_i} dz \tag{2.47}$$

$$op2 = \frac{1.}{\Delta_b} \int_{z_I}^{L_b} dz \tag{2.48}$$

Where:

Δ_b is $L_b - z_I$;
L_b is the position of the moving boundary;
z_I is the fixed upper boundary of the node immediately before the last node;
Δ_i is the length of the node i; and
z_i is the boundary of node i.

The nodes in the boiling region are counted in ascending order along the direction of the secondary stream. In this way the first node is the one closest to the exit of the downcomer and the last node is the one closest to the superheated region. The integral operator op1 is used for all nodes except the last one. The integral operator op2 is used only for the last node, which contains the moving boundary. The reason for this is that the $z_i's$ are considered to be fixed and L_b (the moving boundary) is changing in time.

The use of the integral operator op1 over the differential mass balance as given by equation 2.44, gives an equation to calculate the mass flux leaving the node i, G_i.

$$G_i = G_{i-1} - (\rho_g - \rho_f)\Delta_i\dot{\alpha}_i \tag{2.49}$$

The use of the integral operator op1 over the differential energy balance as given by the equation 2.45, on account of equation 2.49, gives an expression to calculate the node exit void fraction.

$$\dot{\alpha}_i = \frac{Q_i - \frac{c_4(x_i - x_{i-1})G_{i-1}}{\Delta_i}}{c_4(\rho_g - c_6 x_i)} \tag{2.50}$$

The value for the heat rate, Q_i, is calculated by:

$$Q_i = 2.\pi r_o N h_{wb}(\frac{T_{w3} + T_{w4}}{2.} - T_{sat})\frac{1.}{A_s} \tag{2.51}$$

Where h_{wb} is the heat transfer from the wall to the boiling liquid.

The use of the integral operator op1 over the differential momentum balance as given by equation 2.46, returns an equation which is used to calculate the pressure at the interface between nodes i and $i-1$.

$$\begin{aligned} P_{i-1} = P_i &+ (\frac{1}{2}((\frac{(1.-x_i)^2}{(1.-\alpha_i)\rho_f} + \frac{x_i^2}{\alpha_i \rho_g})G_i^2 - (\frac{(1.-x_{i-1})^2}{(1.-\alpha_{i-1})\rho_f} + \frac{x_{i-1}^2}{\alpha_{i-1}\rho_g})G_{i-1}^2) \\ &+ \Delta_i g(\rho_f + c_6\frac{\alpha_i + \alpha_{i-1}}{2.}) + \Delta_i \frac{dG}{dt} \\ &+ f_{crd} f_b R_i \frac{\Delta_i}{2.\rho_f D_{eqb}}(\frac{G_i + G_{i-1}}{2.})^2)10.^{-6} \end{aligned} \tag{2.52}$$

In the equation 2.52, when i is set to 0, is used to calculate the pressure at the bottom of the downcomer region, P_{db}, by adding a term corresponding to the pressure drop caused by the orifice located between the bottom of the downcomer and the bottom of the boiling region.

$$P_{db} = P_0 + kor\frac{G_{db}^2}{\rho_f} \tag{2.53}$$

Where kor is the value of the orifice coefficient.

The exit quality of the node is related to the exit void fraction [16]. This relationship is given by:

$$x_i = \frac{s_i \rho_g \alpha_i}{\rho_g + (s_i \rho_g - \rho_f)\alpha_i} \tag{2.54}$$

Where s_i is the slip ratio. The slip ratio is a function of the void fraction [16]. This relationship is given by:

$$s_i = \frac{1. - \alpha_i}{k_{sba} - \alpha_i + (1. - k_{sba})\alpha_i^{r_{ba}}} \tag{2.55}$$

Where k_{sba} and r_{ba} [24] are pressure dependent parameters given by:

$$k_{sba} = 0.71 + (3.0639e-4)P_{ss} \tag{2.56}$$

$$r_{ba} = 3.33 - (6.09742e-4)P_{ss} + (5.2785e-6)P_{ss}^2 \tag{2.57}$$

The friction factor is considered to be a constant for all the nodes. The Martinelli-Nelson correction factor is a function of the quality at the node exit. Reference [24] provides several plots that relate the Martinelli-Nelson correction factor with the quality for several pressures. The data of these plots were used to obtain a fifth order polynomial fit for the value of operating pressure of the OTSG. This relationship is given by:

$$
\begin{aligned}
R_i = 3.68965 &+ 1.87793x_i + 249.617x_i^2 - 736.569x_i^3 \\
&+ 934.539x_i^4 - 432.318x_i^5
\end{aligned}
\tag{2.58}
$$

The use of the integral operator op2 over the mass, and the energy balance requires the use of the chain rule and the Leibnitz's rule in order to commute the integration over the height and the partial derivative in time.

$$
\frac{1.}{\Delta_b}\frac{d}{dt}\int_{z_I}^{L_b} \alpha dz = \frac{d}{dt}\left(\frac{1.}{\Delta_b}\int_{z_I}^{L_b} \alpha dz\right) - \left(-\frac{1.}{\Delta_b^2}\right)\dot{\Delta}_b \int_{z_I}^{L_b} \alpha dz \tag{2.59}
$$

$$
\int_{z_I}^{L_b} \frac{\partial \alpha}{\partial t} dz = \frac{d}{dt}\int_{z_I}^{L_b} \alpha dz - \alpha(L_b, t)\dot{L}_b \tag{2.60}
$$

Where $\dot{\Delta}_b$ is obtained as $\dot{L}_b$.

The application of the integral operator op2 over the differential mass balance as given by equation 2.44, gives an equation to calculate the mass flux leaving the boiling region, G_b.

$$
G_b = G_I - \frac{1}{2}c_6(\alpha_I - 1.)\dot{L}_b \tag{2.61}
$$

Where the subindex "I" refers to quantities entering the last node.

The application of the integral operator op2 over the differential energy balance as given by the equation 2.45, gives an equation to calculate the moving boundary position L_b.

$$
\dot{L}_b = \frac{2.\Delta_b\left(Q - \frac{c_4(1.-x_I)G_I}{\Delta_b}\right)}{\rho_f c_4(\alpha_I - 1.)} \tag{2.62}
$$

Where c_4 is defined as:

$$c_4 = h_g - h_f \tag{2.63}$$

The application of the integral operator op2 over the differential momentum balance as given by equation 2.46, gives an equation to calculate the pressure at the interface between the last node and the node "I", P_I.

$$\begin{aligned} P_I = P_{ss} \quad &+ \quad (\frac{1}{2}(\frac{G_b^2}{\rho_g} - (\frac{(1.-x_I)^2}{\rho_f(1.-\alpha_I)} + \frac{x_I^2}{\rho_g \alpha_I})G_I) + \Delta_b \frac{dG}{dt} + \frac{G_I - G_b}{2}\frac{dL_b}{dt} \\ &+ \quad \Delta_b g(\rho_f + \frac{c_6(1.+\alpha_I)}{2.}) \\ &+ \quad f_{crd} f_b R_b \frac{\Delta_b}{2.\rho_f D_{eqb}}(\frac{G_b + G_I}{2.})^2)10.^{-6} \end{aligned} \tag{2.64}$$

The Martinelli-Nelson correction factor for the last node is calculated using equation 2.58 for a value of quality equal to one.

2.4.5 The Downcomer Region: Considered as an Accumulation Tank

The mass balance for the mixture in the downcomer region is given by:

$$\frac{d(V_{dc}(\rho_f + (\rho_g - \rho_f)\alpha_{dc}))}{dt} = W_{fw} + W_{bp} - W_{db} \tag{2.65}$$

Where:

V_{dc} is the downcomer volume;
ρ_f is the density of saturated liquid;
ρ_g is the density of saturated gas;
α_{dc} is the percent in volume occupied by the gas;
W_{fw} is the inlet feedwater mass flow rate; and
W_{db} is the liquid mass flow rate leaving the downcomer.

The energy balance for the mixture in the downcomer region is given by:

$$\frac{d(V_{dc}(\rho_f h_f + (\rho_g h_g - \rho_f h_f)\alpha_{dc}))}{dt} = W_{fw} h_{fw} + W_{bp} h_g - W_{db} h_f \tag{2.66}$$

Where:

h_f is the enthalpy of the saturated liquid; and

h_{fw} is the enthalpy of the feedwater.

A momentum balance is used to calculate the flow exiting the downcomer, W_{db}:

$$\begin{aligned} \dot{W}_{db} &= (\frac{(W_{fw} + W_{bp})^2 - W_{db}^2}{A_{dc}\rho_{dc}} - 10.^6 A_{dc}(P_{db} - P_{dc}) - \\ & f_l \frac{L_{bp} W_{db}^2}{2.D_{edc} A_{dc} \rho_{dc}} + A_{dc} g L_{bp} \rho_{dc}) \frac{1.}{L_{bp}} \end{aligned} \quad (2.67)$$

Where:

A_{dc} is the downcomer flow area;

P_{db} is the pressure at the bottom of the downcomer;

P_{dc} is the pressure at the top of the downcomer;

f_l is the friction factor;

D_{edc} is the equivalent diameter of the downcomer; and

L_{bp} is the height of the bleeding port.

The momentum balance includes the difference between the pressure at the bottom, P_{db}, and the pressure at the top, P_{dc}, of the downcomer. The pressure at the bottom of the downcomer is calculated by the equation 2.53. The pressure at the top is considered to be equal to the pressure of the superheated region, P_s, plus a pressure drop, ΔP_{ext} set externally by the feedwater pump.

$$P_{dc} = P_s + \Delta P_{ext} \quad (2.68)$$

The average density of the downcomer, ρ_{dc}, is calculated by:

$$\rho_{dc} = \rho_f + c_6 \alpha_{dc} \quad (2.69)$$

A differential equation is obtained for the void fraction, α_i, from the mass balance as given by equation 2.65:

$$\dot{\alpha}_{dc} = \frac{W_{fw} + W_{bp} - W_{db}}{V_{dc} c_6} \quad (2.70)$$

An algebraic equation is obtained for the steam bleed flow, W_{bp}, from the energy balance as given by equation 2.66:

$$W_{bp} = (W_{fw}h_{f}w - W_{db}h_f - (W_{fw} - W_{db})\frac{c_5}{c_6})\frac{1.}{\frac{c_5}{c_6} - h_g} \tag{2.71}$$

The constants c_5 and c_6 are defined respectively by:

$$c_5 = \rho_g h_g - \rho_f h_f \tag{2.72}$$

$$c_6 = \rho_g - \rho_f \tag{2.73}$$

And finally, the water level in the downcomer, L_{dc}, is given by:

$$L_{dc} = (1. - \alpha_{dc})L_{bp} \tag{2.74}$$

2.4.6 The Downcomer Region: Considering Phase Separation

The downcomer considering steam and water as independent phases requires independent mass and energy balances for each phase. The mass balance for the steam phase is given by:

$$\frac{d(\rho_g A_{dc}(L_{bp} - L_{dc}))}{dt} = W_{bp} - W_c \tag{2.75}$$

Where:

ρ_g is the density of saturated gas;
A_{dc} is the downcomer flow area;
L_{bp} is the height of the bleeding port;
L_{dc} is the height of the water column at the bottom of the downcomer;
W_{bp} is the bleeding flow of superheated steam; and
W_c is the steam condensation flow rate.

The energy balance for the steam phase is given by:

$$\frac{d(\rho_g h_g A_{dc}(L_{bp} - L_{dc}))}{dt} = W_{bp}h_{bp} - W_c h_c + 10^6(L_{bp} - L_{dc})A_{dc}\frac{dP_{dc}}{dt} \tag{2.76}$$

Where:

h_g is the enthalpy of the saturated steam at the downcomer;
h_{bp} is the enthalpy of the bleed superheated steam;
h_c is the enthalpy of the condensing steam; and
P_{dc} is the pressure at the top of the downcomer.

The mass balance for the water phase is given by:

$$\frac{d(\rho_f A_{dc} L_{dc})}{dt} = W_{fw} + W_c - W_{db} \tag{2.77}$$

Where:

ρ_f is the density of saturated liquid;
W_{fw} is the inlet feedwater mass flow rate; and
W_{db} is the liquid mass flow rate leaving the downcomer.

The energy balance for the water phase is given by:

$$\frac{d(\rho_f h_f A_{dc} L_{dc})}{dt} = W_{fw}h_{fw} + W_c h_c - W_{db}h_f \tag{2.78}$$

Where:

h_f is the enthalpy of the saturated liquid; and
h_{fw} is the enthalpy of the feedwater.

The unknowns in this model are L_{dc}, W_c, h_c, P_{dc}, and W_{db}. From the mass and energy balance equations for the water and the steam phase, equations for L_{dc}, h_c, W_c, and P_{dc} are obtained.

$$\dot{L}_{dc} = \frac{W_{fw}}{A_{dc}\rho_f} + \frac{W_c}{A_{dc}\rho_f} - \frac{W_{db}}{A_{dc}\rho_f} - \frac{L_{dc}\frac{d\rho_f}{dP}}{\rho_f}\dot{P}_{dc} \tag{2.79}$$

$$h_c = h_f + \frac{W_{fw}(h_f - h_{fw})}{W_c} \tag{2.80}$$

$$W_c = \frac{W_{bp}}{cd_{dc1}} - \frac{cf_{dc2}}{cf_{dc1}}\dot{P}_{dc} + \frac{\rho_g(W_{fw} - W_{db})}{\rho_f cf_{dc1}} \tag{2.81}$$

$$\dot{P}_{dc} = \frac{cf_{dc4}}{cf_{dc3}}W_{bp} + \frac{cf_{dc5}}{cf_{dc3}}W_{fw} - \frac{cf_{dc6}}{cf_{dc3}}W_{db} \tag{2.82}$$

Where the factors cf_{dc1}, cf_{dc2}, cf_{dc3}, cf_{dc4}, cf_{dc5}, and cf_{dc6} are defined respectively by:

$$cf_{dc1} = 1. - \frac{\rho_g}{\rho_f} \tag{2.83}$$

$$cf_{dc2} = A_{dc}((L_{bp} - L_{dc})\frac{d\rho_g}{dP} + L_{dc}\frac{\rho_g}{\rho_f}\frac{d\rho_f}{dP}) \tag{2.84}$$

$$cf_{dc3} = (L_{bp} - L_{dc})A_{dc}(10^6 - \rho_g\frac{dh_g}{dP}) + (h_f - h_g)\frac{cf_{dc2}}{cf_{dc1}} \tag{2.85}$$

$$cf_{dc4} = h_g - h_{bp} + \frac{h_f - h_g}{cf_{dc1}} \tag{2.86}$$

$$cf_{dc5} = h_f - h_{fw} + cf_{dc6} \tag{2.87}$$

$$cf_{dc6} = \frac{(h_f - h_g)\rho_g}{cf_{dc1}\rho_f} \tag{2.88}$$

The momentum balance is used to calculate the flow exiting the downcomer, W_{db}:

$$\begin{aligned} \dot{W}_{db} &= (\frac{(W_{fw} + W_{bp})^2 - W_{db}^2}{A_{dc}\rho_{dc}} - 10.^6 A_{dc}(P_{db} - P_{dc}) - \\ &\quad f_l\frac{L_{bp}W_{db}^2}{2.D_{edc}A_{dc}\rho_{dc}} + A_{dc}gL_{bp}\rho_{dc})\frac{1.}{L_{bp}} \end{aligned} \tag{2.89}$$

Where:

P_{db} is the pressure at the bottom of the downcomer;

P_{dc} is the pressure at the top of the downcomer;

f_l is the friction factor;

D_{edc} is the equivalent diameter of the downcomer.

The momentum balance includes the difference between the pressure at the bottom, P_{db} and the pressure at the top of the downcomer, P_{dc}.

The average density of the downcomer, ρ_{dc}, is calculated by:

$$\rho_{dc} = \frac{\rho_g(L_{bp} - L_{dc}) + \rho_f L_{dc})}{L_{bp}} \tag{2.90}$$

The superheated bleed steam mass flow rate is calculated by an orifice equation:

$$W_{bp} = C_{bp}\sqrt{(P_{bp} - P_{dc})\rho_{s2}} \tag{2.91}$$

Where C_{bp} is the orifice coefficient. The pressure P_{bp} is the pressure at the bleeding port at the side of the node 2 of the superheated region, and is given by:

$$P_{bp} = P_s + 10^6(\rho_{s1} g(L_t - L_{bp}) + r_s f_s \frac{W_s^2(L_t - L_{bp})}{2D_{eqs}\rho_{s1}A_s^2}) \tag{2.92}$$

2.4.7 The Steam Pressure Proportional-Integral Controller

A proportional-integral (PI) controller is used to regulate the pressure at the turbine header, P_{tb}, which has a set value (P_{set}) equal to 885 psi. The PI acts by regulating the steam flow, W_s, leaving the OTSG. The pressure at the turbine header, P_{tb}, is calculated, considering a frictional pressure loss between the steam generator and the turbine and is given by:

78009153 $\times 10^{-5}$

$$P_{tb} = P_s - K_{tb}\frac{W_s^2}{2\rho_{s1}} \tag{2.93}$$

Where K_{tb} is a friction coefficient.

The equations used to model the PI controller are given below. The proportional part is given by:

$$p = kc(s - x) \tag{2.94}$$

Where:

kc is the proportional gain; 1.0

s is equal to $\frac{P_{set}}{925.}$; and $P_{set} = 885$

x is equal to $\frac{P_{tb}}{925.}$.

The integral part is given by:

$$\frac{di}{dt} = \frac{p}{ti} \qquad i_0 = 0.0 \tag{2.95}$$

Where ti is the integral time constant. $t_i = 10.0$

The PI control is calculated as the sum of the proportional and integral parts:

$$u = p + i \tag{2.96}$$

And the steam flow is calculated in terms of the PI control action by:

$$\dot{W}_s = \frac{W_{s0}(1 - \overset{10.0}{c_{st}}u) - W_s}{\underset{0.1}{\tau_s}} \tag{2.97}$$

Where:

$W_{s0} = W_{fw0}$

τ_s is a time constant;

W_{s0} is the average value of the flow obtained from plant data; and

c_{st} is an adjustable constant.

The reason for using a differential equation to calculate the steam flow, W_s, is to avoid the algebraic loop of having the steam flow depending on the pressure at the turbine header, P_{tb}. The values of the PI constants are given in Appendix A.

2.5 Model Validation in the Non-Oscillatory Regime

In order to validate the model in the non-oscillatory regime, a comparison is made between the average values obtained from the plant signals for the 61.4 % in reactor power and the values generated by the OTSG model considering the two different mathematical descriptions used for the downcomer: the accumulation tank and the separation of phases. Table 2.1 shows in the first column the available power plant

Table 2.1: Comparison of power plant average data with the results generated with the OTSG model

	Power Plant Aver.	*Sep. of Phases Model*	*Acc. Tank Model*
P_s (psi)	901.	900.81	900.82
W_s (lb/s)	830.96	830.95	830.97
T_{s1} (F)	—	586.7	586.7
L_b (ft)	16.1	16.075	16.067
T_{p4} (F)	—	562.9	562.9
L_{dc} (ft)	—	12.73	10.0

average data, in the second column the results using the OTSG model containing the separation of phases description for the downcomer, and in the third column the results using the OTSG model containing the accumulation tank description for the downcomer. These results show good agreement among the two models and the averaged plant data. It also shows that in terms of the model outputs no difference is observed between the downcomer described as an accumulation tank and considering the phase separation. Although, the phase separation description is more complete because it does not use an assumption to calculate the pressure at the top of the downcomer as equal to the pressure at the top of the superheated region plus an external ΔP and allows the calculation of the condensation rate.

2.6 Model Stability in the Non-Oscillatory Regime

In order to evaluate the model stability in the non-oscillatory regime, a power transient is imposed on the OTSG and its response is analyzed. To generate the effect of change in the reactor power, the model inputs: the temperature of the hot leg, the feedwater flow, and the feedwater enthalpy are given to the program in a tabular form as a function of several reactor powers. Unfortunately, the power plant data available were only for the power level at 61.4 %. The input information necessary for the other power schedules were obtained from the previous work of Chen [5].

The OTSG model using the separation of phases for the downcomer is set to run in the steady state with the reactor power level at 61.4 % for 100 seconds. At this time, the reactor power is increased in a ramp, up to 71.4 %, during 400 seconds, and stabilized at that value. Figure 2.3, Figure 2.4, Figure 2.5, and Figure 2.6 show the time profile of: the reactor power imposed for the transient POWV, the water level in the boiling region L_b, the OTSG steam pressure P_s, and the cold leg temperature T_{p4}, respectively. In all the figures the abscissa is the time in seconds. As the reactor power goes up, the steam pressure P_s and the water level L_b goes up, and the cold leg temperature T_{p4} goes down, as expected. The responses shown here indicate that the OTSG model considering the separation of phases in the downcomer behaves correctly for an increase in the reactor power. The results obtained for 71.4 % power agrees with the ones in Chen's work [5]. An interesting behavior was observed for a particular pair of complex eigenvalues. For the 61.4 % power this eigenvalue was equal to (-0.0088+/-1.1457j), for the 71.4 % power this eigenvalue was equal to (-0.0144+/-1.0216j). Note that as the power increases the system stability improves because the real part of this complex pair increases in the negative direction. The relevance of this complex pair of eigenvalues comes from the fact that the system change into the oscillatory regime is reflected by its real part change into a positive value. Similar results are also obtained for the OTSG model considering the downcomer as an accumulation tank.

2.7 Comparison With Previous Works

The OTSG model presented in this chapter is a continuation of the work by Chen [5]. Several improvements over Chen's work were introduced: (a) the flow between the downcomer region and the boiling region is calculated using a dynamic momentum balance rather than the static momentum balance used in Chen's model, (b) for the downcomer region considering separation of phases the condensation rate is calculated by the formal application of the energy conservation rather than the an empirical relation used in Chen's model, and (c) a multinodal approach was used here to describe the boiling region rather than the single node approach used by Chen. It is necessary to emphasize that Chen was interested in

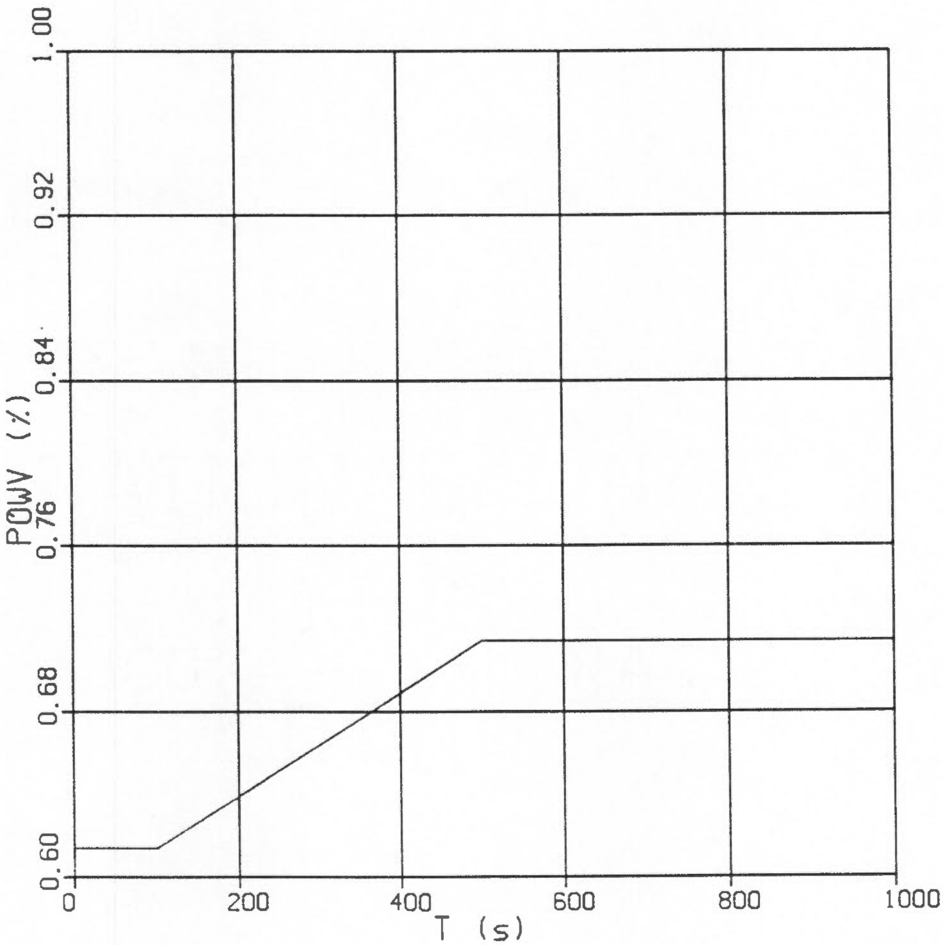

Figure 2.3: Induced reactor power (POWV) transient.

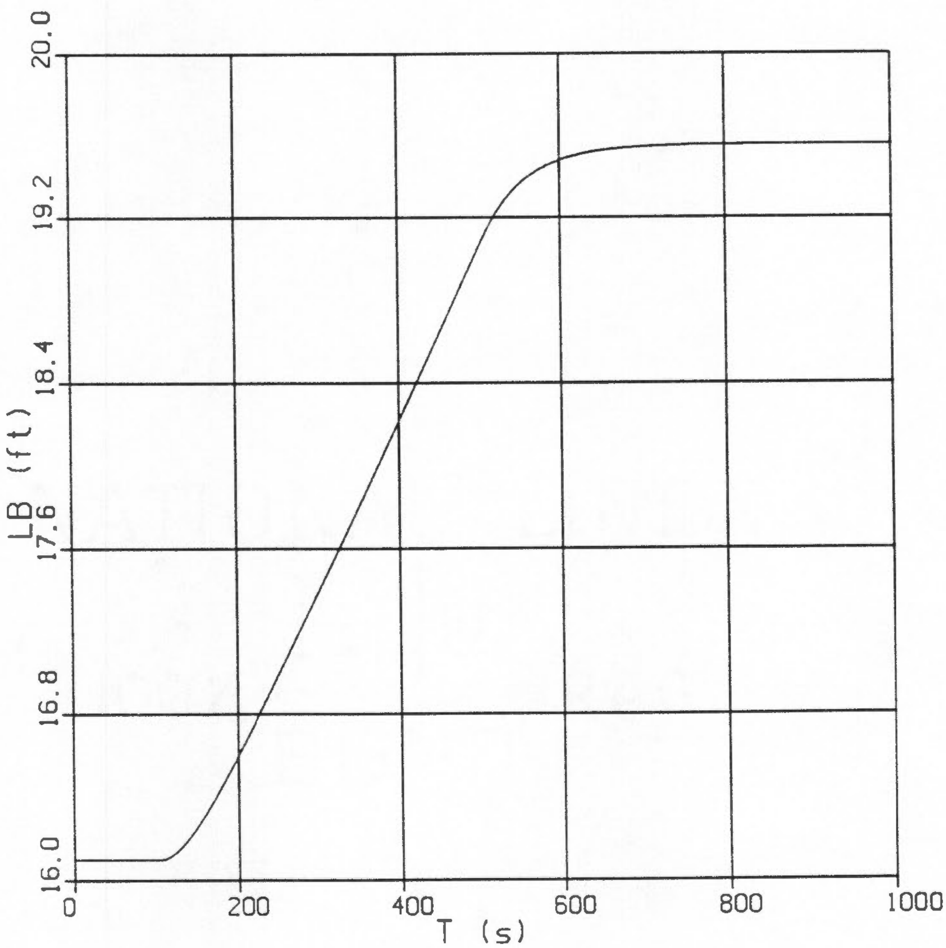

Figure 2.4: Time profile of the water level (L_b) in the boiling region during the power transient

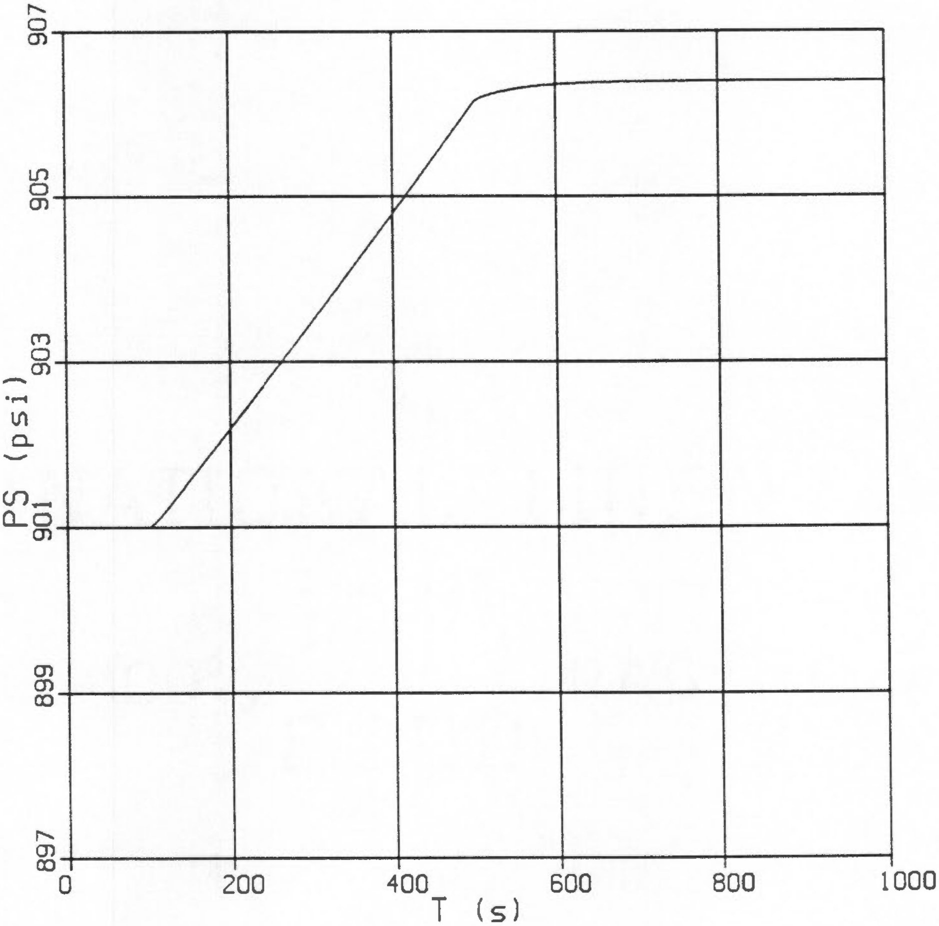

Figure 2.5: Time profile of the OTSG steam pressure (P_s) during the power transient.

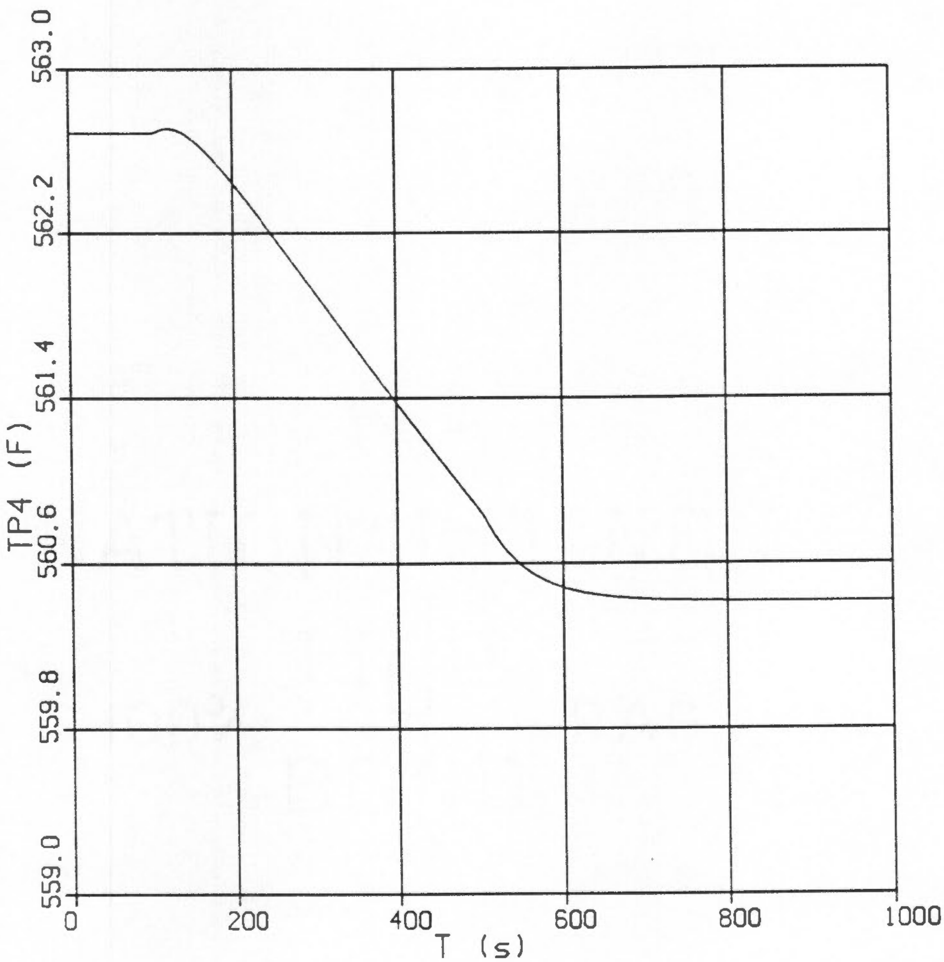

Figure 2.6: Time profile of the OTSG cold leg temperature (T_{p4}) during the power transient.

observing the response of the OTSG to small perturbations around the steady state conditions of several values of reactor power, and his non-linear model was used to validate the responses of his linear model.

Another important previous work in modeling the OTSG is the one found in the Modular Modeling System [6] (MMS) developed by B&W. The most relevant differences between the present model and the MMS model are: (a) the MMS model uses a dynamical momentum balance to calculate the flow between the downcomer and boiling region, but it does not contain the details used in the development of the model presented in this chapter and (b) the MMS uses only three nodes to describe the entire secondary side of the OTSG: a superheated node, a boiling node, and a downcomer node. The MMS considers the downcomer as an accumulation tank and the pressure at the top of the downcomer is assumed equal to the pressure calculated at the superheated steam side. A comparison was made previously, between the downcomer described using separation of phases and as an accumulation tank shows no difference in the results, and the assumption over the downcomer pressure is somewhat limiting. An unreported attempt was made, using the MMS model to study the oscillatory behavior observed in the OTSG and concluded that no steady oscillation could be reproduced by the MMS model.

Chapter 3

The Study of the Oscillatory Behavior of the Once-Through Steam Generator

3.1 Introduction

This chapter deals with the analysis of the oscillatory regime detected in the OTSG and with its theoretical explanation in terms of the model developed in this dissertation. The research issues of interest are the understanding of the origin and nature of the oscillation and whether or not chaotic signatures are present. The latter issue is of relevance not only from the academic point of view but also from the engineering point of view as reported in a recent workshop on chaotic phenomena [1]. Since the behavior of experimental signals in the time domain is better understood in the frequency domain, a thorough analysis of the power spectral density (PSD) for several state variables was performed. This study was also necessary to provide information for the subsequent analysis of the possible presence of chaotic dynamic components in the OTSG oscillatory phenomenon.

3.2 The Power Spectral Density Analysis of Power Plant Data

The PSD's of the power plant data were obtained by using the fast Fourier transform technique [25]. Figure 3.1, and Figure 3.2 show the PSD for the OTSGA steam pressure signal P_{sa} and turbine header steam pressure loop A P_{sha}, respectively. The ordinates of these figures is in $\frac{1}{Hz}$ and the abscissas is in Hz. The common features of these figures are the sharp peak occurring at 0.212 Hz, and the sloping broadband spectra in the frequency range between 0.03 and 0.1 Hz. The 0.212 Hz peak is identified as the natural oscillation frequency of the OTSG and its second harmonic (at 0.422 Hz) is also observed from these PSD's. The relevant observations to be made about these PSDs are their general arrangements, where the OTSG natural frequency appears after the broadband spectrum and the broadband exponential decreases as a function of the frequency. Similar observations can be made for the steam pressure, P_{sb}, measured in the OTSGB.

Figure 3.3 shows the PSD for the reactor power signal Pow, which contains the OTSG natural frequency of oscillation. The broadband spectrum structure does not appear in this PSD, which could indicate that the process that caused the broadband spectrum was probably filtered out.

In summary it can be concluded that the pressure resonance at 0.212 Hz propagates to all the plant variables, whereas the broadband spectrum limits its appearance to plant variables closely related with the OTSG.

3.3 The Power Spectral Density Analysis of the Model Steam Pressure Signal

A steam pressure oscillation is obtained in the OTSG model by increasing the value of a friction correction factor introduced in the friction ΔP calculated along the boiling channel. This friction correction factor is introduced to take into account the restriction effect caused by the reduction in flow area due to the metal tube holders. This restriction effect causes the flow to slow down and as a result the

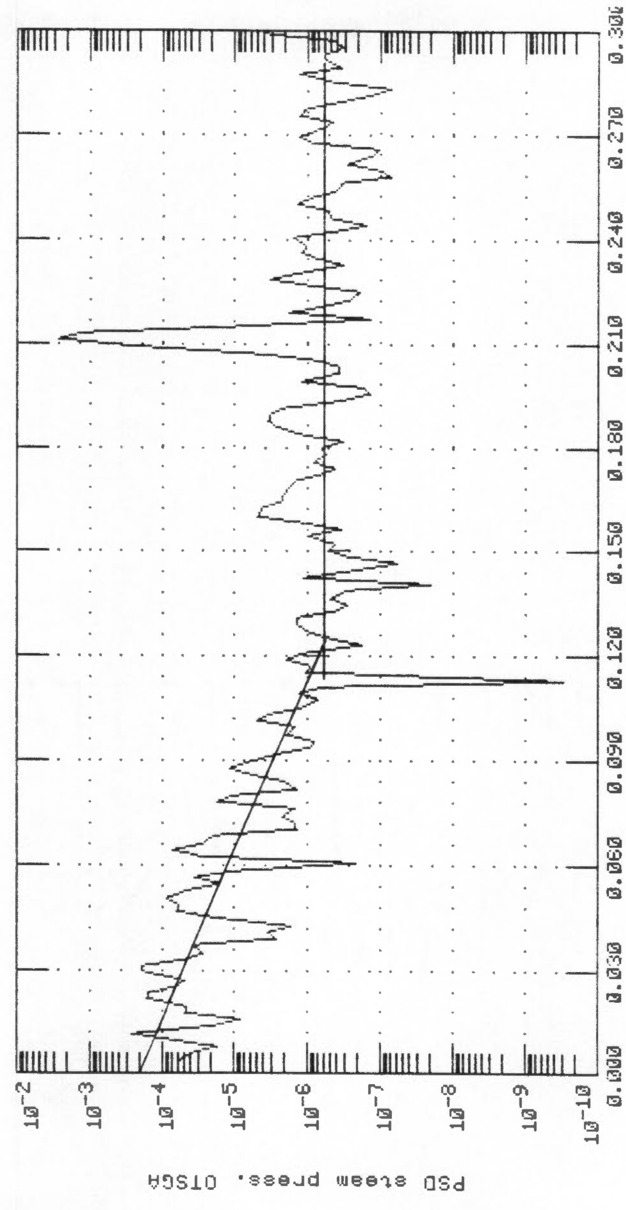

Figure 3.1: Power spectral density of the OTSGA steam pressure signal (P_{sa}).

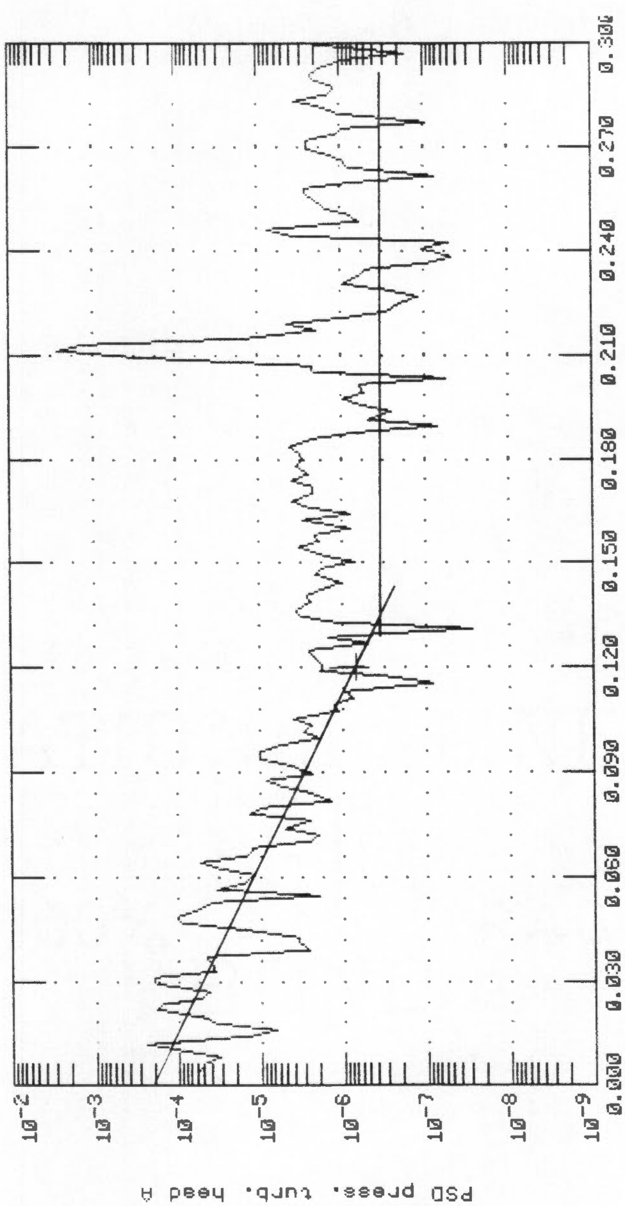

Figure 3.2: Power spectral density of the turbine header loop A pressure signal (P_{sha}).

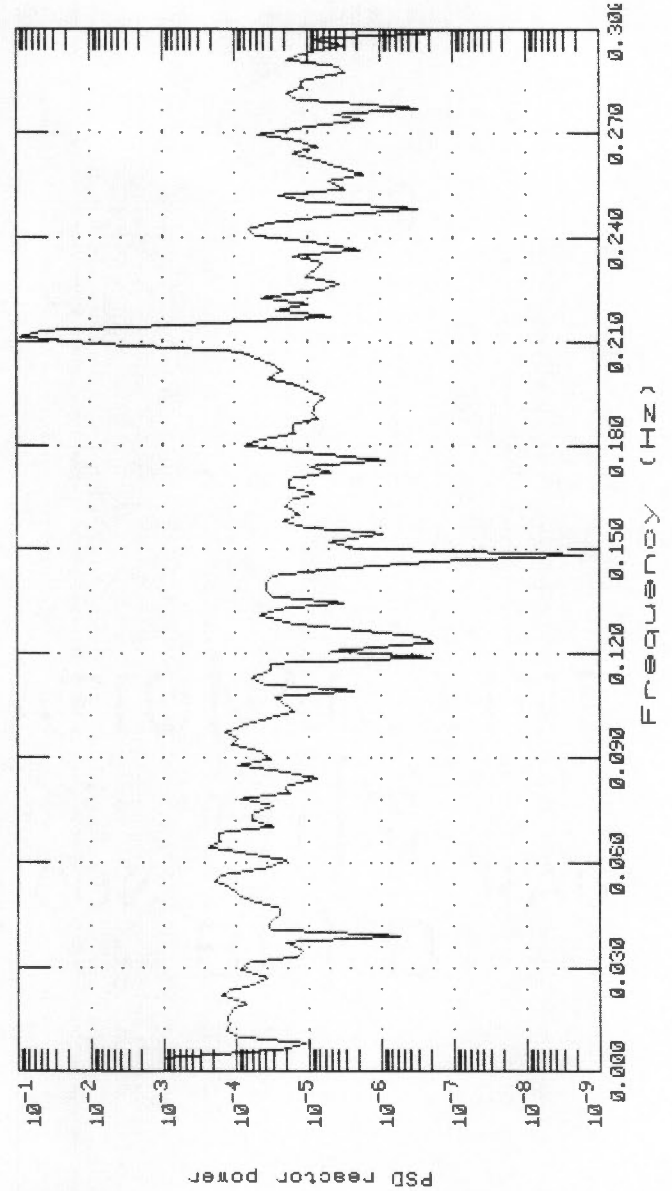

Figure 3.3: Power spectral density of the reactor power signal (*Pow*).

mixture receives more heat, stays longer in the section, and develops more void. The expansion builds up pressure and forces the flow toward both the up- and down-stream directions. After the mixture is pushed through, the volume flow rate is suddenly increased by fresh mixture with lower void fraction and the process repeats itself [26]. In order to observe this phenomena, due to its nature, it is necessary to take into account the spatial dependency along the boiling region, hence the necessity of nodalizing the boiling region. Without the nodalization of the boiling region this phenomena can not be observed. This explains why previous models did not generate the observed oscillation.

Figure 3.4 and Figure 3.5 show the steam pressure, P_s in psi, obtained using the OTSG model considering the downcomer as an accumulation tank and considering the separation of phases in the downcomer, respectively. Both figures show that the amplitude of the oscillation peak-to-peak is around 16 psi which is the value observed in the power plant data.

Figure 3.6 and Figure 3.7 show the limit cycle obtained by plotting the cold leg temperature, T_{p4} in F, against the steam pressure, P_s in psi, for the OTSG model considering the downcomer as an accumulation tank and considering the phase separation in the downcomer respectively. The ray effect observed in both figures is due to the sampling rate (1 s) used, characterizing signal undersampling. As the sampling rate is reduced this effect disappears.

Figure 3.8 and Figure 3.9 shows the PSD of the steam pressure obtained with the OTSG model considering the downcomer as an accumulation tank and considering the separation of phases in the downcomer. Both PSDs exhibit the OTSG natural frequency of oscillation. The OTSG model considering the downcomer as an accumulation tank generates an oscillation frequency value of 0.18 Hz, while the OTSG model considering the separation of phases in the downcomer generates a slighter better value of frequency, 0.19 Hz, when compared with the frequency value obtained from the power plant data (0.212 Hz).

The values of frequencies calculated above were obtained with both models using 16 nodes in the boiling region. Tests were performed to check the stabilization of the frequency value with the increase of the number of nodes in the boiling region. The OTSG model, considering the separation of phases in the downcomer, was run with

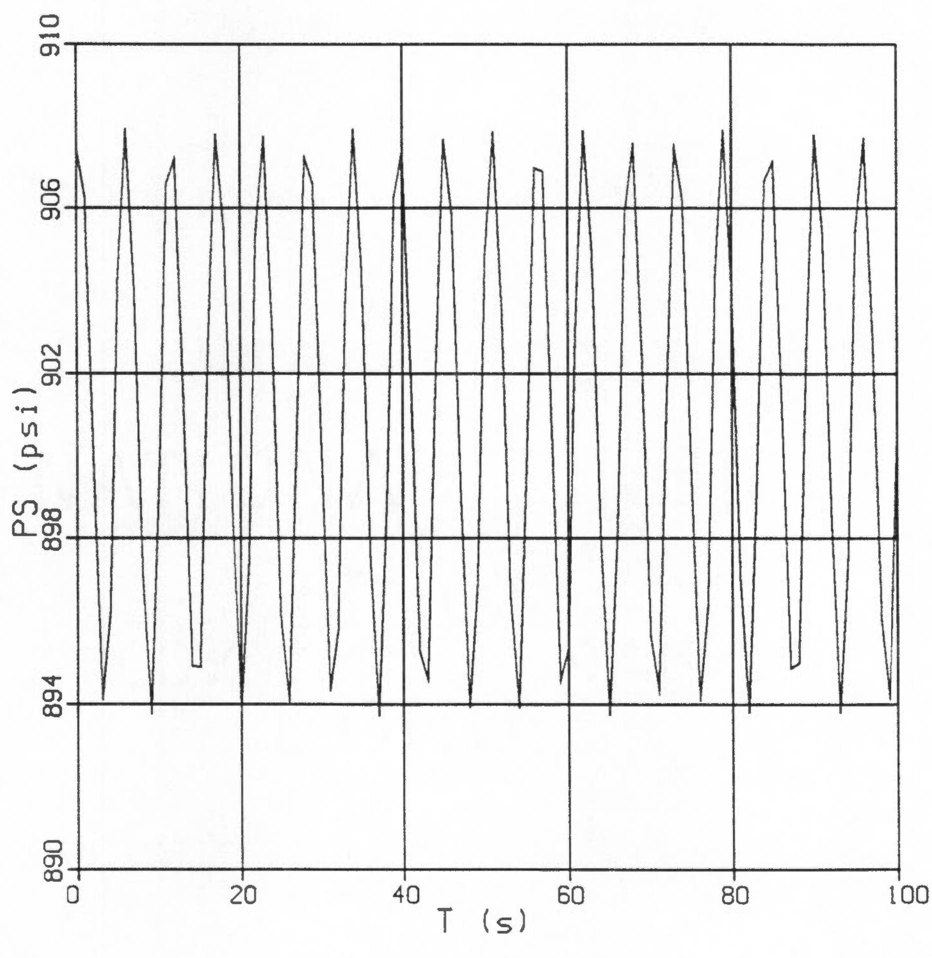

Figure 3.4: Steam pressure (P_s) generated with the OTSG model considering the downcomer as an accumulation tank.

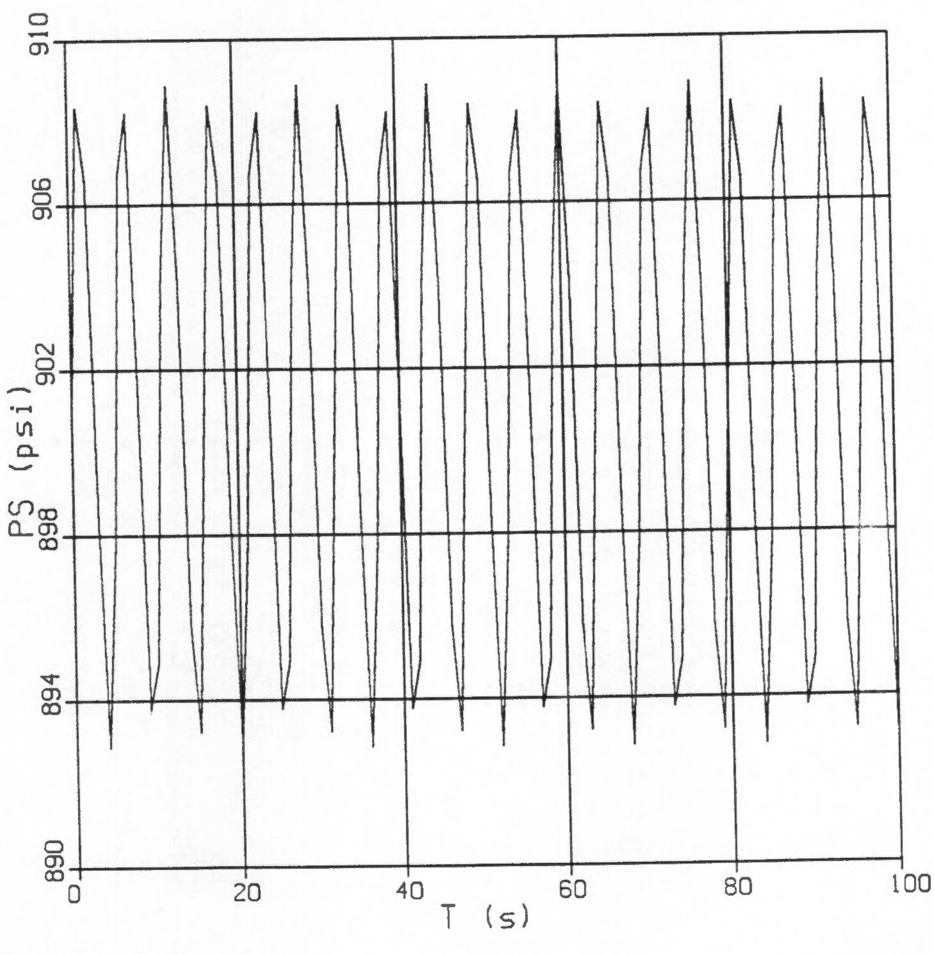

Figure 3.5: Steam pressure (P_s) generated with the OTSG model considering the separation of phases in the downcomer.

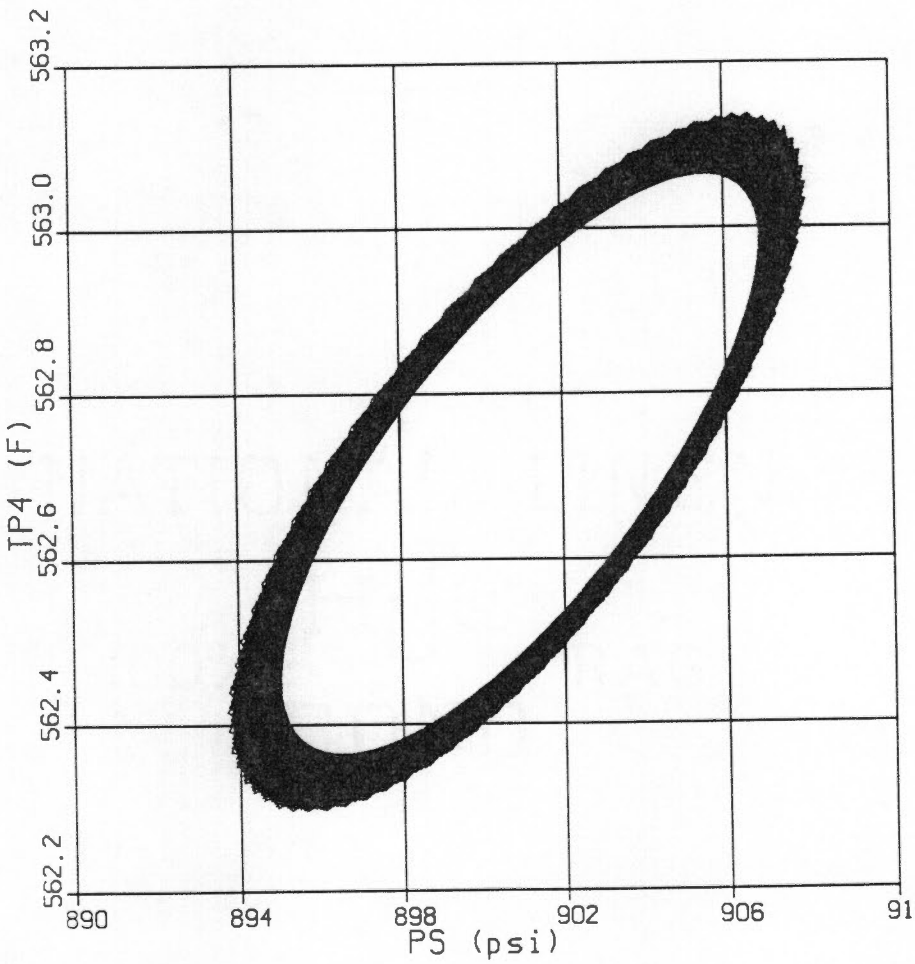

Figure 3.6: Limit cycle obtained by plotting the cold leg temperature (T_{p4}) versus steam pressure (P_s) generated with the OTSG model considering the downcomer as an accumulation tank.

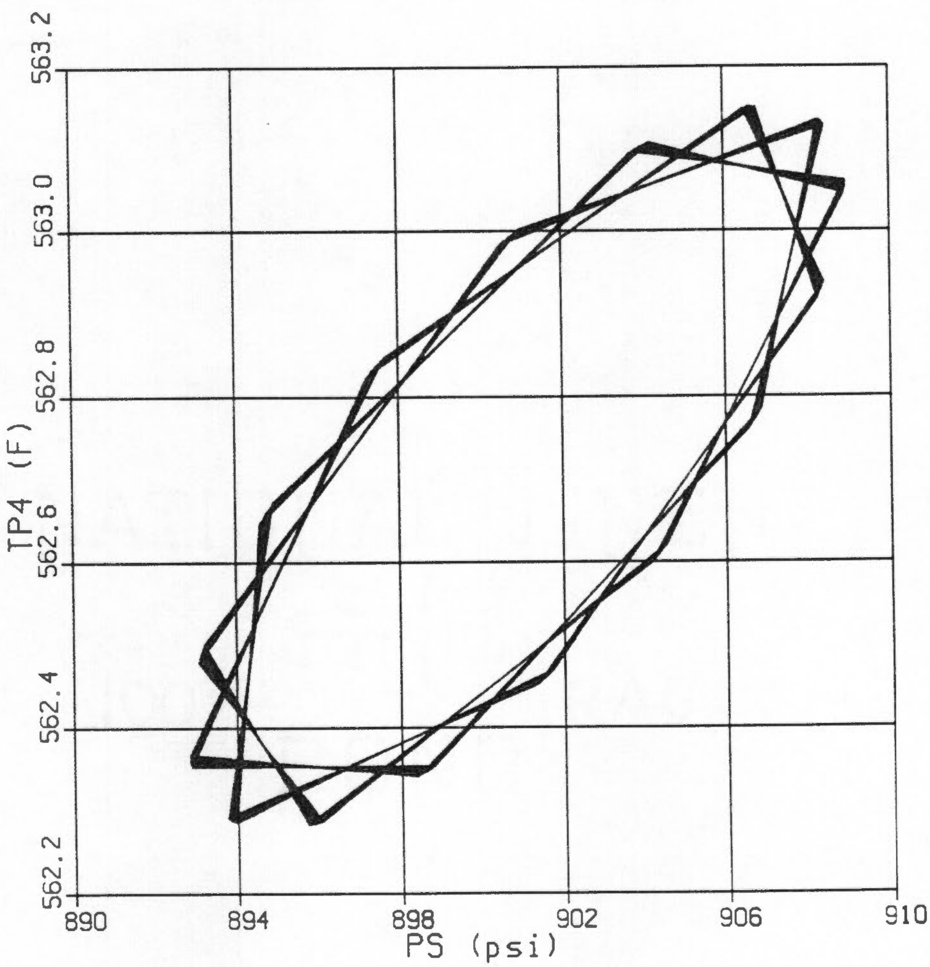

Figure 3.7: Limit cycle obtained by plotting the cold leg temperature (T_{p4}) versus the steam pressure (P_s) generated with the OTSG model considering the separation of phases in the downcomer.

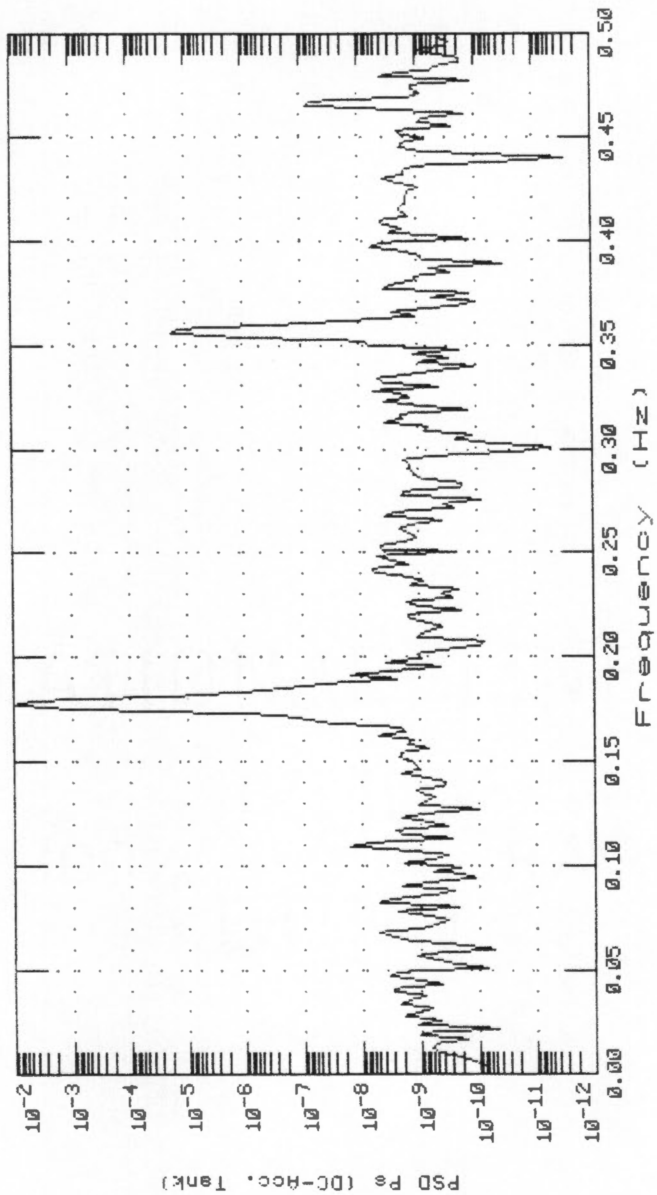

Figure 3.8: Power spectral density of the steam pressure (P_s) generated with the OTSG model considering the downcomer as an accumulation tank.

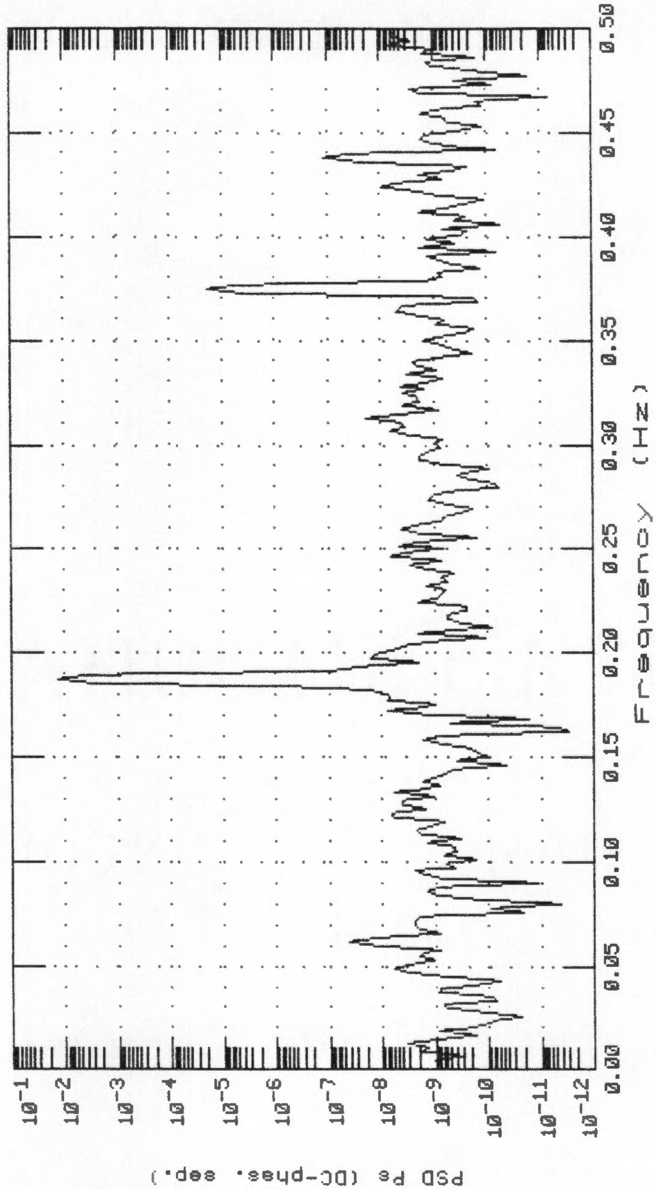

Figure 3.9: Power spectral density of the steam pressure (P_s) generated with the OTSG model considering the separation of phases in the downcomer.

the boiling region divided into 24 nodes and the same value of oscillatory frequency, 0.19 Hz, was obtained. The disadvantage of using the 24 nodes program is that it runs slower than real time in the oscillatory regime.

All the model runs described so far used a value of 0.03 $\frac{s^2 psift}{lb}$ for the friction coefficient of the pressure drop caused by the orifice at the bottom of the downcomer. This value, according to the OTSG description corresponds to the orifice 75% closed. The OTSG model considering the separation of phases in the downcomer set in the oscillatory regime was run with this coefficient set in 0.04 $\frac{s^2 psift}{lb}$ which to represents the orifice 100% closed. Figure 3.10 shows that with the coefficient increase, the steam pressure oscillation dies out which reproduces quite well the OTSG plant behavior. Note that the expression "100 % closed" is an improper use of the language maintained here for consistency with the plant description. This expression means that the movable plate at the bottom of the downcomer has been placed in its most internal position and that there is still a small annular area to allow the water flow between the downcomer and the tube region.

The present OTSG models are limited to moderate changes in power when operating in the oscillatory regime, due to the consideration that only the uppermost node in the boiling region has moving boundaries. Indeed, as the power changes the amplitude of the oscillation increases to a point that the moving boundary calculated in the last node of the boiling region reaches the upper boundary of the previous node as this happens the program crashes. This effect is more pronounced for the case where power is decreased because for this case the value of the moving boundary decreases.

A comparison is made of the steam pressure PSD's generated by the two OTSG models, Figure 3.8 and Figure 3.9, with the PSD obtained from the measured results. Figure 3.1, reveals that the models although giving a good representation of the oscillatory regime, fails to reproduce the broadband spectrum exhibited in the plant data's PSD. Since the broadband spectrum feature is one of the characteristics of the presence of chaos [7], a non-linear analysis of the data was deemed both necessary and interesting. The necessary tools for this study will be presented in the next chapter of this dissertation.

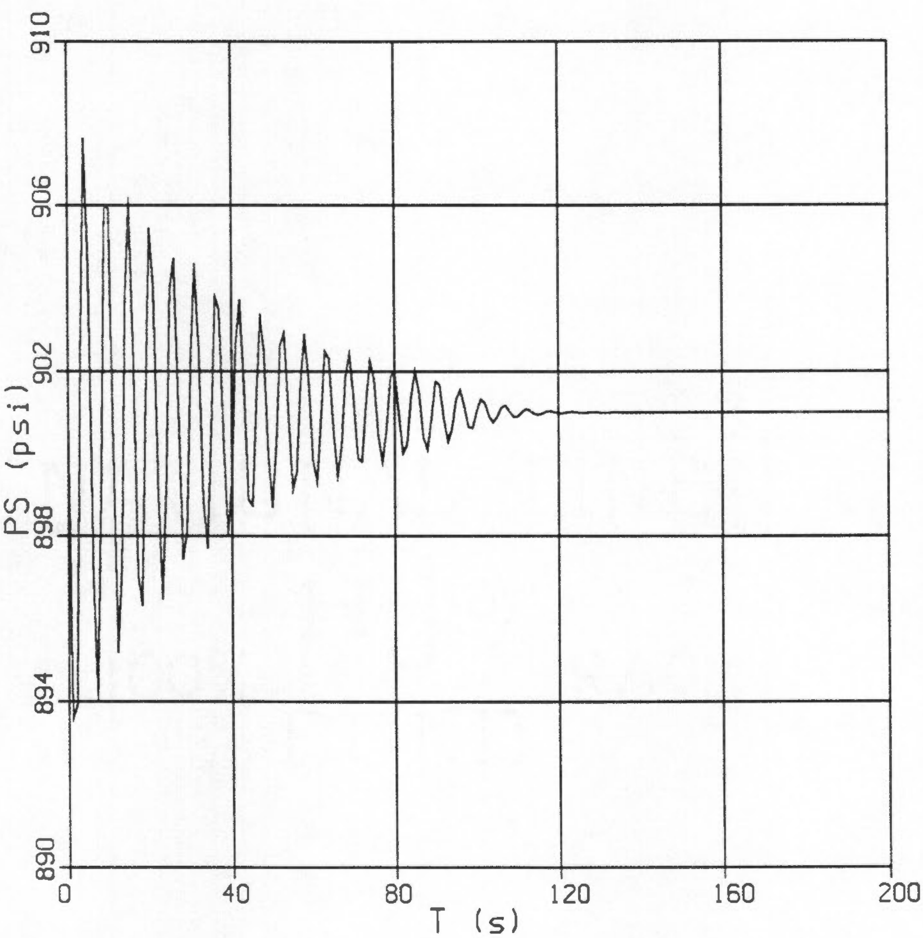

Figure 3.10: Steam pressure (P_s) generated with the OTSG model considering the separation of phases in the downcomer in which the value of the coefficient of the pressure drop corresponding to the orifice at the bottom of the downcomer was increased to represent the orifice fully closed.

Chapter 4

Chaotic Dynamics Analysis of Dynamical Systems and Time Series

4.1 Introduction

The purpose of this chapter is to introduce the definitions and algorithms used in the study of chaotic phenomena in physical systems and to develop procedures for the identification of chaotic signatures in time series data.

4.2 Basic Definitions and Procedures

In this section several definitions are presented. These definitions are presented first, the discussion of the applications of these definitions with examples are presented in the next sections.

The Poincare section is defined as any surface transverse to the bundle of phase space trajectories [27].

The Poincare map is defined as the action that takes all points in a Poincare section to their image points by following trajectories until they first return to the Poincare section [27].

A Lyapunov Exponent is defined as the number that measures the exponential expansion or contraction in time of two adjacent trajectories in phase space with very close but different initial conditions [7]. Similar definitions for the Lyapunov exponents can also be found in [27] and [28].

Fractal is defined as the geometric property of a set of points in a n-dimensional space having the quality of self-similarity at different length scales and having a noninteger dimension less than n ([7],[29],[30]).

The fractal dimension is defined as the quantitative property of a set of points in an n-dimensional space which measures the extent to which the points fill a subspace as the number of points becomes very large [7].

A value for the fractal dimension can be obtained as one counts the minimum number of cubes of size ϵ needed to cover a set of points, if this number behaves as ϵ^{-d} as $\epsilon \rightarrow 0$, the exponent d is called the capacity of the fractal dimension ([7],[31]).

An attractor is defined as a set of points or a subspace in phase space toward which a time history approaches after transients die out [7].

The same definition presented above for attractors applies to the strange attractor, except that the strange attractor is associated exclusively with the chaotic orbits in phase space. A strange attractor is also said to be the attractor that in phase space has a fractal dimension [7].

The signature of chaos in a given physical system is identified by a positive Lyapunov exponent, a fractal dimension of the attractor and known routes to chaos such as a cascade of period doubling pitchfork bifurcations[15]. In the event that a complete analytical model exists, as for instance the Lorenz and Rossler models (see Appendix B), the Lyapunov exponent can be obtained analytically and the strange attractor projection can be described simply by plotting any variable against another. However, in the case of experimental systems or industrial devices only signal time series are available. In this situation the Lyapunov exponent and the strange attractor projection determination must be carried out from the available time series data. To overcome this difficulty, the concept of pseudo-phase space is introduced, which is a virtual space where the coordinates are created by applying a time delay to the original time series. The coordinates of the pseudo-phase space are called pseudo-coordinates ([32],[28],[33],[34]). The proper choice of the time delay is critical. If the time delay is too large the attractor reconstruction folds onto itself. If the time delay is too short the attractor stretches along a line. By the utilization of the method of delays, as many coordinates as is needed can be generated, obviously, limited by the length of the time series. On the basis of the pseudo-phase space concept, Lyapunov exponents and strange attractors projections are determined in terms of three parameters: the time delay itself, the orbital average period, and the evolution time. The orbital average period is the mean time to complete one attractor orbit. The evolution time is the time length necessary to follow two initially close trajectories to calculate the rate of divergence (or convergence).

4.3 Poincare Maps

The determination of the time series points that belong to the same Poincare section requires the visualization of the characteristics that binds these points to the Poincare section. An easy way to accomplish this is to select all the values that represent the maximum peak of the oscillation. This set of points can be displayed graphically, where the abscissa contains the peaks, and the ordinate contains the peaks shifted by one maximum. This graph is called the Poincare map.

Two programs were written in C language [35] to implement the construction of the Poincare maps. The program LGMAPP reads the time series, finds the maxima and writes them into a file. The program LGDEL reads this file and plots the Poincare map on a personal computer screen. These two programs were used with time series arising from the Rossler and the Lorenz systems. A brief description of the Rossler and Lorenz equations used in this work are given in Appendix B.

Figure 4.1, and Figure 4.2 show the Poincare maps of the Rossler x variable, and the Lorenz z variable respectively. Both figures are in agreement with the ones found in the literature ([36],[32],[27]) hence verifying the programs used to generate them.

4.4 Power Spectral Density

The power spectral density (PSD) of a chaotic signal is a basic tool for the determination of the parameters for the strange attractor reconstruction, calculation of

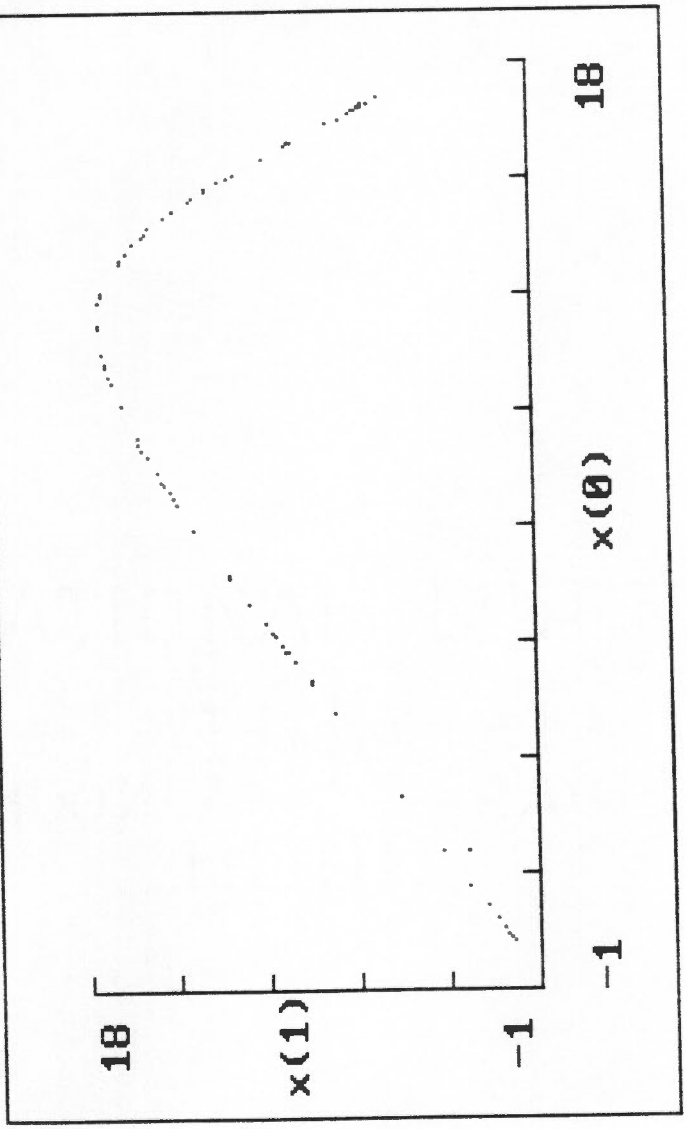

Figure 4.1: Poincare map for the x-Rossler variable.

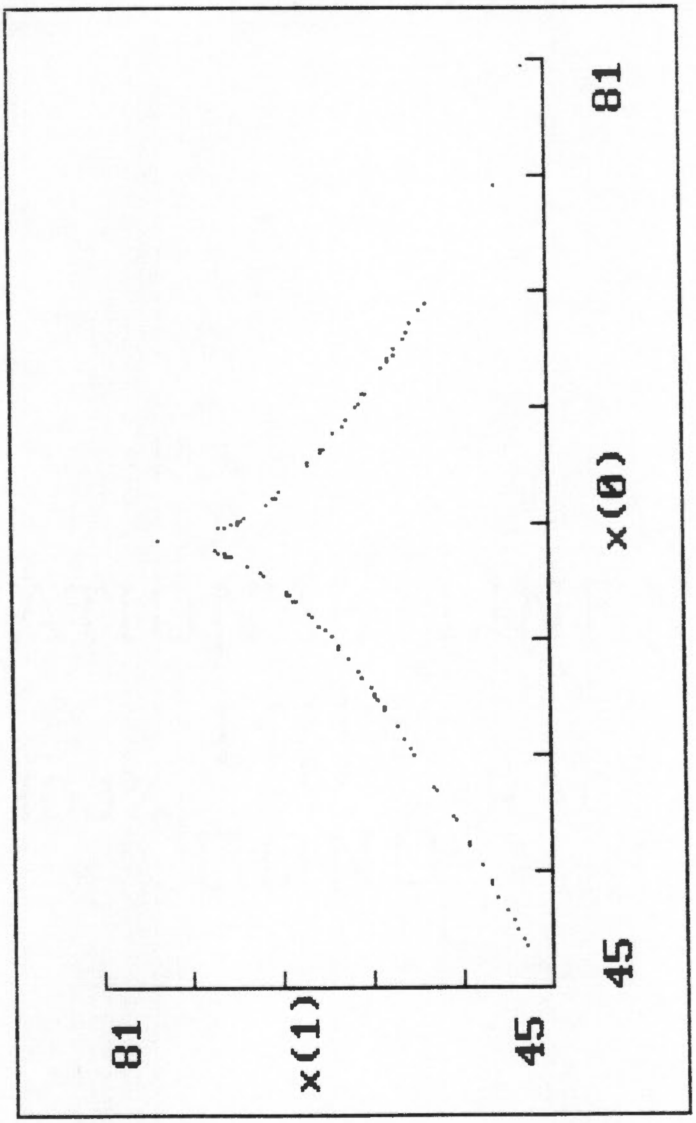

Figure 4.2: Poincare map for the z-Lorenz variable.

the Lyapunov exponent, and the identification of chaotic signatures [37].

The PSD for the x-Rossler and z-Lorenz signals are displayed in Figure 4.3 and Figure 4.4, respectively. The sampling time used for the time series collection was 0.1 second for the x-Rossler and 0.01 second for the z-Lorenz. The two relevant features in both graphs are the resonance peaks at the corresponding frequencies (0.164 Hz for the x-Rossler and 2.18 Hz for the z-Lorenz) of their respective orbital average periods, and the broadband region between the resonance and the plateau at high frequencies. Note that in both examples the broadband power density decays exponentially with frequency. This last feature has been observed in all known chaotic signals [38], although no mathematical proof exists. In contrast it has been shown analytically [38] and experimentally [39] that in the case of stochastic noise the PSD in the broadband region decays inversely proportional to powers of the frequency. As proposed by Gorman and Robbins [37] the specific properties of the PSD for the chaotic signals, as observed above, provides a reliable test for the identification of chaotic signatures in physical systems.

The PSD also serves as the basis for the calculation of the parameters used in the calculation of the Lyapunov exponents and the generation of the attractor reconstruction: the average period, the evolution time, and the time delay. The average period is calculated by taking the inverse of the PSD peak frequency. Which gives a value of 6.1 seconds for the Rossler case, and 0.46 seconds for the Lorenz case. These values are in accordance with the values given in reference [28]. The evolution time is obtained by taking the inverse of the higher frequency value at the end point of the broadband region [40]. This gives a value of 0.46 second for the Rossler system, and a value of 0.069 seconds for the Lorenz system. The time delay is obtained by dividing the evolution time by the desired pseudo-space dimension [40] to be used in the attractor reconstruction.

4.5 The Determination of the Lyapunov Exponents

Two programs were used to calculate the Lyapunov exponent. One of the programs was developed by the author using an algorithm developed by Wolf [28], the other

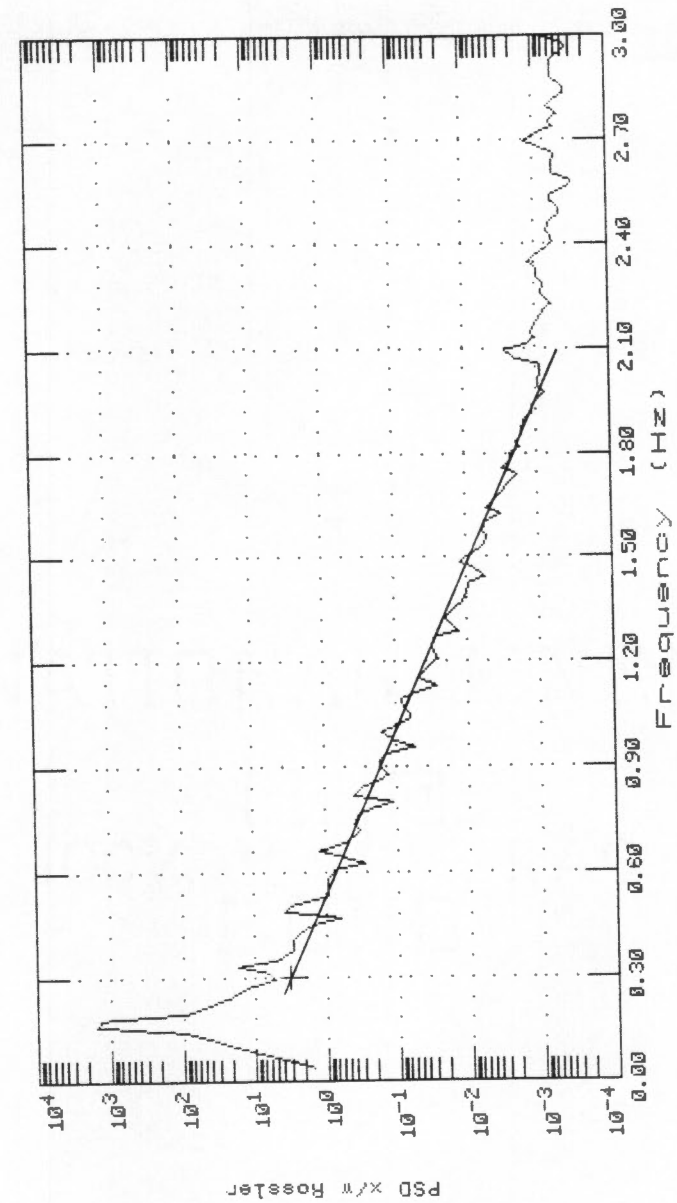

Figure 4.3: Power spectral density for the x-Rossler signal showing an exponential decay.

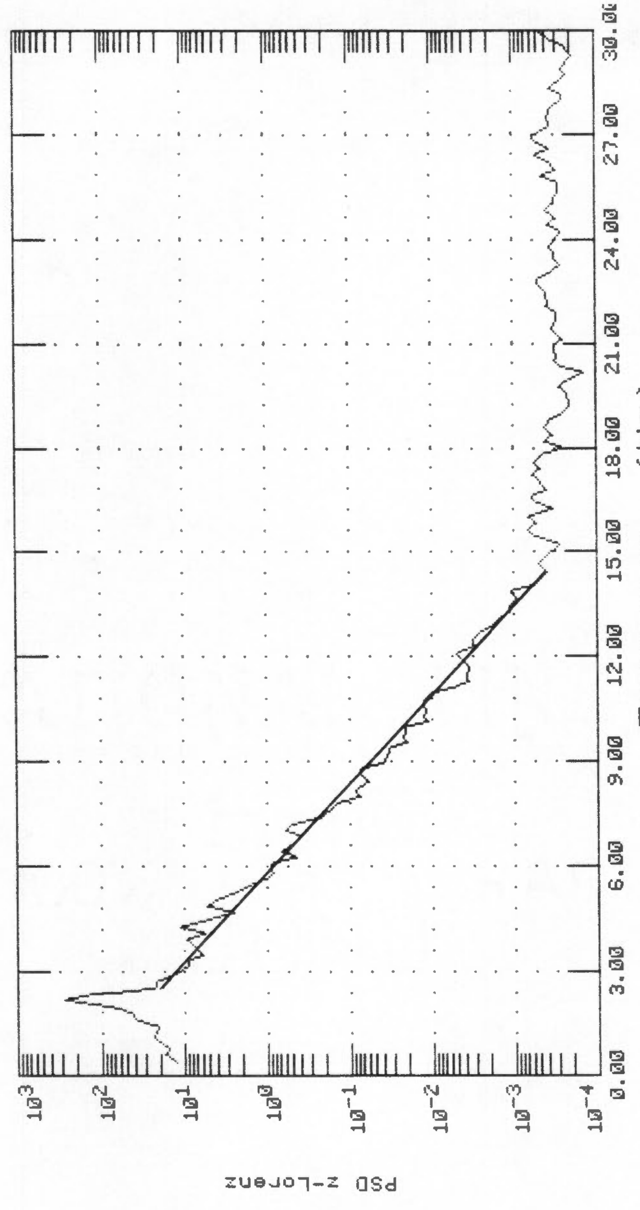

Figure 4.4: Power spectral density for the z-Lorenz signal showing an exponential decay.

program was developed at ORNL [40]. The results of both programs are compared since there are some differences in the algorithms used by both programs. Wolf's program searches for two initially close trajectories and then performs the evolution in time to calculate the rate of expansion. The determination of the next set of closed trajectories is taken after the evolution. This gives the number of iterations to be the total number of points of the time series divided by the evolution time. The ORNL's program uses the average period to determine the number of iterations and calculates the evolutions departing from each point of the orbital cycle. The results of these two programs were verified by comparison with the analytical values of the Lyapunov exponents for the x-Rossler and the z-Lorenz signals, and are presented in Table 4.1.

4.6 The Attractor Projection

Attractors, as defined in Section 4.2, can be classified as classical attractors and strange attractors. Included in the classical attractor category are the steady state equilibrium condition of a dynamical system which is represented by a point in phase space, the periodic solution of an oscillatory system, which is represented by a limit cycle in phase space, and the quasiperiodic phenomena which is represented by a toroidal surface in phase space. Strange attractors are related exclusively with chaotic phenomena and have fractal dimensions [7].

Figure 4.5 shows the projection of the Rossler strange attractor in the XY plane (y versus x Rossler signals). The phase space trajectory spirals away from the initial point into the strange attractor. Note the folding of the trajectories in the upper right corner of the graph.

Table 4.1: Comparison of the Lyapunov exponents calculated with the ORNL's and Wolf's programs and analytical results.

	ORNL's program	*Wolf's program*	*analytical values*
x-Rossler	0.12	0.11	0.13
z-Lorenz	2.5	2.4	2.16

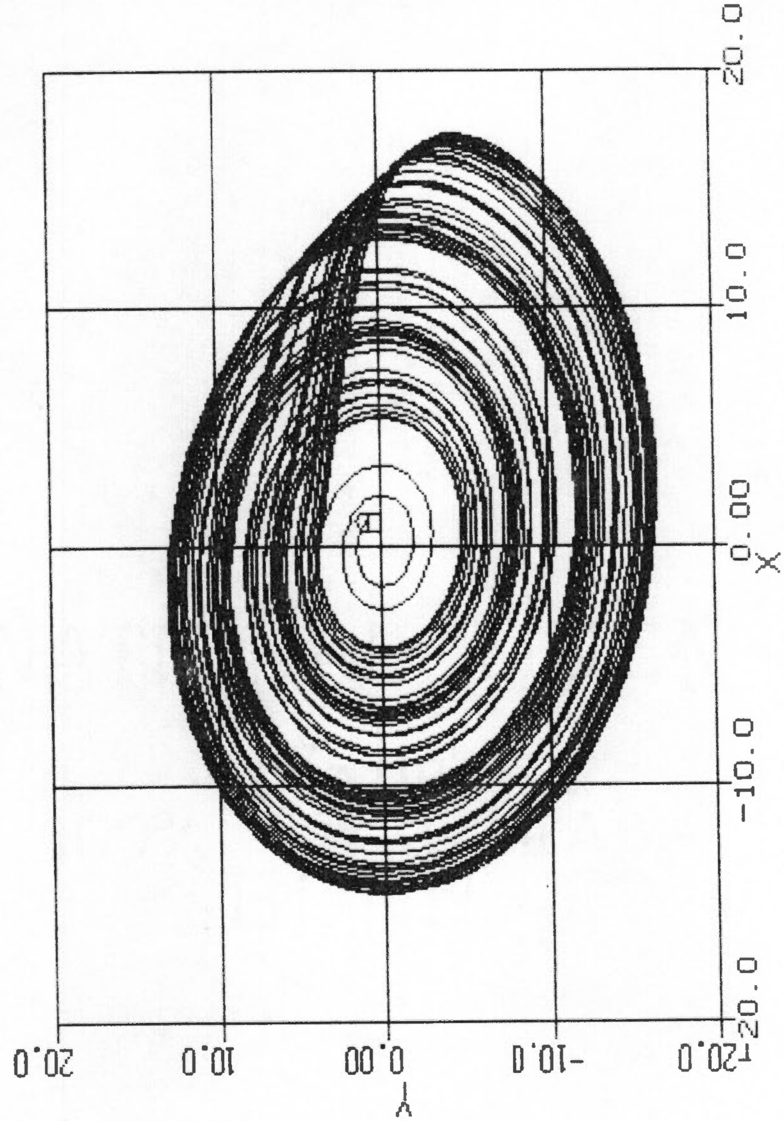

Figure 4.5: XY projection of the Rossler strange attractor.

To illustrate the use of the pseudo-phase space method discussed in Section 4.2 a x-Rossler time series was generated with a sampling rate of 0.1 seconds. From the PSD in Figure 4.3, a time delay of two samples is obtained. Figure 4.6 shows on the abscissa, the x-Rossler signal and on the ordinate, itself delayed by two samples. Note that the folding of the strange attractor orbits is located at the right bottom part in this diagram.

A comparison between Figure 4.5 and Figure 4.6 reveals some similar features as for instance the arrangement of the orbits. However, the folding effect causes different results in the way the bundle of trajectories falls back onto itself. It is necessary to stress here that a perfect match was not expected. The relevant aspect of this method is the fact that it shows the chaoticity information can be obtained from a single signal. This is the remarkable feature of pseudo-space reconstruction of the attractor.

4.7 The Undersampling Effect in Time Series

In preparation for the use of the previously developed set of tests to identify chaotic signatures from experimental time series, the undersampling effect introduced by instrumental resolution has to be investigated.

The undersampling effect on the Poincare map is shown in Figure 4.7 generated with a x-Rossler signal (undersampled) at a rate of one sample per second. The comparison between Figure 4.7 and Figure 4.1 (for which there is no undersampling) shows that the inverted "U" shape is common to both cases, but the undersampling effect causes the points to occupy a region on the diagram.

The PSD for the same undersampled x-Rossler signal is shown in Figure 4.8. Although degraded one can still observe the typical resonance at 0.164 Hz and the broadband region.

Figure 4.9 displays the Rossler strange attractor reconstruction using an undersampled time series. Note it shows clearly the outside boundary, but both the details of its internal structure and the folding of the trajectories have been lost.

This study has shown that instrumental resolution effects do indeed reduce the effectiveness of the Poincare map and the attractor reconstruction.

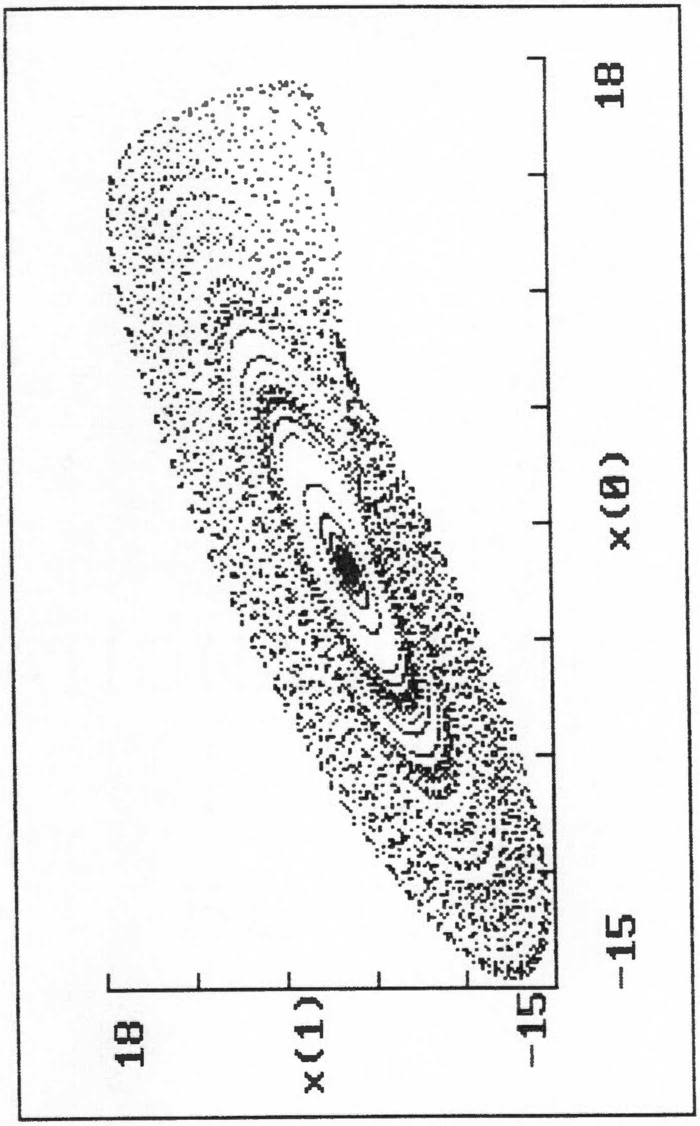

Figure 4.6: X-Rossler signal against itself delayed by two samples.

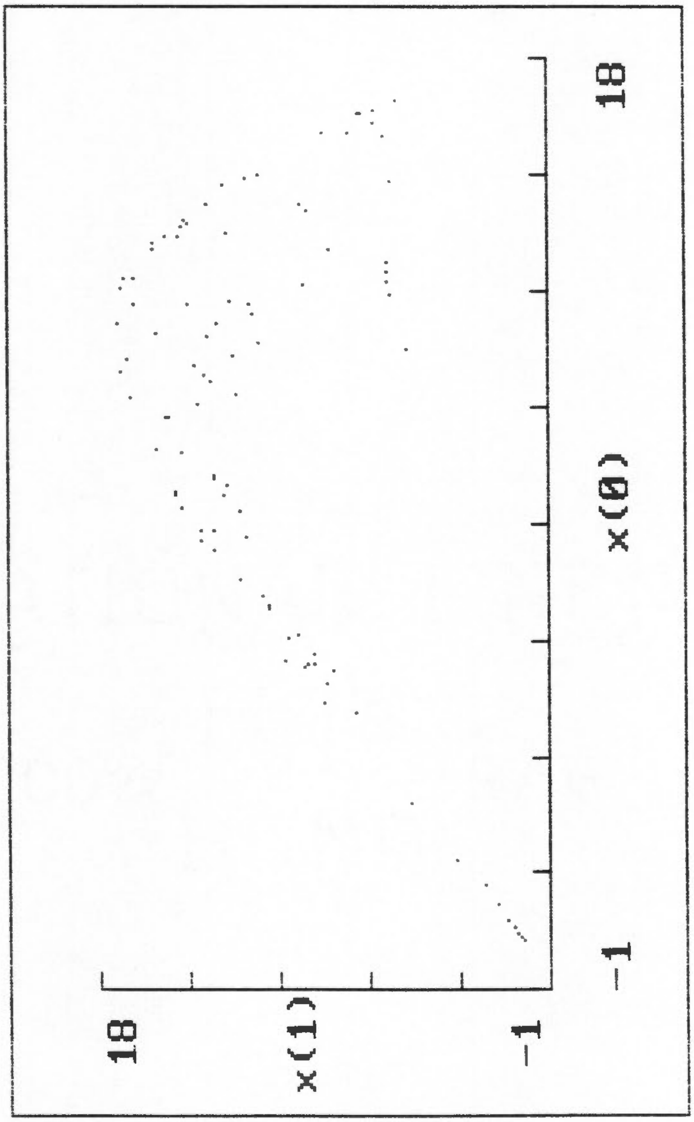

Figure 4.7: Poincare map for the undersampled time series of x-Rossler variable.

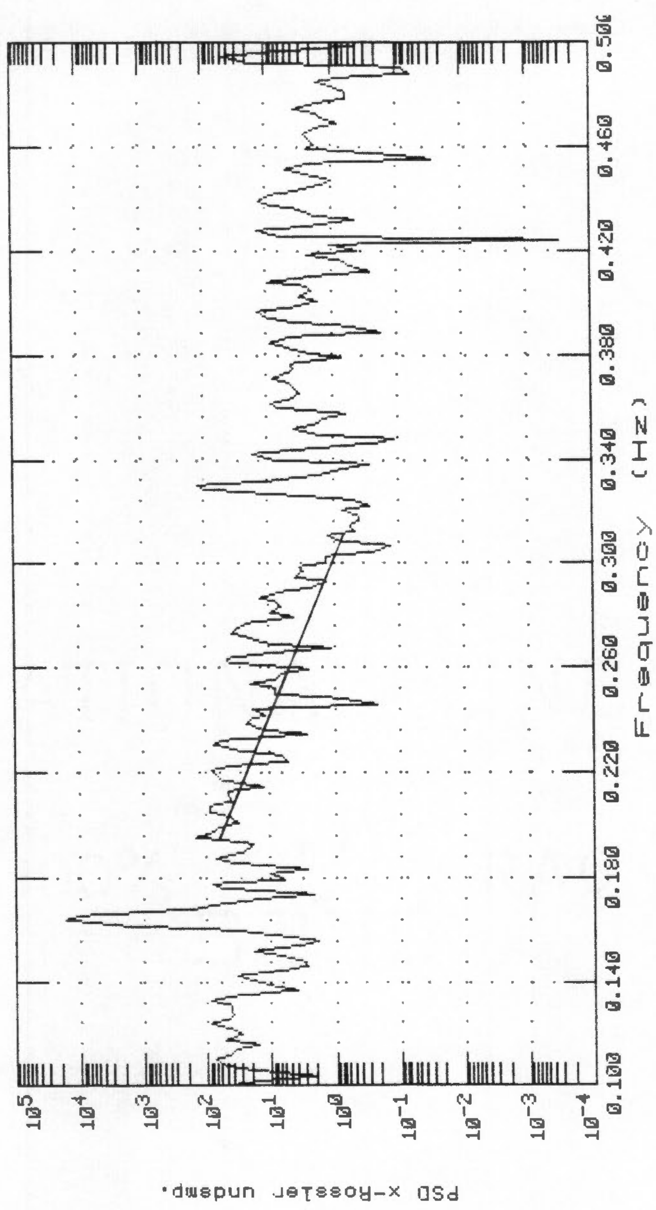

Figure 4.8: Power spectral density for the undersampled x-Rossler signal.

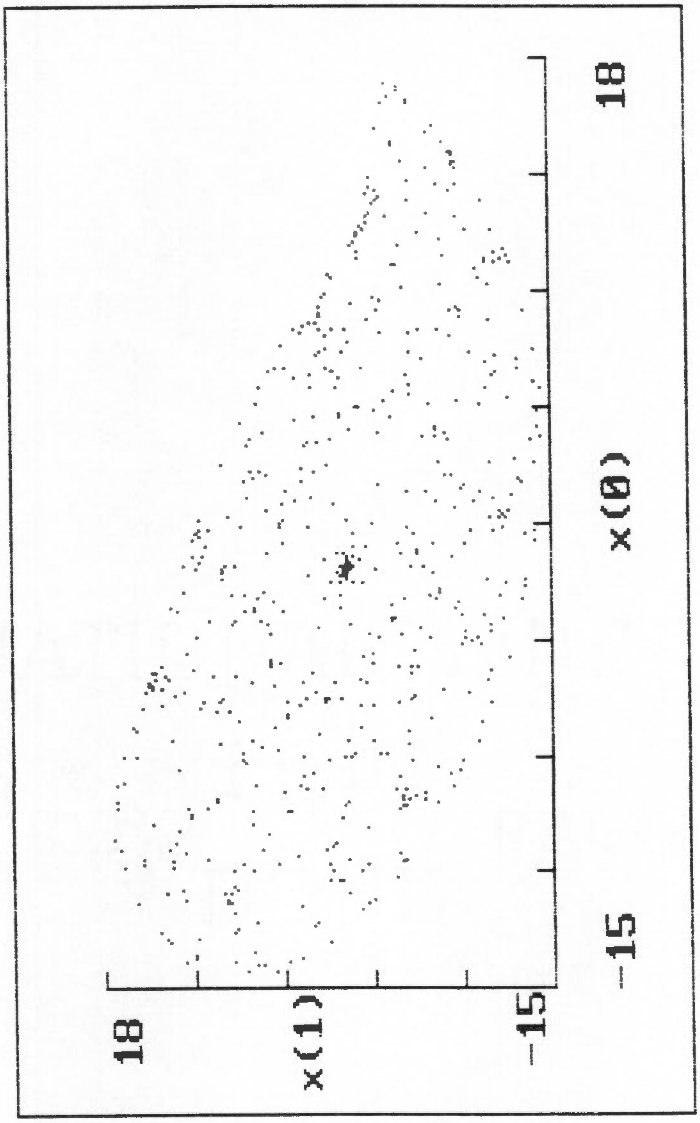

Figure 4.9: Undersampled x-Rossler signal plotted against itself delayed by two samples.

4.8 The Modulation Effects in the Harmonic Oscillator

Disorderly (erratic) behavior of otherwise deterministic physical systems may occur via stochastic and/or chaotic process as acting either internally or as external driving sources. The purpose of this section is to investigate the effects of stochastic and chaotic perturbations on the amplitude of a limit cycle. To this end the system of equations below, which simulates an externally driven oscillator, were used:

$$\dot{x} = y \tag{4.1}$$

$$\dot{y} = G - (2.\,\pi\, f)^2\, x \tag{4.2}$$

$$G = c1\, X_{nsc} + c2\, X_{ros} \tag{4.3}$$

Where:

x is the harmonic oscillator variable;
y is the time derivative of the harmonic oscillator variable;
X_{nsc} is a variable containing band limited white noise [25];
X_{ros} is the x-Rossler variable containing chaos, see Appendix B;
c1 and c2 are adjustable parameters; and
f is the frequency value in (Hz), set equal to 2.12 Hz.

The initial conditions used are $x = 7.8$, and $y = 0$. The analyzed signal had its mean value further shifted to 901.

4.8.1 The Unmodulated Limit Cycle

To provide a basis for comparison the unmodulated limit cycle will be examined first. In ideal conditions (good sampling rate and long time collection) the Poincare map of the harmonic oscillator exhibits a single point. The attractor reconstruction shows either a circle or an ellipse depending on the angle of sight, and the PSD exhibits a peak frequency corresponding to the harmonic oscillator frequency. The undersampling effect was then included in the data collection for harmonic oscillator (a 0.1 second sampling time and 60 seconds of data collection). Signal undersampling effects did hardly change, from the ideal case, the attractor reconstruction projection and the PSD structures as shown in Figure 4.10, and Figure 4.11 respectively. But drastically changed the Poincare map that degenerates from a point to a D-shape form shown in Figure 4.12.

4.8.2 Modulation by Band Limited White Noise

Setting the parameter c2 equal to zero in equation 4.3, the model was run (sampling time 0.1 second, for 60 seconds) with the BLN function, X_{nsc}. The break frequency of the BLN function was set to 0.42 Hz. The resulting Poincare map is shown in Figure 4.13. Note that the D-shape contour of the undersampled and unmodulated limit cycle (Figure 4.12) is still clearly seen as the fuzzy contour of a region populated by a spread of points due to the random nature of the driving force. The attractor projection reconstructed in the pseudo-phase space is shown in Figure 4.14. Note that the main change with respect to the unmodulated case is the observed fuzziness causing the loss of definition in the pseudo-trajectory in Figure 4.10.

4.8.3 Modulation by x-Rossler Signal

By setting the parameter cl equal to zero in equation 4.3, the model was run (sampling time 0.1 second, for 60 seconds) with the x-Rossler signal, X_{ros} generated by the Rossler equations as described in Appendix B. The resulting Poincare map is shown in Figure 4.15, which exhibit a mixture of the D-shape contour of the unmodulated limit cycle stretched by the superposition of the inverted "U" shape from the x-Rossler Poincare map (Figure 4.1). The strange attractor projection reconstruction for this case is shown in Figure 4.16. Note that a higher degree of fuzziness than the case with the BLN modulation (Figure 4.14) around the main trajectory is observed. The PSD which is displayed in Figure 4.17 exhibits the Rossler resonance at 0.16 Hz, followed by the broadband of chaotic signals (with the exponential decay) and the harmonic oscillator resonance frequency.

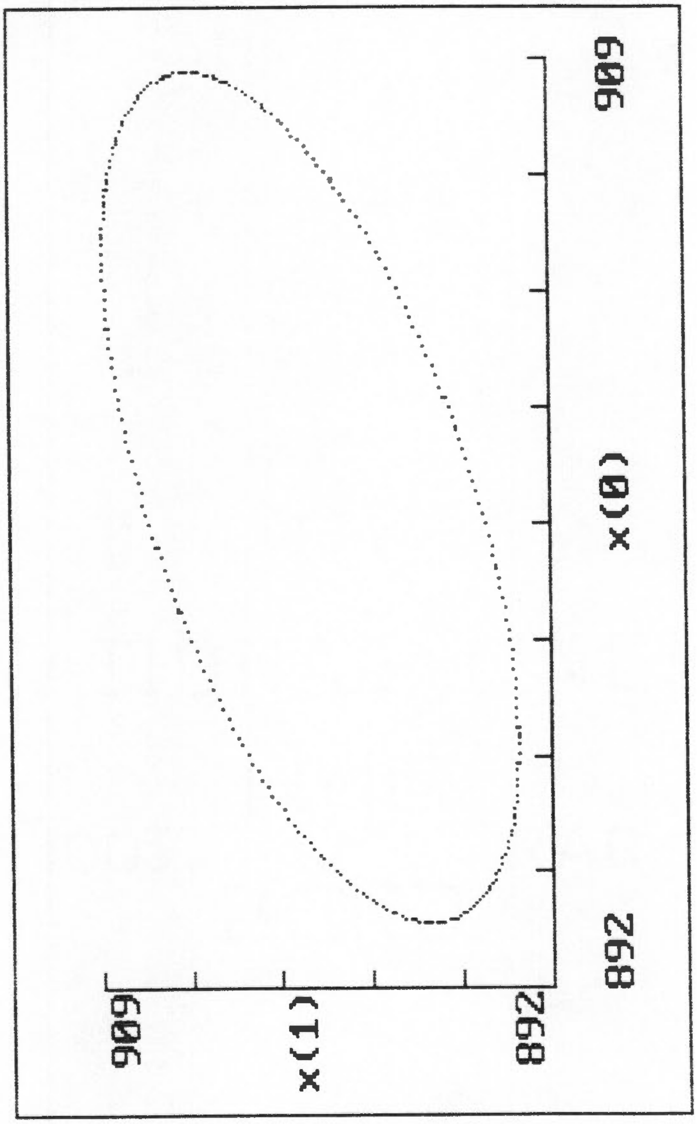

Figure 4.10: Attractor reconstruction for the undersampled harmonic oscillator.

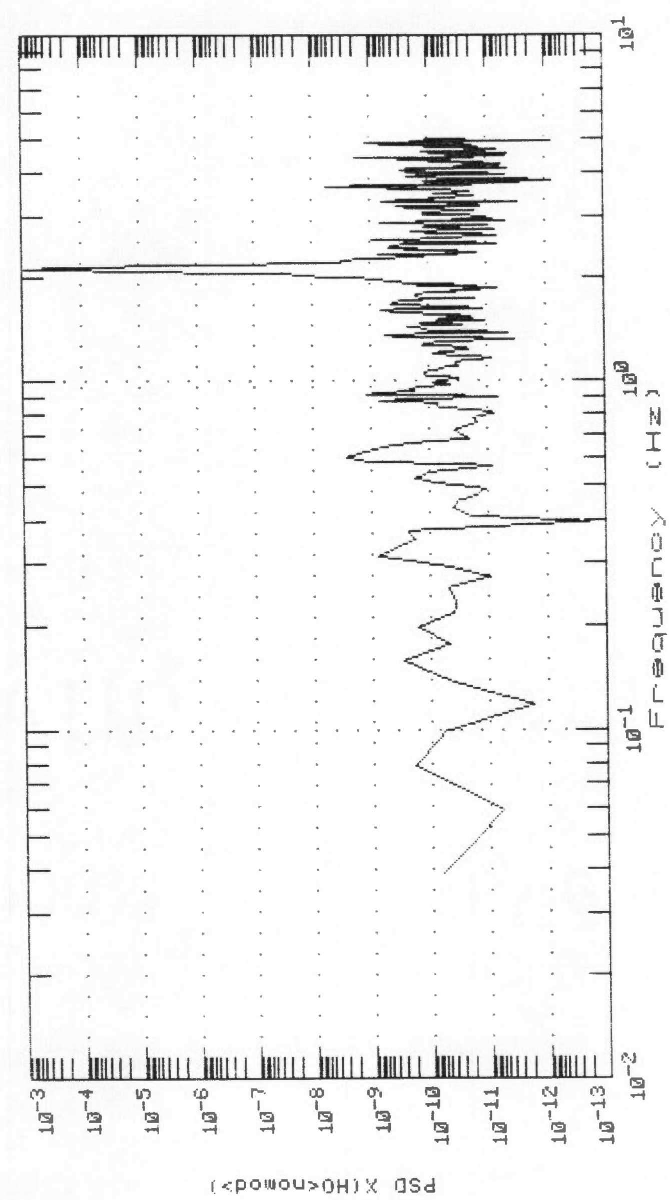

Figure 4.11: PSD for the undersampled harmonic oscillator.

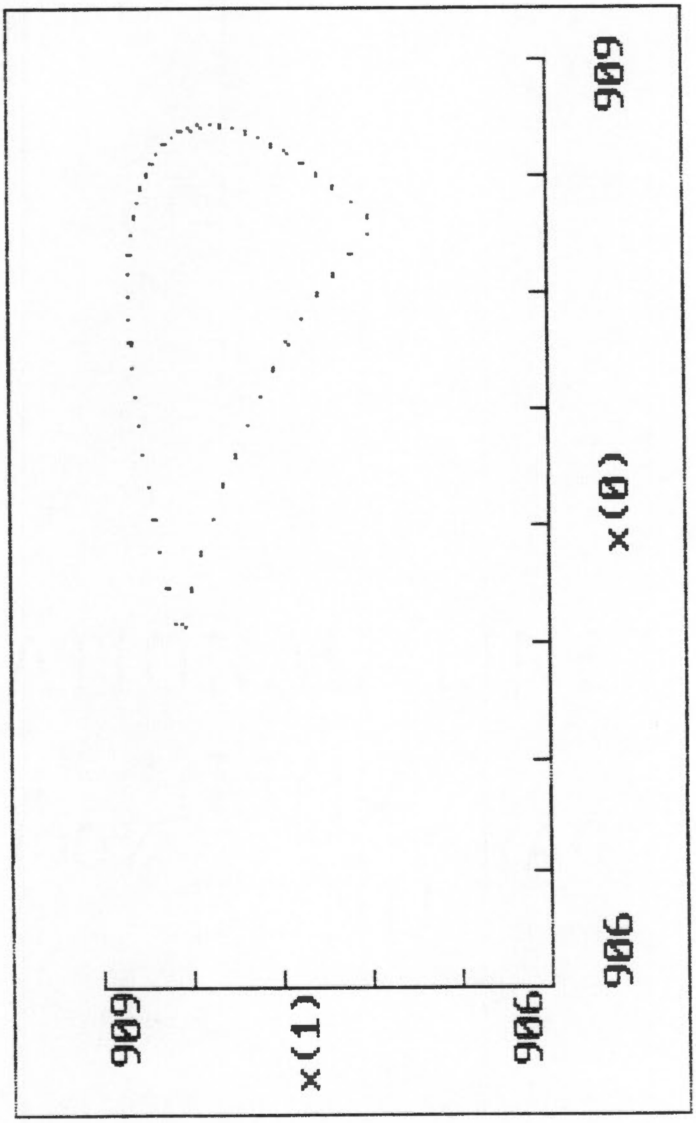

Figure 4.12: Poincare map for the undersampled harmonic oscillator.

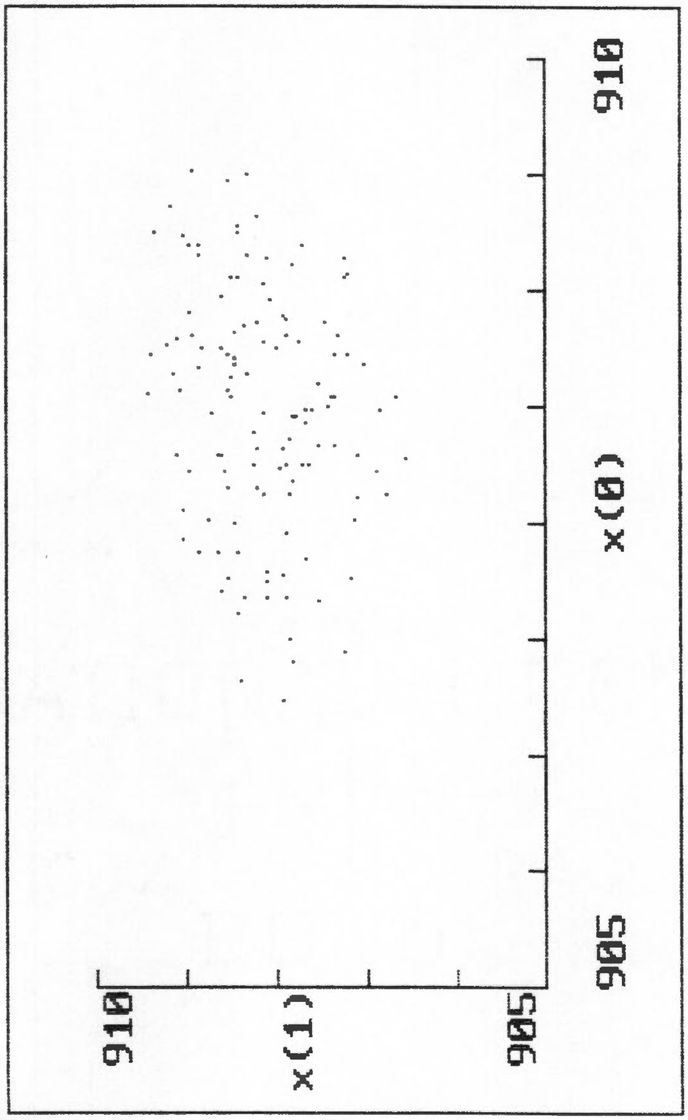

Figure 4.13: Poincare map for the band limited noise modulation of a harmonic oscillator.

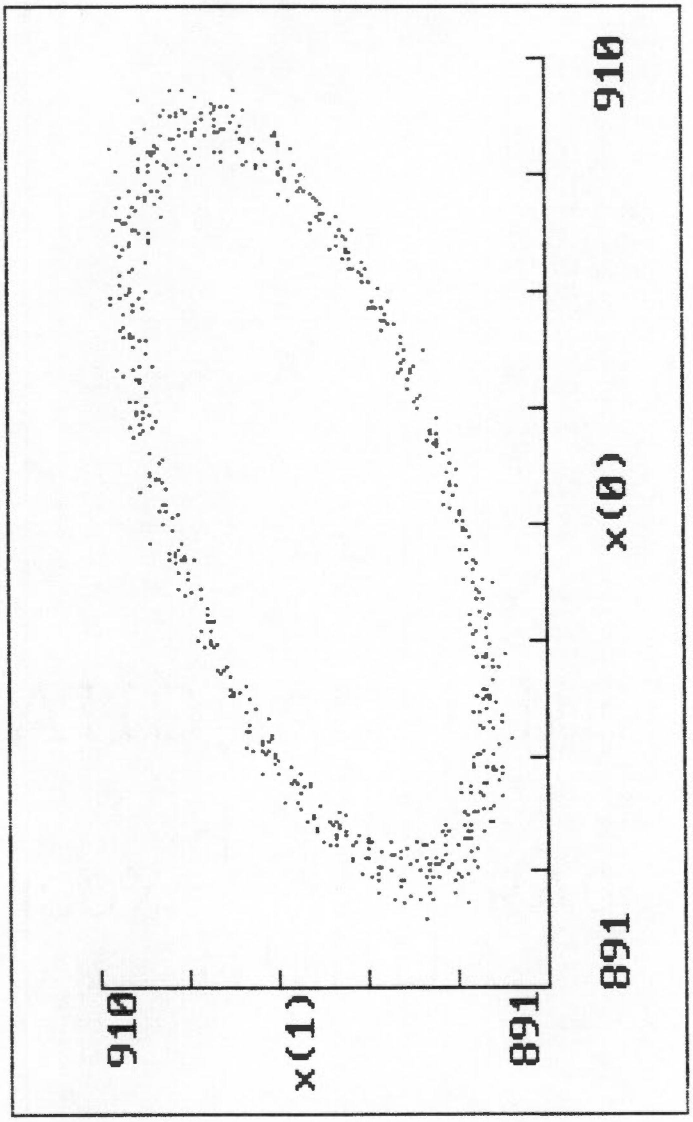

Figure 4.14: Attractor reconstruction for the band limited noise modulation of a harmonic oscillator.

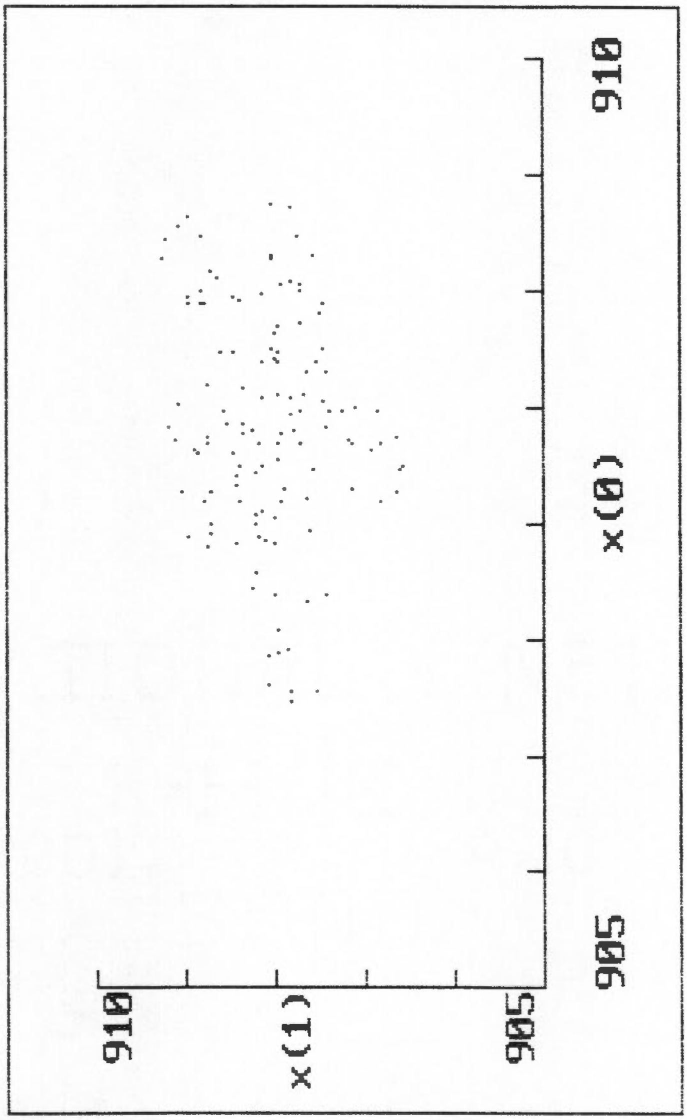

Figure 4.15: Poincare map for the x-Rossler modulation of a harmonic oscillator.

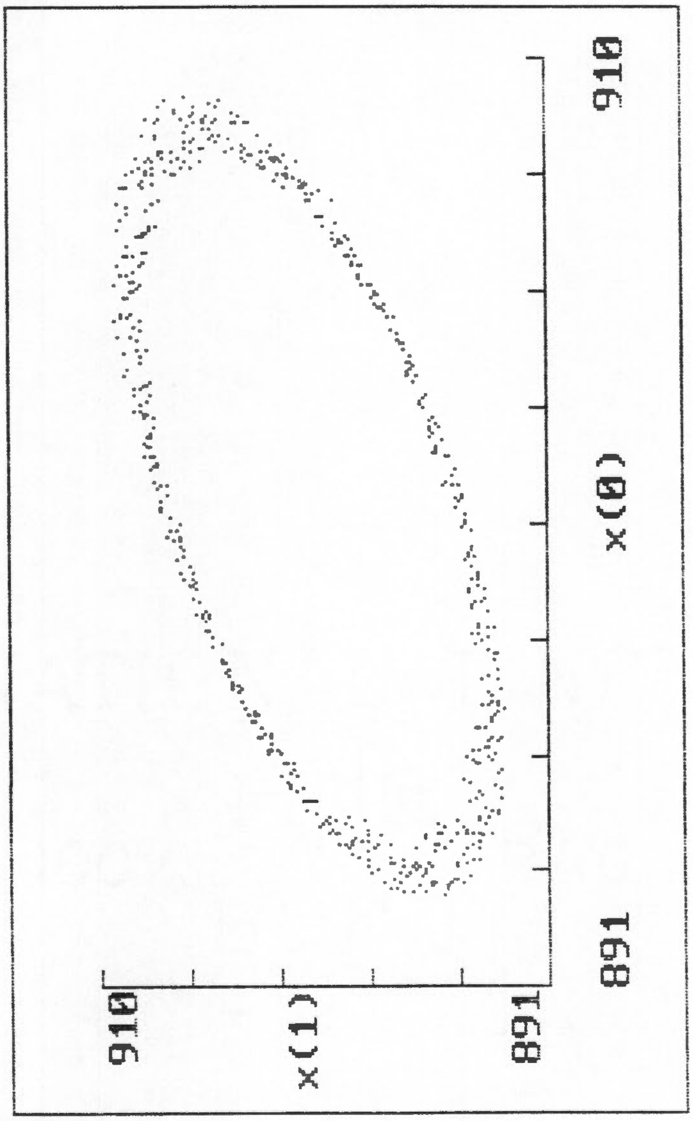

Figure 4.16: Attractor reconstruction for the x-Rossler modulation of a harmonic oscillator.

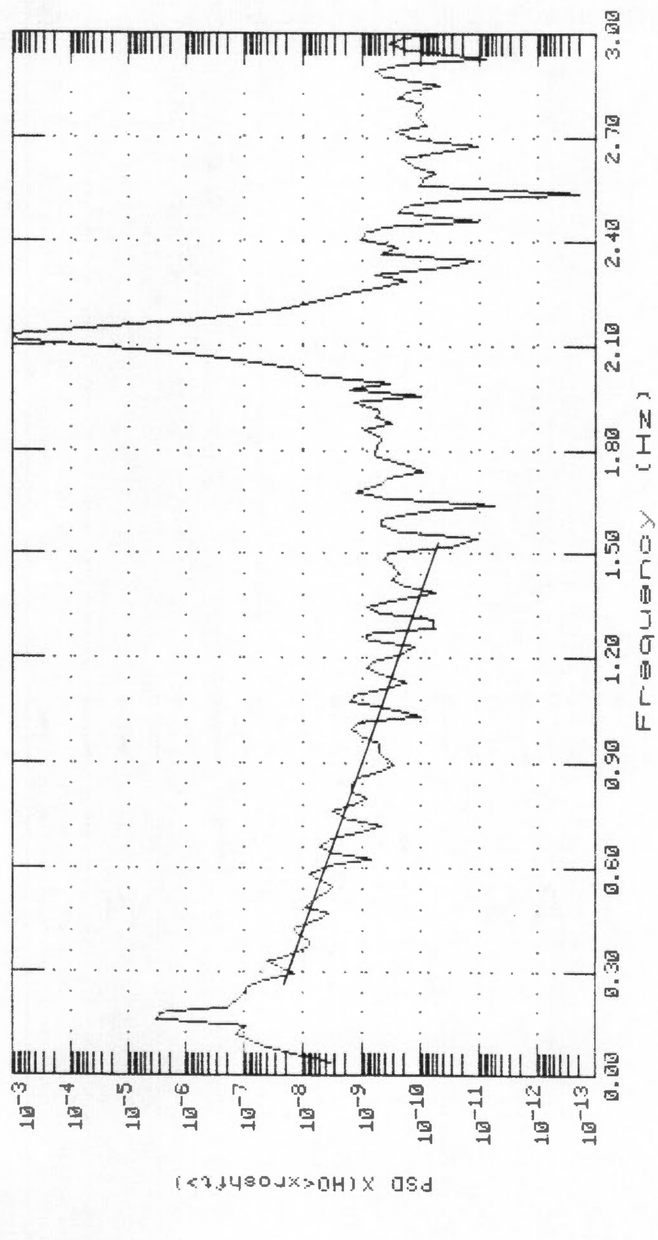

Figure 4.17: PSD for the x-Rossler modulation of a harmonic oscillator.

4.9 Conclusions

It has been shown that in agreement with the original work of Sigeti and Horsthemke [38], there is a marked difference between the structures of the PSD for stochastic and chaotic signals. The former having a broadband decaying as a power law and the latter decaying as an exponential function of the frequency.

The study of the limit cycle modulation has shown some noticeable differences in the structure of Poincare maps and attractor projections reconstructions which aid in the identification of the nature of the driving sources. Although the frequency dependence of the broadband region in the PSD appears to be a better test for signature identification.

Some relevant observations for the identification of chaotic signatures in experimental data sets have been derived from the present study. Instrumental resolution effects leading to signal undersampling may drastically change the structure of the Poincare map and attractor projections. The time length of the data must be sufficient to guarantee that the trajectories in phase space will be followed long enough for an appropriate reconstruction of the attractor. The general consensus seems to be that around 5000 points on the time series are required ([28], [10]). The number of points actually required depends on the size of the strange attractor and if the proper sampling resolution have been used.

Chapter 5

Nonlinear Analysis of the Plant and Simulation Data

The purpose of this chapter is to perform a comparison of the Poincare maps, Lyapunov exponents, attractor reconstruction, and power spectral density of the plant data with the corresponding tests for chaotic signatures described in Chapter 4. The objective of this comparison is to determine whether or not there is a chaotic signature in the plant data.

5.1 The Poincare Map Analysis of the Plant Data

The Poincare maps obtained from the OTSGA steam pressure, P_{sa}, and from the reactor power, POW, signals are displayed in Figures 5.1 and 5.2 respectively. Both maps are more stretched and the points are more unevenly distributed than the map corresponding to the BLN modulation of the harmonic oscillator in Figure 4.13. Qualitatively, the experimental maps present a certain degree of similarity with the Poincare map for the Rossler Modulated harmonic oscillator in Figure 4.15.

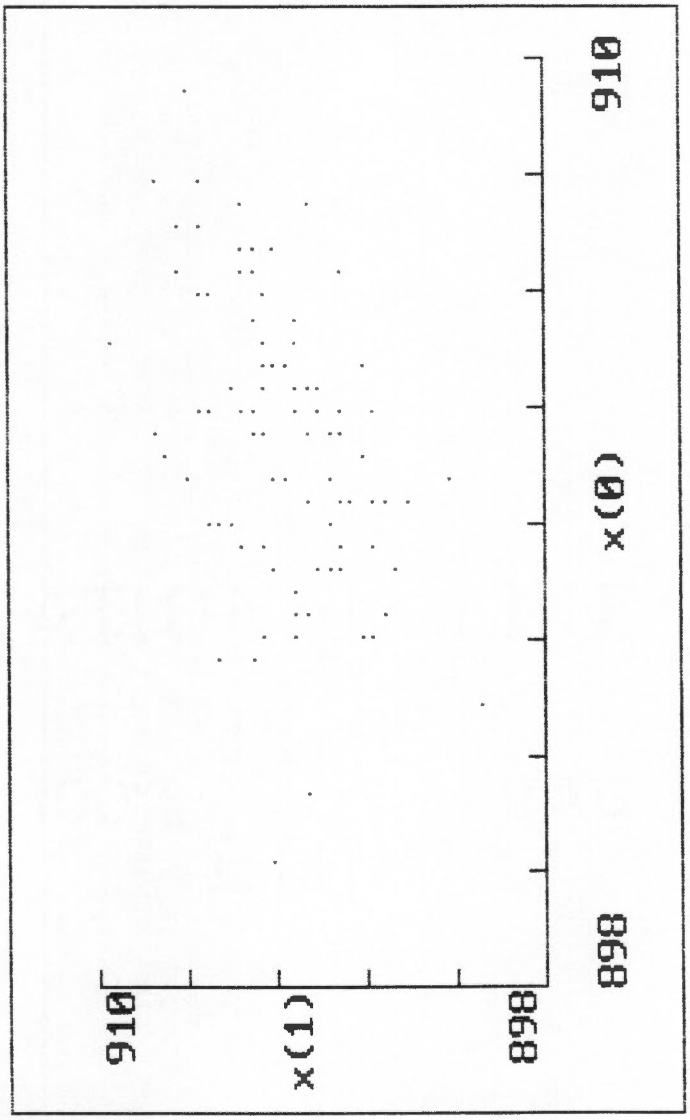

Figure 5.1: Poincare map obtained from the OTSGA steam pressure signal (P_{sa}).

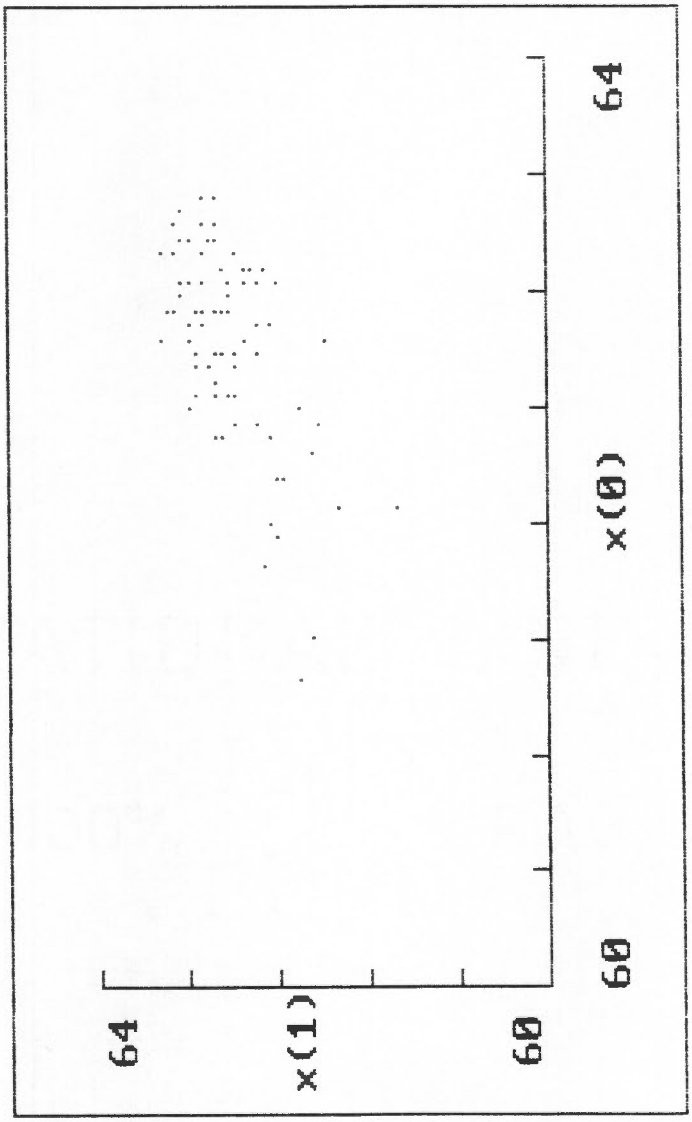

Figure 5.2: Poincare map obtained from the reactor power signal (POW).

5.2 The Lyapunov Exponents Analysis of the Plant Data

The fundamental value of the Lyapunov hierarchy was calculated for three sets of experimental data: the OTSGA steam pressure (P_{sa}), the OTSGB steam pressure (P_{sb}), and the loop A turbine header steam pressure (P_{sha}). Table 5.1 shows the values of the average period (τ_p), evolution time (τ_{evol}), and time delay (τ_d) derived from the PSD for each data set and the results obtained using the ORNL algorithm and the algorithm based on Wolf's formulation. Despite the undersampling effects, which tend to distort the shape of the broadband region in the PSD, there is a good consistency among the values of the Lyapunov exponent for the three sets of data.

5.3 The Attractor Projection Analysis of the Plant Data

This section presents the projections of the reconstructed attractor using the plant data and the methods developed in Section 4.6. Figure 5.3 shows the projection of the attractor obtained by plotting the OTSGA steam pressure, P_{sa}, in the abscissa (xaxs) against the loop A turbine header steam pressure, P_{sha}, in the ordinate (yaxs). The selection of the variables to obtain the projection was made by requiring that the pair of variables belongs to the same secondary loop, that they present a good data spread around its mean value, and that the characteristic broadband spectrum is present in their respective PSD's.

Table 5.1: Comparison of the Lyapunov exponents calculated with the ORNL's and Wolf's programs for the plant data.

	τ_p *(s)*	τ_{evol} *(s)*	τ_d *(s)*	*ORNL's program*	*Wolf's program*
P_{sa}	33.	10.	3.	0.082	0.10
P_{sb}	33.	10.	3.	0.112	0.09
P_{sha}	33.	10.	3.	0.084	0.09

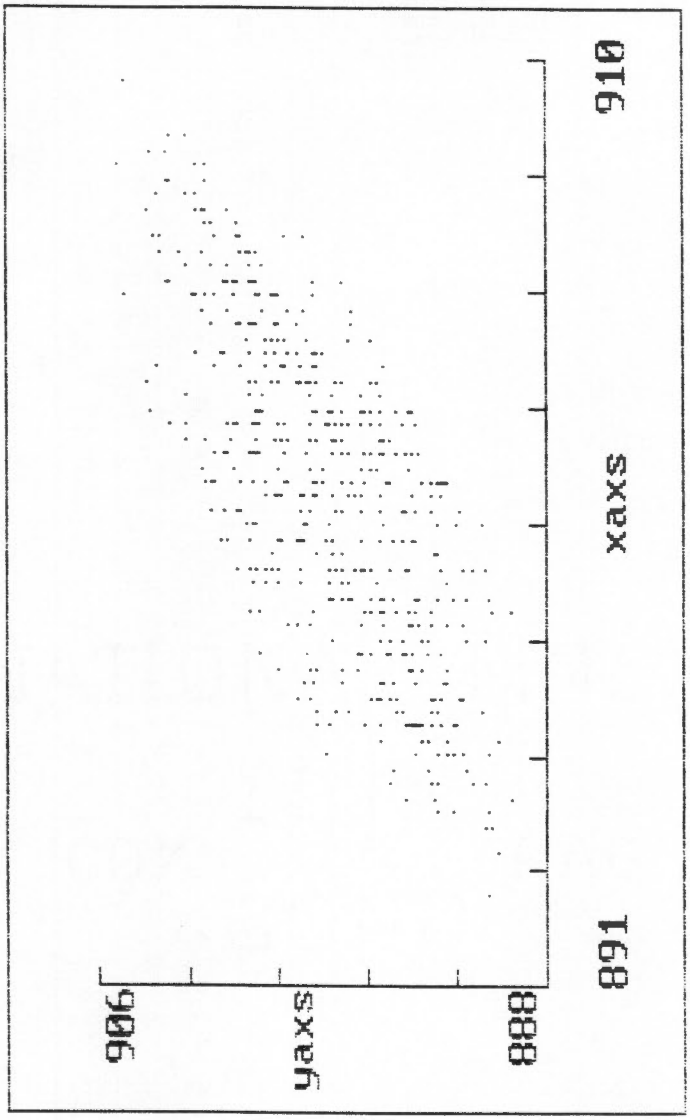

Figure 5.3: Attractor projection obtained by plotting the loop A turbine header steam pressure signal (P_{sha}) versus the OTSGA steam pressure signal (P_{sa}).

Figure 5.4 shows the attractor projection obtained by using the pseudo-phase space approach (Section 4.6). In this figure the OTSGA steam pressure, P_{sa}, is plotted against itself delayed by three samples, the label in the ordinate "x(1)" means the time series delayed and the label in the abscissa "x(0)" means the original time series.

In both instances the reconstructed attractor projections define a region in phase space of elliptical shape, with fuzzy limits due to undersampling effects discussed in Section 4.7. The experimental attractors exhibit a structure similar to the one of the Rossler modulated limit cycle, Figure 4.16, except for the filling of the interior region which is an artifice of the poor quality of the data (undersampling and resolution effects). Similar pseudo-projections are obtained for the OTSGB steam pressure, P_{sb}, and the loop A turbine header steam pressure, P_{sha}.

5.4 Introduction of Chaotic Signatures by Parametric Modulation

In this section, the metal-to-boiling secondary fluid heat transfer coefficient of the OTSG model was modulated by the x-Rossler signal. This test is based on the assumption that a chaotic signature may be induced by the two-phase turbulent flow motion of the steam/water mixture in the boiling region of the OTSG. The steam pressure time series generated by the model were treated to match the sampling rate and record length of the experimental data (one sample per second and 600 seconds for the duration of the signal).

Figure 5.5 presents the Poincare map of the model steam pressure which displays a structure very similar to the one exhibited by the Poincare map derived from the plant steam pressure Figure 5.1.

The PSD of the modulated steam pressure is shown in Figure 5.6.

Since the Rossler resonance (0.16 Hz) is so close to the limit cycle oscillation frequency (0.19 Hz) the characteristic broadband region appears to the right of the limit cycle resonance rather than on its left as is the case for the plant data. Nevertheless, this test together with the corresponding Poincare map (Figure 5.5) lends support to the conclusion that the broadband spectrum in the experimental

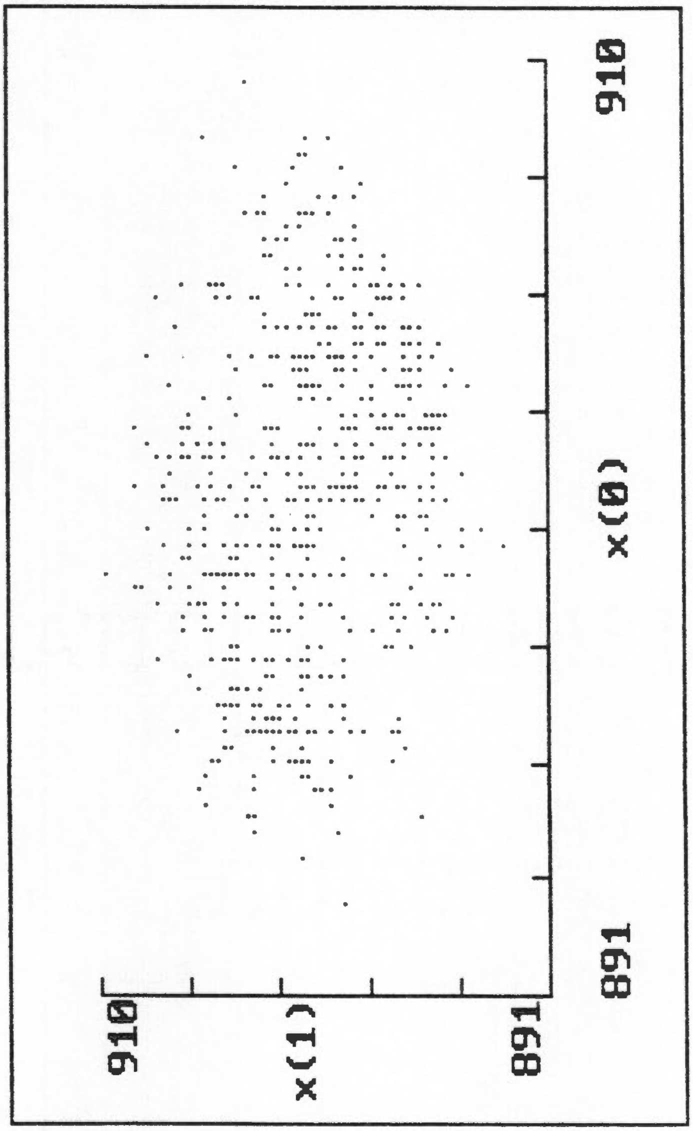

Figure 5.4: Attractor projection obtained from the OTSGA steam pressure (P_{sa}).

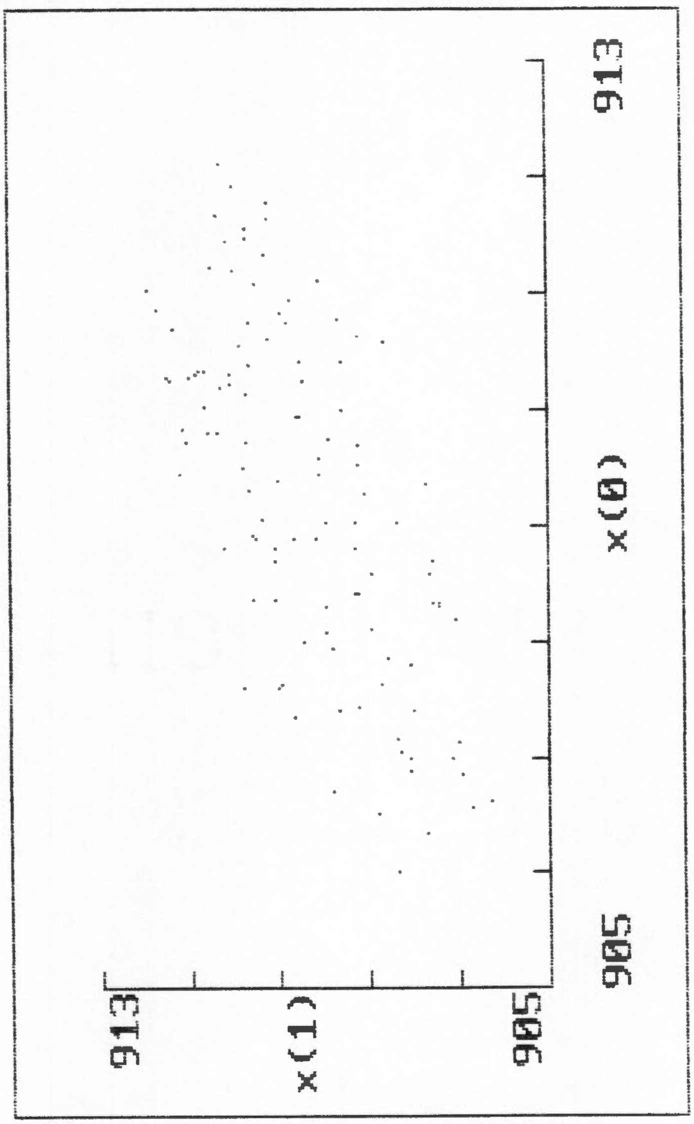

Figure 5.5: Poincare map of the model steam pressure (P_s) obtained by the modulation of the boiling region heat transfer coefficient with the x-Rossler signal

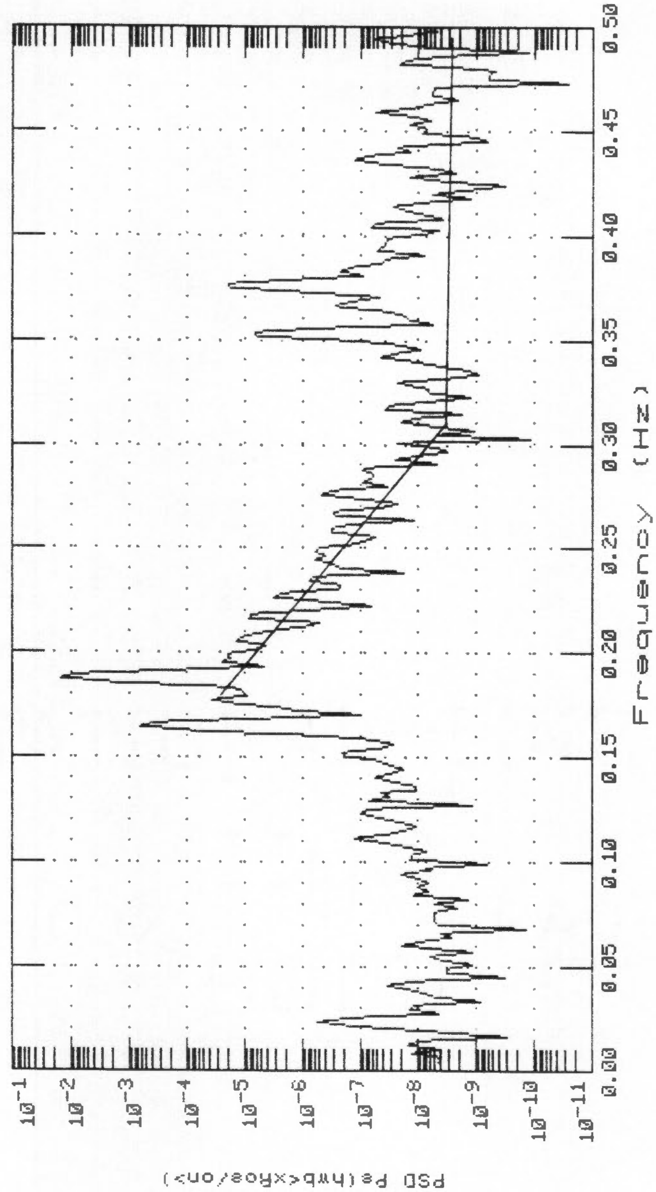

Figure 5.6: PSD of the model steam pressure (P_s) obtained by the modulation of the boiling region heat transfer coefficient with the x-Rossler signal

PSD could in fact arise from chaotic signatures introduced by chaotic components in the boiling heat transfer coefficient, having resonances at frequencies much lower than the Rossler resonance.

5.5 The OTSG Model Route to Chaos

This section addresses the question of whether or not the analytical structure of the model of the OTSG system may lead to a route to chaos via a cascade of pitchfork bifurcations, arising from successive instabilities of the limit cycle. To investigate this question the amplitude of the pressure oscillation was calculated as a function of the value of the friction corrector factor (f_{crd}), which controls the appearance of the limit cycle oscillation. The bifurcation diagram in Figure 5.7 shows the onset of the limit cycle at the value of 30 for the friction corrector factor, indicating the first bifurcation from the equilibrium to the oscillatory behavior. For a value of 31.2 the amplitude of the pressure oscillation is 7.8 psi (15.6 psi peak-to-peak) which is the value observed experimentally. For values of the friction corrector factor larger than 31.2, the amplitude of the limit cycle grows monotonically up to a value at which the amplitude of the moving boundary oscillation reaches the size of the upper most node length and touches the upper boundary of the preceding node leading to the failure of the analytical model. Notice that this failure occurs for unrealistically high values of the friction corrector factor.

From the above study of the bifurcation diagram,it can be concluded that the model does not predict a route to chaos via parametric bifurcations within the physical range of values of the friction correction factor.

5.6 Conclusion

The study of the plant data (Poincare maps, Lyapunov exponents, attractor projection reconstructions and PSD's) provides substantial evidence for the presence of a chaotic signature in the experimental data. Within the model limitations this signature arises from chaotic driving sources, or parametric modulations, or their combination thereof.

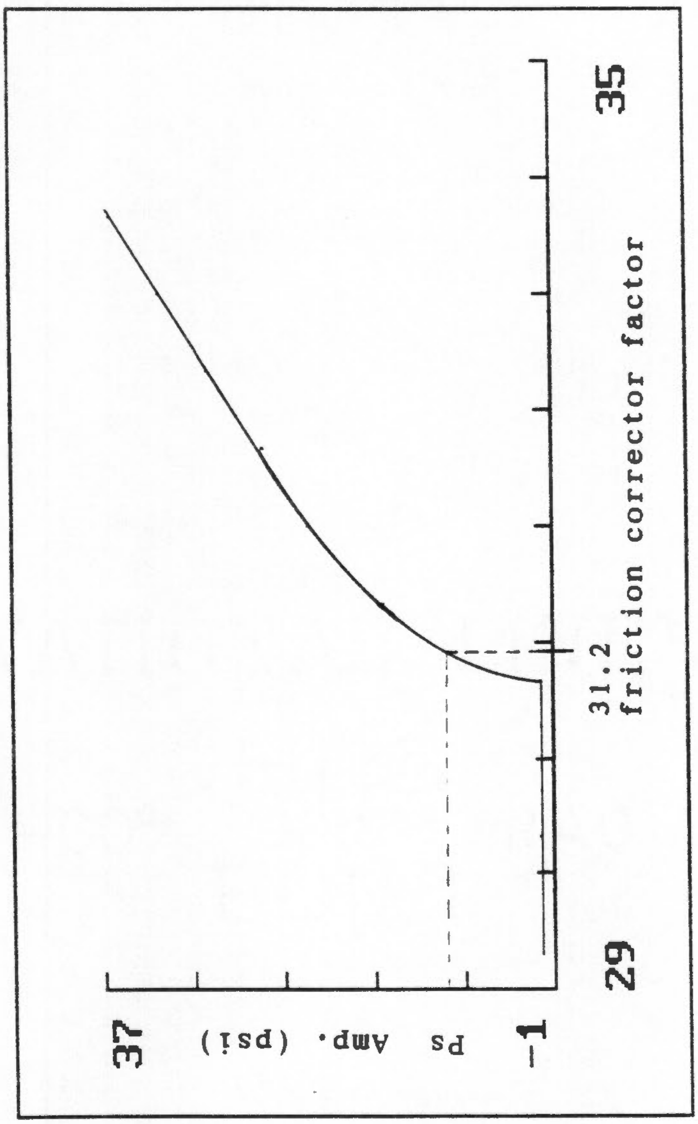

Figure 5.7: Growth of the amplitude of the steam pressure oscillation as the value of the friction multiplier is increased.

Chapter 6

Conclusions, Originality, and Recommendations For Future Work

An analytical model for an Once-Through Steam Generator (OTSG) system has been developed. This model has extended previous work in this area [5] by the use of dynamic rather than static momentum balances and by the implementation of a detailed multinodal description of the boiling region. Up to 24 nodes have been implemented; however stabilized results have been obtained with only 16 nodes which was the number of nodes used throughout this study. The multinodal approach is crucial for the description of the density waves which appear in the boiling region and which dominate the dynamic behavior of the entire system. The causative mechanism of the pressure oscillations has been identified as arising from the increase in pressure drop along the boiling channel which is due to the reduction in flow area introduced by the metal tube holders. Since this effect is measured by the friction corrector factor, f_{crd}, this parameter ultimately controls the onset and evolution of the limit cycle oscillation. Two options have been identified to eliminate the oscillatory behavior. One option is to retrofit the metal tube holders to decrease the pressure drop in the boiling region. Alternatively, the pressure drop in the downcomer region can be increased, by reducing the size of the orifice at the bottom of the downcomer, and consequently decreasing the pressure drop along the boiling region. This latter option is precisely the technical fix adopted by the plant operators.

The analysis of the linearized version of the present model showed the existence of a pair of complex conjugate eigenvalues, responsible for the appearance of the limit cycle. Since their real parts are negative, the OTSG oscillation is stable for small perturbations around the steady state values. The question of global stability has been investigated by the construction of a bifurcation diagram, where the amplitude of the limit cycle is plotted against the friction corrector factor, f_{crd}. It has been shown that the limit cycle is stable (does not experience further bifurcations) within the range of physical values of the friction corrector factor.

The power spectral density (PSD) of the plant data have two marked features: a resonance at the frequency of oscillation of the limit cycle and a broadband region preceding the location of the resonance peak. The model developed in this dissertation does not reproduce the broadband region. Concerning this problem, a detailed simulation study has been performed whereby the amplitude of a limit cycle was modulated by band limited white noise and chaotic sources. The simulation results have shown that both sources generated broadband regions which can be identified by the behavior of their amplitudes as a function of frequency: the BLN generated broadband exhibits a power-law dependence on the frequency, whereas the amplitude of the chaotic broadband decreases exponentially with the frequency. A detailed comparison between the Poincare maps, Lyapunov exponents, attractor reconstruction projections, and power spectral densities of the simulation with the corresponding tests performed on the plant data has led to the conclusion that the Once-Through Steam Generator can be described by a limit cycle oscillation modulated by a chaotic component. In reaching this conclusion the most relevant test has been the exponential shape of the broadband region found in the power spectral density of the plant data.

The search for chaotic signatures in experimental time series is seriously hindered by undersampling effects. Specifically affected by signal degradation are the Poincare maps and the attractor projections. The values obtained for the Lyapunov exponents should be taken with some reservations, although the signal undersampling effects do not change their signs. Hence finding a positive value for the exponent is still a credible test for the chaoticity of the analyzed signal. Fortunately, the power spectral density although somewhat compromised by undersampling effects, still exhibits a clear image of the broadband structure. This study has shown that the best criterion for chaoticity is by far the shape of the frequency dependence of the broadband structure in the signal PSD.

6.1 Originality

The original work in this dissertation can be classified into two categories: model development and implementation of a battery of tests for chaotic signature identification in experimental time series. The first category includes the development of a nodal method with a time-varying node limit which has led to the identification of the causative mechanism for the observed limit cycle oscillations. None of the previous models for the Once-Through Steam Generator could account for the oscillatory behavior of the plant. In the second category the novel use must be stressed, of otherwise well established tests, in simulation studies of degraded signals to implement an algorithm for the identification of chaotic signals.

6.2 Recommendations for Future Work

The model developed in this work should be extended to allow the motion of all the nodal boundaries rather than just the uppermost nodal limits. This modification would be of theoretical interest as it would allow the exploration of a larger region of the bifurcation diagram.

The study of the interaction between the two steam generators in the plant is strongly recommended. It is also recommended that an analytical study of the eigenvalue dependency with power be performed. Future work should stress the availability of good quality signals.

BIBLIOGRAPHY

Bibliography

[1] J. H. Kim and J. Stringer, *Proceedings of the Workshop on Applications of Chaos.* San Francisco, California: Electric Power Research Institute - EPRI Office of Exploratory Research, 1990.

[2] J. Dorning and J. Kim, "Some past and possible future applications of nonlinear dynamics and chaos to practical engineering systems," *EPRI Workshop on Applications of Chaos*, vol. 1, 1990.

[3] Rizwan-uddin and J. J. Dorning, "A Chaotic Attractor in a Periodically Forced Two-Phase flow System," *Nuclear Science and Engineering*, vol. 100, pp. 393–404, December 1988.

[4] Rizwan-uddin and J. J. Dorning, "Chaotic Dynamics of a Triply-Forced Two-Phase Flow System," *Nuclear Science and Engineering*, vol. 105, pp. 123–135, June 1990.

[5] A. T. Chen, *A Digital Simulation for Nuclear Once-Through Steam Generators, Ph.D Dissertation.* The University of Tennessee Department of Nuclear Engineering, Pasqua Engineering Bldg., Knoxville, TN 37996-2300: The University of Tennessee, Knoxville, 1976.

[6] T. Babcock and W. Co., *Modular Modeling System (MMS): A Code for the Dynamic Simulation of Fossil and Nuclear Power Plants.* Lynchburg Research Center, Lynchburg, Virginia, 24505: The Babcock and Wilcox Co., 1983.

[7] F. C. Moon, *Chaotic Vibrations: an Introduction for Applied Scientists and Engineers.* New York, NY, USA: John Wiley and Sons, 1987.

[8] L. Glass *et al.*, "Bifurcation and Chaos in a Periodically Stimulated Cardiac Oscillator," *Physica D*, vol. 7, pp. 89–101, 1983.

[9] A. A. Chernikov *et al.*, "Chaos: How Regular Can It Be?," *Physics Today*, vol. 41, pp. 27–35, November 1988.

[10] S. A. Stafford, *Investigation of the Nonlinear Behavior of a Weakly Ionized Plasma, M.S. Thesis.* The University of Tennessee Electrical and Computer Engineering Department, Knoxville, TN 37996-2100: The University of Tennessee, Knoxville, 1989.

[11] P. Martien *et al.*, "The Chaotic Behavior of the Leaky Faucet," *Physics Letters*, vol. 110A, No. 7,8, pp. 399–404, August 1985.

[12] E. N. Lorenz, "Deterministic Nonperiodic Flow," *J. Atmosp. Sci.*, vol. 20, pp. 130–141, 1963.

[13] O. E. Rossler, "An Equation For Continuous Chaos," *Physics Letters*, vol. 57A, pp. 397–398, July 1976.

[14] O. E. Rossler, "An Equation For Hyperchaos," *Physics Letters*, vol. 71A, pp. 155–157, April 1979.

[15] J. March-Leuba *et al.*, "Universality and Aperiodic Behavior of Nuclear Reactors," *Nuclear Science and Engineering*, vol. 86, pp. 401–404, 1984.

[16] J. March-Leuba, *Dynamic Behavior of Boiling Water Reactors, Ph.D Dissertation.* The University of Tennessee Department of Nuclear Engineering, Pasqua Engineering Bldg., Knoxville, TN 37996-2300: The University of Tennessee, Knoxville, 1984.

[17] M. J. Feigenbaum, "The Transition to Aperiodic Behavior in Turbulent Systems," *Commun. Math. Phys.*, vol. 77, pp. 65–86, 1980.

[18] V. Franceschini, "Bifurcations of Tori and Phase Locking in a Dissipative System of Differential Equations," *Physica D*, vol. 6, pp. 285–304, 1983.

[19] G. Bertolotti *et al.*, "Once-Through Steam Generator OCONEE-1 Operation," *Energia Nucleare*, vol. 21, pp. 484–494, September 1974.

[20] T. Wilson and N. E. Clapp, "Personal communication: Memos from B&W," April 1991.

[21] N. E. Clapp, "Personal communication: letter from Arkansa Power and Light Co.," February 1990.

[22] Mitchell and Gauthier, *ACSL Reference Manual.* Concord, Mass. 01742: Mitchell and Gauthier Associates, 1987.

[23] W. J. Garland, *Water and Steam Properties Programs.* 82 Rayne Ave., Oakville, Ontario, L6H 1C2, Canada: EACS - Engineering and Computing Services, 1991.

[24] P. J. Otaduy-Bengoa, *Modeling of the Dynamic Behavior of Large Boiling Water Reactor Cores, Ph.D Dissertation.* The University of Florida, Department of Nuclear Engineering: The University of Florida, 1979.

[25] J. March-Leuba, "Personal communication: Software for Power Spectrum Density Calculation and routine for band limited white noise generation.," November 1990.

[26] Y. Hsu and R. W. Graham, *Transport Processes in Boiling and Two-Phase Systems.* La Grange Park, Illinois, USA: American Nuclear Society, 1986.

[27] J. Thompson and H. Stewart, *Nonlinear Dynamics and Chaos.* New York, NY: John Wiley and Sons, 1989.

[28] A. Wolf *et al.*, "Determining Lyapunov Exponents from a Time Series," *Physica D*, vol. 16, pp. 285–317, 1985.

[29] B. B. Mandelbrot, "On the Quadratic Mapping," *Physica D*, vol. 7, pp. 224–239, 1983.

[30] H. O. Peitgen *et al.*, *The Science of Fractal Images.* 175 Fifth Avenue, New York, NY 10010, USA: Springer-Verlag, 1988.

[31] H. Lorenz, *Lecture Notes in Economics and Mathematical Systems.* Berlin, RDF: Spring-Verlag, 1989.

[32] D. S. Broomhead and G. P. King, "Extracting Qualitative Dynamics from Experimental Data," *Physica D*, vol. , pp. 217–236, 1986.

[33] T. S. Parker and L. O. Chua, "Chaos: A Tutorial for Engineers," *Proceedings of the IEEE*, vol. 75, No. 8, pp. 982–1008, August 1987.

[34] C. S. Daw *et al.*, "Chaotic Characteristics of a Complex Gas-Solids Flow," *Physical Review A*, vol. 41, No. 2, pp. 1179–1181, January 1990.

[35] R. Lafore, *Microsoft C Programming for the PC.* 4300 West 62nd Street, Indianapolis, Indiana 46268: Howard W. Sams and co., 1989.

[36] E. Ott, "Strange Attractors and Chaotic Motions of Dynamical Systems," *Reviews of Modern Physics*, vol. 53 , No. 4, Part 1, pp. 655–671, October 1981.

[37] M. Gorman and K. Robbins, "The implications of chaotic dynamics for applications in physical sciences and engineering," *Proceedings of the Workshop on Applications of Chaos*, vol. 1, pp. 2.1–2.10, 1990.

[38] D. Sigeti and W. Horsthemke, "High-frequency power spectra for systems subject to noise," *Physical Review A*, vol. 35, pp. 2276–2282, 1987.

[39] J. R. Roth, *Notes for the Plasma Diagnostic course - EE561-562.* Electrical Engineering Department: University of Tennessee, 1988-1989.

[40] N. E. Clapp, "Personal communication: Program for Lyapunov Exponent Calculation," February 1990.

[41] J. C. Roux *et al.*, "Representation of a Strange Attractor an Experimental Study of Chemical Turbulence," *Physics Letters*, vol. 77A, No. 6, pp. 391–393, June 1980.

APPENDIXES

APPENDIX A

Below are the copies of the two OTSG models developed. These programs can be ran in any mainframe, workstation or personal computer that has the ACSL software available. The water properties routines must be provided by the user. The use of the MACRO that allows the nodalization of the boiling region is given in its general form in order to save space. The necessary MACROS to run both programs are displayed only in the first program.

```
dissert165e        Wed Apr 15 13:28:48 1992        1

Program for simulation of otsg
' written by Lamartine Guimaraes '
' all rights reserved '
' 2/17/91 - version 3.0 '
' British units '
' last change 04/15/92'

****************************************************************
                                                               *
" THIS PROGRAM CONTAINS THE ONCE-THROUGH STEAM GENERATOR MODEL  *
                                                               *
  WITH THE DOWNCOMER DESCRIBED CONSIDERING THE SEPARATION       *
                                                               *
  OF PHASES (STEAM/WATER).  "                                  *
                                                               *
****************************************************************

" ============================================================ "
" ********************** BLGWN  **************************** "
" ============================================================ "

" This macro generates a band limited gausian white noise. "
" The filtering is accomplished by a simple 10 point addition. "
" By giving different IDs several white noise sequences can "
" be used concurrently "

" INTERCONNECTIONS : "
"       ID      : a 3 character ID for this particular noise " .

" REQUIRED INPUT : "
"       T&ID    : Current time "
"       DT&ID   : Desired sampling time (break freq. set @ 0.8/(2*DT&ID))"
"       AV&ID   : Desired average of generated noise "
"       SD&ID   : Desired standard deviation of generated noise "

" OUTPUT : "
"       N&ID    : Filtered noise @ time T&ID "

MACRO BLGWN(ID)
MACRO RELABEL L1, L2, L3, L4, L5, L6, L7, F1, F2, G1, G2 ,G3
        INTEGER I&ID, J&ID
        DIMENSION ZN&ID(22)                S" ZN&ID(11) = NOISE @ ZT0&ID "
        DIMENSION ZNW&ID(20)
        CONSTANT ZN&ID  = 22*0.
        CONSTANT ZNW&ID = 20*0.
        CONSTANT ZT0&ID = 0.

        PROCEDURAL (N&ID = T&ID, DT&ID)
          IF(T&ID .EQ. 0.) ZT0&ID = 0.  S" Reset for multiple runs "
"---------------------------------------------------"
"   Reset all the variables  "
          IF(T&ID .GT. 0.) GOTO G3
              DO G1 I&ID=1, 22
               ZN&ID(I&ID)=0.
G1..          CONTINUE
              DO G2 I&ID=1, 20
               ZNW&ID(I&ID)=0.
G2..          CONTINUE
G3..      CONTINUE
"---------------------------------------------------"
          IF(CINT .LT. DT&ID) GOTO L1
            WRITE(6,F1)
F1..        FORMAT(' <BLGWN>  ERROR.  CINT > DT&ID.  SET CINT SMALLER')
            TERMT(.TRUE.)
```

```
L1..      IF(T&ID .GT. ZT0&ID + DT&ID) GOTO L2
            I&ID = IFIX(10.*(T&ID - ZT0&ID)/DT&ID)
            X&ID = 10.*(T&ID - ZT0&ID)/DT&ID - FLOAT(I&ID)

            IF(I&ID .LE.10  .AND.  I&ID.GE.-10) GOTO L6
              WRITE(6,F2) T&ID, ZT0&ID, I&ID
F2..          FORMAT(' <BLGWN>  ERROR.  TIME OUT OF RANGE'/...
                     '            T&ID   = ', G15.5/...
                     '            ZT0&ID = ', G15.5/...
                     '            I&ID   = ', I10)
              TERMT(.TRUE.)
              GOTO L5

L6..        N&ID = ZN&ID(11 + I&ID)*(1.-X&ID)...
              + ZN&ID(11 + I&ID + 1.)*X&ID
            GOTO L5

L2..      DO L3 I&ID = 1, 11              $" Shift old filtered noise "
L3..        ZN&ID(I&ID) = ZN&ID(I&ID + 10)

          DO L4 I&ID = 12, 21             $" Generate new noise "
            ZN&ID(I&ID) = 0.
            DO L7 J&ID = 1, 19
              ZNW&ID(J&ID) = ZNW&ID(J&ID + 1)
L7..          ZN&ID(I&ID) = ZN&ID(I&ID) + ZNW&ID(J&ID)
              ZNW&ID(20) = GAUSS(AV&ID, 4.47*SD&ID)  $" 4.47 = SQRT(10)"
              ZN&ID(I&ID) = (ZN&ID(I&ID) + ZNW&ID(10)) / 20.
L4..      CONTINUE
          ZN&ID(22) = ZN&ID(21)
          ZT0&ID = ZT0&ID + DT&ID
          GOTO L1

L5..      CONTINUE
        END $" Procedural "
MACRO END $" BLGWN "

      macro pidaw(id)

      p&id = kc&id*(s&id-x&id)
      di&id = p&id/ti&id + (v&id-u&id)/tt&id
      i&id = intvc(di&id,io&id)
      xd&id = derivt(xo&id,x&id)
      dd&id = nd&id*(-kc&id*xd&id - d&id/td&id)
      d&id = intvc(dd&id,0.)
      u&id = p&id + i&id + d&id

      macro end  $ " end macro pidaw"

macro rosler(id)
'Rossler source '

dx&id = - (y&id + z&id)
dy&id = x&id + a&id * y&id
dz&id = b&id + z&id * (x&id - c&id)
x&id = intvc(dx&id,x&id&0)
y&id = intvc(dy&id,y&id&0)
z&id = intvc(dz&id,z&id&0)

macro end $ "end macro rosler"

macro lstndl(id,nd)
'computes last (clsest to the superheated region) node ...
 of boiling region'
```

```
G&id = G&nd - c6*(af&nd-1.)*drl&id/2.
Q&id = Qt
drl&id = (Q&id - c4*(1.-x&nd)*G&nd/del&id)*del&id*2./...
            (Rf*c4*(af&nd-1.))
dL&id = drl&id
L&id = intvc(dL&id,Lb0)
pac&id = (G&id*G&id/Rg - ((1.-x&nd)*(1.-x&nd)/((1.-af&nd)*Rf)+...
              x&nd*x&nd/(af&nd*Rg))*G&nd*G&nd)/(2.*gc*144.)
pgr&id = del&id*(Rf + c6*(1.+af&nd)/2.)/144.
pfr&id = fcrd*fb*rb&id*del&id*(G&id+G&nd)*(G&id+G&nd)/...
            (8.*Rf*Des*gc*144.)
pbr&id = (G&nd - G&id)*drl&id/(288.*gc) + ...
            del&id*auxdb/(144.*gc*Adc)
adp&id = pac&id + pgr&id + pfr&id + pbr&id
drp&id = adp&id - del&id*Adc*Pdb/(Adc*Lbp)
P&nd = Pss + adp&id - del&id*Adc*Pdb/(Adc*Lbp)

macro end $ "end macro lstndl"

macro genndl(id,nd,aft)
'computes general node of boiling, located between the first ...
  and the last node.'

G&id = G&nd - c6*del&id*reg&id
Q&id = Qt
reg&id = (Q&id - c4*(x&id - x&nd)*G&nd/del&id)/...
            (c4*(Rg-c6*x&id))
daf&id = reg&id
af&id = intvc(daf&id,af0&id)
pac&id = (((1.-x&id)*(1.-x&id)/((1.-af&id)*Rf) + ...
            x&id*x&id/(af&id*Rg))*G&id*G&id - ...
            ((1.-x&nd)*(1.-x&nd)/((1.-af&nd)*Rf) + ...
            x&nd*x&nd/(af&nd*Rg))*G&nd*G&nd)/(2.*gc*144.)
pgr&id = (Rf+c6*(af&id+af&nd)/2.)*del&id/144.
rb&id = 3.68965 + 1.87793*x&id + 249.617*x&id*x&id - ...
        736.569*x&id*x&id*x&id + 934.539*x&id*x&id*x&id*x&id - ...
        432.318*x&id*x&id*x&id*x&id*x&id
pfr&id = fcrd*fb*rb&id*del&id*(G&id+G&nd)*(G&id+G&nd)/...
            (8.*Rf*Des*gc*144.)
pbr&id = del&id*auxdb/(144.*gc*Adc)
adp&id = adp&aft + pac&id + pgr&id + pfr&id + pbr&id
drp&id = pac&id + pgr&id + pfr&id + pbr&id - del&id*Adc*Pdb/(Adc*Lbp)
P&nd = P&id + pac&id + pgr&id + pfr&id + pbr&id ...
            - del&id*Adc*Pdb/(Adc*Lbp)
x&id = slp&id*Rg*af&id/srb&id
srb&id = Rf + (slp&id*Rg-Rf)*af&id
slp&id = (1. - af&id)/den&id
den&id = (ks&id-af&id+(1.-ks&id)*(abs(af&id))**rr&id)
ks&id = 0.71 + 3.0639e-4*Psat
rr&id = 3.33 - 6.09742e-4*Psat + 5.27853e-6*Psat*Psat

macro end  $  "end macro genndl"


macro fstnl(id,db,aft)
'computes the first (closest to the downcomer) node ...
 of boiling region'

G&id = G&db - c6*del&id*reg&id
Q&id = Qt
reg&id = (Q&id - ((1.-x&id)*hff+x&id*hgg-hfdc)*G&db/del&id)/...
            (c4*(Rg-c6*x&id))
daf&id = reg&id
```

```
af&id = intvc(daf&id,af0&id)
pac&id = (((1.-x&id)*(1.-x&id)/((1.-af&id)*Rf) + ...
          x&id*x&id/(af&id*Rg))*G&id*G&id - ...
          G&db*G&db/Rfdc)/(2.*gc*144.)
pgr&id = (Rf+c6*af&id/2.)*del&id/144.
rb&id = 3.68965 + 1.87793*x&id + 249.617*x&id*x&id - ...
        736.569*x&id*x&id*x&id + 934.539*x&id*x&id*x&id*x&id - ...
        432.318*x&id*x&id*x&id*x&id*x&id
pfr&id = fcrd*fb*rb&id*del&id*(G&id+G&db)*(G&id+G&db)/...
         (8.*Rf*Des*gc*144.)
pbr&id = del&id*auxdb/(144.*gc*Adc)
adp&id = adp&aft + pac&id + pgr&id + pfr&id + pbr&id + ...
         kor*G&db*G&db/(2.*Rfdc)
aux1 = 1. + Adc*Lb/(Adc*Lbp)
drp&id = pac&id + pgr&id + pfr&id + pbr&id + ...
         kor*G&db*G&db/(2.*Rfdc) - del&id*Adc*Pdb/(Adc*Lbp)
P&db = (Pss + adp&id)/aux1
x&id = slp&id*Rg*af&id/srb&id
srb&id = Rf + (slp&id*Rg-Rf)*af&id
slp&id = (1. - af&id)/den&id
den&id = (ks&id-af&id+(1.-ks&id)*(abs(af&id))**rr&id)
ks&id = 0.71 + 3.0639e-4*Psat
rr&id = 3.33 - 6.09742e-4*Psat + 5.27853e-6*Psat*Psat

macro end $ "end macro fstnl"

       initial
       constant tmax=600.
       constant ROp=44.75,ROw=526.0,ROfw=51.71
       constant Cpp=1.3355,Cpw=0.109
       constant Ap=26.3,Aw=6.81,As=44.4,Adc=23.33
       constant Lt=52.11,Lbp=32.11
       constant Ri=0.0232,Ro=0.02605
       constant Wpin=18472.2,N=15531.,J=778.16
       constant PI = 3.1415927,gc=32.17,g=32.17
       constant hpw=1.53
       constant Rm=1.,fb=0.017,fs=0.013,fl=0.011
       constant Des=0.06902,Dedc=1.374
       constant b5=2.5e-4,b6=0.589,b7=1.,tin=100.,ten=500.
       constant ampp = 0., fexp = 0.212

       table tp0tab,1,3 /0.4,0.75,0.95,...
                        588.8,594.9,598.9/
       table hfwtab,1,3 /0.4,0.75,0.95,...
                        327.,394.5,421.3/
       table wfw0tb,1,4 /0.4,0.614,0.75,0.95,...
                        518.538,830.962,1010.38,1348.43/
       table hwstb,1,3 /0.4,0.75,0.95,...
                       0.032778,0.058056,0.075556/

    ' constants to be ajusted '
        constant pow = 0.614
        constant hwb0 = 0.69
        constant kor = 0.03, rs=2., fcrd=31.2, rbb = 21.
        constant dpext0 = 1.
        constant wfw0 = 830.962
        constant cbp = 190.
        constant f1=0.,f2=0.,f3=0.,f4=0.,f6=0,f7=0.,f8=0.,frq=1.33832
        constant f10=0.,f14=0.,f15=1.,f51=0.,f52=0.
        constant avsc2=0., sdsc2=0.1, dtsc2=3.
        constant aros=0.15,bros=0.2,cros=10.
        constant xros0=5.,yros0=0.,zros0=0.
        constant taus=0.1,ktb=8.00953e-5,pset=885.
        constant deltaz = 0.92
```

```
' initial values for integration '
   constant ...
       AFON10 = 0.955058 ,AFON11 = 0.962801 ,AFON12 = 0.969374 ,...
       AFON13 = 0.975025 ,AFON14 = 0.979935 ,AFON15 = 0.984242 ,...
        AFON1 = 0.543038 ,AFON2 = 0.712425  ,AFON3 = 0.795617 ,...
        AFON4 = 0.845398 ,AFON5 = 0.878662  ,AFON6 = 0.902516 ,...
        AFON7 = 0.920485 ,AFON8 = 0.934522  ,AFON9 = 0.945797 ,...
          LB0 = 16.09890 ,LDC0 = 12.22560   ,PDC0 = 900.9140 ,...
          PS0 = 901.0000 ,TP10 = 592.5300   ,TP20 = 590.1450 ,...
         TP30 = 574.2260 ,TP40 = 562.6900   ,TS10 = 586.7370 ,...
         TS20 = 571.6840 ,TW10 = 591.8860   ,TW20 = 589.2010 ,...
         TW30 = 560.1410 ,TW40 = 552.4830   ,WDB0 = 1011.930 ,...
          WS0 = 830.9660

     constant kcpre = 1., tipre = 10., ttpre = 100., tdpre = 100.,...
              ndpre = 0., xopre = 1. , iopre = 0.  , cfwpre = 0.01, ...
              cstpre = 10.

     cinterval cint = 0.4
     algorithm ialg = 2
     nsteps nstep = 1000
     maxterval maxt=1.

     a1 = ROp * Ap * Cpp/2.
     a2 = ROw * Aw * Cpw/2.
     a4 =  hpw * Ri * PI * N/a1
     a5 = Wpin * Cpp/a1
     a6 = hpw * Ri * PI * N/a2
     a18 = Rm * f1/(2. * Dedc * gc * Adc)
     Vdc = Adc * Lbp
     wfwts=2.99146
     xrosun=xros0
     xros=xros0
     nsc2un=0.
     sinus =1.
     integer nao
     constant nao=1

     end

     dynamic

     discrete
 ' this section allows the power plant data for the feedwater flow ...
  be used as input to the model '
      interval dtsamp=1.
      nsc2un = nsc2
      sinus = sin(frq*t)
      xrosun = xros/10.
      procedural(wfwts)
      if(nao.eq.1)goto 111
      read(11,*)wfwts
      111..continue
      end
      end

      derivative otsg
      procedural(powv=pow,t,b5,b6,b7,PI,fexp,ampp)
      if(b7.GT.0.)goto 11
      if(t.lt.tin)powa=pow
      if(t.ge.tin.and.t.le.ten)powa=b5*t + b6
      powv=powa * (1. + ampp * sin(2. * PI * fexp * t))
      goto 12
```

```
      11..continue
      powv=pow * (1. + ampp * sin(2. * PI * fexp * t))
      12..continue
      end

'band limited noise call'
      blgwn("sc2")
      tsc2=t

'rossler chaotic source call'
"     rosler(ros)"

' pressure controller '
      pidaw("pre")
      xpre = ptb/925.
      vpre = upre
      spre = pset/925.
      ptb = ps - ktb*Ws*Ws/(2.*ROs1)

"includes band limited noise,...
 noise on the heat transfer, sinusoidal on the inputs, ...
 sinusoidal forcing function on the momentum "

      Tp0 = tp0tab(powv)*(1. + f8*sin(frq*t) + f10*nsc2)
      power = powv * 2568.
      Wds  = wfw0*(1. - cstpre*upre)
      dWs = (Wds - Ws)/taus
      hws = hwstb(powv)
      dpext = f7*sin(frq*t)
      Wfw = wfw0tb(powv)*(1. + f2*sin(frq*t) + f4*nsc2un ...
          + f6*xrosun)*f15 + f14*wfwts*277.778
      hfw = hfwtab(powv)
      hwb = hwb0*(1. + f51*nsc2 + f52*xros)

' water properties for the superheated steam upper node'
      pssi1 = 6.894757e-3*ps
      tssi1 = (ts1 - 32.)/1.8
      ROs1 = 6.242796e-2*dgsup(pssi1,tssi1)
      hs1 = 4.299209e-1*hgsup(pssi1,tssi1)
      drs1dt = 1.1237033e-1*drgdtp(pssi1,tssi1)
      drs1dp = 4.304256e-4*drgdpt(pssi1,tssi1)
      Cps1 = 7.7385762e-1*cpgsup(pssi1,tssi1)
      dhs1dp = 2.9642e-3*dhgdpt(pssi1,tssi1)
      dhs1dt = 7.7385762e-1*dhgdtp(pssi1,tssi1)

' water properties for the superheated steam lower node'
      pssi2 = 6.894757e-3*ps2
      tssi2 = (ts2 - 32.)/1.8
      ROs2 = 6.242796e-2*dgsup(pssi2,tssi2)
      hs2 = 4.299209e-1*hgsup(pssi1,tssi1)
      drs2dt = 1.1237033e-1*drgdtp(pssi2,tssi2)
      drs2dp = 4.304256e-4*drgdpt(pssi2,tssi2)
      Cps2 = 7.7385762e-1*cpgsup(pssi2,tssi2)
      dhs2dp = 2.9642e-3*dhgdpt(pssi2,tssi2)
      dhs2dt = 7.7385762e-1*dhgdtp(pssi2,tssi2)

' water properties for the boiling region'
      psatsi = 6.894757e-3*psat
      Tsatt = 32. + 1.8*tsat(Psatsi)
      Rg = 6.242796e-2*dg(psatsi)
      Rf = 6.242796e-2*df(psatsi)
      hgg = 4.299209e-1*hg(psatsi)
      hff = 4.299209e-1*hf(psatsi)
      c4 = hgg - hff
```

```
      c5 = Rg * hgg - Rf * hff
      c6 = Rg - Rf
      a7 = hws * Ro * PI * N/a2
      a8 = hwb * Ro * PI * N/a2

' water properties for the downcomer region'
      pdcsi = 6.894757e-3*pdc
      Tdc = 32. + 1.8*tsat(Pdcsi)
      Rgdc = 6.242796e-2*dg(pdcsi)
      Rfdc = 6.242796e-2*df(pdcsi)
      hgdc = 4.299209e-1*hg(pdcsi)
      hfdc = 4.299209e-1*hf(pdcsi)
      dvfcdp = 1.1044301e-1*dvfdp(pdcsi)
      dvgcdp = 1.1044301e-1*dvgdp(pdcsi)
      drgcdp = - Rgdc*Rgdc*dvgcdp
      drfcdp = - Rfdc*Rfdc*dvfcdp
      dhgcdp = 2.9642e-3*dhgdp(pdcsi)
      dhfcdp = 2.9642e-3*dhfdp(pdcsi)

' equations for the primary side '
      dtp1 = a5 * (tp0 - tp1)/(Lt - Lb) - a4 * (tp1 - tw1)
      dtp2 = a5 * (tp1 - tp2)/(Lt - Lb) - a4 * (tp2 - tw2)
      dtp3 = a5 * (tp2 - tp3)/Lb - a4 * (tp3 - tw3)
      dtp4 = a5 * (tp3 - tp4)/Lb - a4 * (tp4 - tw4)

' equations for the metal '
      dtw1 = - DRLB * (tw2 - tw1)/(2. * (Lt - Lb)) ...
             + a6 * (tp1 - tw1) - a7 * (tw1 - ts1)
      dtw2 = - DRLB * (2. * tw3 - tw2 - tw1)/(2. * (Lt - Lb)) ...
             + a6 * (tp2 - tw2) - a7 * (tw2 - ts2)
      dtw3 = - DRLB * (tw4 + tw3 - 2. * tw2)/(2. * Lb) ...
             + a6 * (tp3 - tw3) - a8 * (tw3 - tsatt)
      dtw4 = - DRLB * (tw4 - tw3)/(2. * Lb) ...
             + a6 * (tp4 - tw4) - a8 * (tw4 - tsatt)

' equations for the secondary superheated steam side '
      vss = (Lt - Lb)*As/2.
      cfss1 = vss*ROs2*dhs2dt
      cfss2 = vss*(144./J - ROs2*dhs2dp)
      cfss3 = 1. - vss*drs2dt*(hgg - hs2)/cfss1
      cfss4 = vss*(drs2dp + drs2dt*cfss2/cfss1)
      cfss5 = vss*ROs1*dhs1dt
      cfss6 = vss*(144./J - ROs1*dhs1dp)
      cfss7 = vss*(drs1dp + drs1dt*cfss6/cfss5)
      cfss8 = 1. - vss*drs1dt*(hs2 - hs1)/cfss5
      cfss9 = cfss7 + cfss4*cfss8
      cfss10 = vss*(cfss8*drs2dt*Qs2/cfss1 + drs1dt*Qs1/cfss5)
      cfss11 = As*(ROs1 + cfss8*ROs2)/2.
      Qs1 = PI*Ro*N*hws*(Lt - Lb)*(Tw1 - Ts1)
      Qs2 = PI*Ro*N*hws*(Lt - Lb)*(Tw2 - Ts2)
      w2 = Wb - Wbp - vss*(drs2dp*drps + drs2dt*drts2) + ...
           As*ROs2*drlb/2.
      drps = (cfss3*cfss8*Wb - cfss8*Wbp - Ws - cfss10 + ...
             cfss11*drlb)/cfss9
      drts1 = w2*(hs2 - hs1)/cfss5 + cfss6*drps/cfss5 + Qs1/cfss5
      drts2 = wb*(hgg - hs2)/cfss1 + cfss2*drps/cfss1 + Qs2/cfss1
      delPs1 = ROs1*(Lt - Lb)/(2.*144.) + rs*fs*Ws*Ws*(Lt - Lb)/ ...
             (4.*Des*gc*ROs1*As*As*144.)
      Ps2 = Ps + delps1
      delPss = ROs2*(Lt - Lb)/(2.*144.) + rs*fs*Ws*Ws*(Lt - Lb)/ ...
             (4.*Des*gc*ROs2*As*As*144.)
      Pss = Ps2 + delPss
      dPs = drps
      dTs1 = drts1
```

```
      dTs2 = drts2
      Psat = Pss

' equations for the downcomer using separation of phases '
      hbp = hs2
      vsdc = Adc*(Lbp - Ldc)
      vldc = Adc*Ldc
      cfdc1 = 1. - Rgdc/Rfdc
      cfdc2 = vsdc*drgcdp + vldc*Rgdc*drfcdp/Rfdc
      cfdc3 = vsdc*(144./J - Rgdc*dhgcdp) + (hfdc - hgdc)*cfdc2/cfdc1
      cfdc4 = hgdc - hbp + (hfdc - hgdc)/cfdc1
      cfdc6 = (hfdc - hgdc)*Rgdc/(cfdc1*Rfdc)
      cfdc5 = hfdc - hfw + cfdc6
      delPbp = ROs1*(Lt - Lbp)/144. + rs*fs*Ws*Ws*(Lt - Lbp)/ ...
              (2.*Des*gc*ROs1*As*As*144.)
      Pbp = Ps + delpbp
      Wbp = cbp*sqrt(abs((Pbp - Pdc)*ROs2))
      drpdc = cfdc4*Wbp/cfdc3 + cfdc5*Wfw/cfdc3 - cfdc6*Wdb/cfdc3
      Wc = Wbp/cfdc1 - cfdc2*drpdc/cfdc1 + ...
           Rgdc*(Wfw - Wdb)/(Rfdc*cfdc1)
      hc = hfdc + (hfdc - hfw)*Wfw/Wc
      dLdc = (Wfw + Wc - Wdb)/(Adc*Rfdc) - Ldc*drfcdp*drpdc/Rfdc
      dPdc = drpdc
      ROdc = Rgdc*(Lbp - Ldc)/Lbp + Rfdc*Ldc/Lbp
      Fw = a18 * Lbp * Wdb * Wdb/ROdc
      dWdb = (((Wfw + Wbp) * (Wfw + Wbp) - Wdb * Wdb)/(Adc * ROdc) -...
              144. * gc * Adc * (Pdb - Pdc - dpext) - ...
              gc * Fw + Adc * g * Lbp * ROdc)/Lbp
      auxdb = (((Wfw + Wbp) * (Wfw + Wbp) - Wdb * Wdb)/(Adc * ROdc) +...
              144.*gc*Adc*(Pdc + dpext) - gc*Fw + Adc*g*Lbp*ROdc)/Lbp


' equation for the secondary boiling liquid side '
      twb = (tw3 + tw4)/2.
      Qt = 2.*PI*Ro*N*hwb*(Twb - tsatt)/As

'   last node  '
      delb = Lb - z15
      Wb = Gb*As
      lstndl("b","n15")

'   node 15'
      z15 = 15.*deltaz
      deln15 = deltaz
      genndl("n15","n14","b")

************************************************************
                                                          *
" FOR REASON OF SPACE THE FORMAT FOR NODES 2 THROUGH 14    *
                                                          *
  IS GIVEN IN A GENERAL FORM "                             *
                                                          *
'   node i'                                                *
      z_i = ( i )*deltaz                                   *
      deln_i = deltaz                                      *
      genndl("n_i","n_(i-1)","n_(i+1)")                    *
                                                          *
" FOR  2 =< i => 14 , E.G. i=13                            *
                                                          *
'   node 13'                                               *
      z13 = 13.*deltaz                                     *
      deln13 = deltaz                                      *
      genndl("n13","n12","n14")                            *
                                                          *
```

```
************************************************************

'   first node '
      z1 = deltaz
      deln1 = deltaz
      Gdb = Wdb/As
      fstn1("n1","db","n2")
      pbb = pdb - kor*Gdb*Gdb/(2.*Rfdc)

' integration of state variables '
      tp1 = intvc(dtp1,tp10)
      tp2 = intvc(dtp2,tp20)
      tp3 = intvc(dtp3,tp30)
      tp4 = intvc(dtp4,tp40)
      tw1 = intvc(dtw1,tw10)
      tw2 = intvc(dtw2,tw20)
      tw3 = intvc(dtw3,tw30)
      tw4 = intvc(dtw4,tw40)
      Ps = intvc(dPs,Ps0)
      Ts1 = intvc(dTs1,Ts10)
      Ts2 = intvc(dTs2,Ts20)
      Ldc = intvc(dLdc,Ldc0)
      Pdc = intvc(dPdc,Pdc0)
      Wdb = intvc(dWdb,Wdb0)
      Ws = intvc(dWs,Ws0)
      end
      termt(t.ge.tmax)
      end
end
```

```
Program for simulation of otsg
' written by Lamartine Guimaraes '
' all rights reserved '
' 2/17/91 - version 3.0 '
' British units '
' last change 04/15/92'

******************************************************************
                                                                 *
" THIS PROGRAM CONTAINS THE ONCE-THROUGH STEAM GENERATOR MODEL   *
                                                                 *
  WITH THE DOWNCOMER DESCRIBED AS AN ACCUMULATOR TANK.           *
                                                                 *
  FOR SPACE ECONOMY REASONS THE MACROS USED BY THIS PROGRAM      *
                                                                 *
  ARE PRINTED WITH THE FIRST PROGRAM. "                          *
                                                                 *
******************************************************************

      initial
      constant tmax=600.
      constant ROp=44.75,ROw=526.0,ROfw=51.71
      constant Cpp=1.3355,Cpw=0.109
      constant Ap=26.3,Aw=6.81,As=44.4,Adc=23.33
      constant Lt=52.11,Lbp=32.11
      constant Ri=0.0232,Ro=0.02605
      constant Wpin=18472.2
      constant N=15531.,J=778.16,PI = 3.1415927
      constant gc=32.17,g=32.17
      constant hpw=1.53
      constant fb=0.017,fs=0.013,fl=0.011
      constant Des=0.06902,Dedc=1.374
      constant b5=5.94444e-5,b6=3.70278e-1,b7=1.
      constant ampp = 0., fexp = 0.212

      table tp0tab,1,3 /0.4,0.75,0.95,...
                        588.8,594.9,598.9/
      table hfwtab,1,3 /0.4,0.75,0.95,...
                        327.,394.5,421.3/
      table wfw0tb,1,4 /0.4,0.614,0.75,0.95,...
                        518.538,830.962,1010.38,1348.43/
      table hwstb,1,3 /0.4,0.75,0.95,...
                        0.032778,0.058056,0.075556/

  ' constants to be ajusted '
      constant pow = 0.614
      constant hwb = 0.69
      constant kor = 0.03
      constant dpext0 = -1.4
      constant rs=2.
      constant fcrd=7.5
      constant fslp=3.5
      constant rbb = 21.
      constant nnodes = 16.
      constant wfw0 = 830.962
      constant cst = 0.922
      constant f1=0.,f2=0.,frq=0.05
      constant f3=0.,f4=0.
      constant avsc1=0.,avsc2=0.
      constant sdsc1=0.1,sdsc2=0.1
      constant dtsc1=3.,dtsc2=3.
      constant taus=0.05,ktb=8.00953e-5,pset=885.
      constant zb0 = 12.
      Ws0 = Wfw0
```

```
' initial values for integration '
    constant ...
       AFON10 = 0.900723 ,AFON11 = 0.918993 ,AFON12 = 0.935342 ,...
       AFON13 = 0.949904 ,AFON14 = 0.962820 ,AFON15 = 0.974231 ,...
        AFON1 = 0.639476 ,AFON2 = 0.676601  ,AFON3 = 0.712066 ,...
        AFON4 = 0.745614 ,AFON5 = 0.777063  ,AFON6 = 0.806295 ,...
        AFON7 = 0.833256 ,AFON8 = 0.857946  ,AFON9 = 0.880409 ,...
       ALFDC0 = 0.687874 ,LB0 = 16.08990    ,PS0 = 900.9970 ,...
         TP10 = 592.5300 ,TP20 = 590.1440   ,TP30 = 574.2270 ,...
         TP40 = 562.6900 ,TS10 = 586.7370   ,TS20 = 571.6840 ,...
         TW10 = 591.8040 ,TW20 = 589.2010   ,TW30 = 560.1350 ,...
         TW40 = 552.4770 ,WDB0 = 1012.090   ,WS0 = 830.9430

      constant kcpre = 1., tipre = 10., ttpre = 100., tdpre = 100., ...
               ndpre = 0., xopre = 1. , iopre = 0.  , cfwpre = 0.01, ...
               cstpre = 10.

      cinterval cint = 1.
      algorithm ialg = 2
      nsteps nstep = 1000
      maxterval maxt=1.

      a1 = ROp * Ap * Cpp/2.
      a2 = ROw * Aw * Cpw/2.
      a4 =  hpw * Ri * PI * N/a1
      a5 = Wpin * Cpp/a1
      a6 = hpw * Ri * PI * N/a2
      a18 = f1/(2. * Dedc * gc * Adc)
      Vdc = Adc * Lbp
      deltaz = zb0/nnodes

      end

      dynamic

      derivative otsg

      procedural(powv=pow,t,b5,b6,b7,PI,fexp,ampp)
      if(b7.GT.0.)goto 11
      if(t.lt.500.)powa=pow
      if(t.ge.500.and.t.le.4100.)powa=b5*t + b6
      powv=powa * (1. + ampp * sin(2. * PI * fexp * t))
      goto 12
      11..continue
      powv=pow * (1. + ampp * sin(2. * PI * fexp * t))
      12..continue
      end

      blgwn("sc1")
      blgwn("sc2")
      tsc1=t
      tsc2=t

 ' pressure controller '
      pidaw("pre")
      xpre = ptb/925.
      vpre = upre
      spre = pset/925.
      ptb = ps - ktb*Ws*Ws/(2.*ROs1)
      Tp0 = tp0tab(powv)
      power = powv * 2568.
      tws = (tw1 + tw2)/2.
      twb = (tw3 + tw4)/2.
```

```
      Wds  = wfw0*(1. - cstpre*upre)
      dWs = (Wds - Ws)/taus
      hws = hwstb(powv)
      Wfw = wfw0tb(powv)
      hfw = hfwtab(powv)

' Calculation of the superheated steam properties upper node'
      pssi1 = 6.894757e-3*ps
      tssi1 = (ts1 - 32.)/1.8
      ROs1 = 6.242796e-2*dgsup(pssi1,tssi1)
      hs1 = 4.299209e-1*hgsup(pssi1,tssi1)
      drs1dt = 1.1237033e-1*drgdtp(pssi1,tssi1)
      drs1dp = 4.304256e-4*drgdpt(pssi1,tssi1)
      Cps1 = 7.7385762e-1*cpgsup(pssi1,tssi1)
      dhs1dp = 2.9642e-3*dhgdpt(pssi1,tssi1)
      dhs1dt = 7.7385762e-1*dhgdtp(pssi1,tssi1)

' Calculation of the superheated steam properties lower node'
      pssi2 = 6.894757e-3*ps2
      tssi2 = (ts2 - 32.)/1.8
      ROs2 = 6.242796e-2*dgsup(pssi2,tssi2)
      hs2 = 4.299209e-1*hgsup(pssi2,tssi2)
      drs2dt = 1.1237033e-1*drgdtp(pssi2,tssi2)
      drs2dp = 4.304256e-4*drgdpt(pssi2,tssi2)
      Cps2 = 7.7385762e-1*cpgsup(pssi2,tssi2)
      dhs2dp = 2.9642e-3*dhgdpt(pssi2,tssi2)
      dhs2dt = 7.7385762e-1*dhgdtp(pssi2,tssi2)

' Calculation of the saturation properties of boiling region'
      psatsi = 6.894757e-3*psat
      Tsatt = 32. + 1.8*tsat(Psatsi)
      Rg = 6.242796e-2*dg(psatsi)
      Rf = 6.242796e-2*df(psatsi)
      hgg = 4.299209e-1*hg(psatsi)
      hff = 4.299209e-1*hf(psatsi)
      c4 = hgg - hff
      c5 = Rg * hgg - Rf * hff
      c6 = Rg - Rf
      a7 = hws * Ro * PI * N/a2
      a8 = hwb * Ro * PI * N/a2

' equations for the primary side '
      dtp1 = a5 * (tp0 - tp1)/(Lt - Lb) - a4 * (tp1 - tw1)
      dtp2 = a5 * (tp1 - tp2)/(Lt - Lb) - a4 * (tp2 - tw2)
      dtp3 = a5 * (tp2 - tp3)/Lb - a4 * (tp3 - tw3)
      dtp4 = a5 * (tp3 - tp4)/Lb - a4 * (tp4 - tw4)

' equations for the metal '
      dtw1 = - DRLB * (tw2 - tw1)/(2. * (Lt - Lb)) ...
             + a6 * (tp1 - tw1) - a7 * (tw1 - ts1)
      dtw2 = - DRLB * (2. * tw3 - tw2 - tw1)/(2. * (Lt - Lb)) ...
             + a6 * (tp2 - tw2) - a7 * (tw2 - ts2)
      dtw3 = - DRLB * (tw4 + tw3 - 2. * tw2)/(2. * Lb) ...
             + a6 * (tp3 - tw3) - a8 * (tw3 - tsatt)
      dtw4 = - DRLB * (tw4 - tw3)/(2. * Lb) ...
             + a6 * (tp4 - tw4) - a8 * (tw4 - tsatt)

' equations for the secondary superheated steam side '
      vss = (Lt - Lb)*As/2.
      cfss1 = vss*ROs2*dhs2dt
      cfss2 = vss*(144./J - ROs2*dhs2dp)
      cfss3 = 1. - vss*drs2dt*(hgg - hs2)/cfss1
      cfss4 = vss*(drs2dp + drs2dt*cfss2/cfss1)
      cfss5 = vss*ROs1*dhs1dt
```

```
        cfss6 = vss*(144./J - ROs1*dhs1dp)
        cfss7 = vss*(drs1dp + drs1dt*cfss6/cfss5)
        cfss8 = 1. - vss*drs1dt*(hs2 - hs1)/cfss5
        cfss9 = cfss7 + cfss4*cfss8
        cfss10 = vss*(cfss8*drs2dt*Qs2/cfss1 + drs1dt*Qs1/cfss5)
        cfss11 = As*(ROs1 + cfss8*ROs2)/2.
        Qs1 = PI*Ro*N*hws*(Lt - Lb)*(Tw1 - Ts1)
        Qs2 = PI*Ro*N*hws*(Lt - Lb)*(Tw2 - Ts2)
        w2 = Wb - Wbp - vss*(drs2dp*drps + drs2dt*drts2) + ...
             As*ROs2*drlb/2.
        drps = (cfss3*cfss8*Wb - cfss8*Wbp - Ws - cfss10 + ...
               cfss11*drlb)/cfss9
        drts1 = w2*(hs2 - hs1)/cfss5 + cfss6*drps/cfss5 + Qs1/cfss5
        drts2 = wb*(hgg - hs2)/cfss1 + cfss2*drps/cfss1 + Qs2/cfss1
        delPs1 = ROs1*(Lt - Lb)/(2.*144.) + rs*fs*Ws*Ws*(Lt - Lb)/ ...
                (4.*Des*gc*ROs1*As*As*144.)
        Ps2 = Ps + delps1
        delPss = ROs2*(Lt - Lb)/(2.*144.) + rs*fs*Ws*Ws*(Lt - Lb)/ ...
                (4.*Des*gc*ROs2*As*As*144.)
        Pss = Ps2 + delPss
        dPs = drps
        dTs1 = drts1
        dTs2 = drts2
        Psat = Pss

' equations for the downcomer as an accumulation tank '
        dalfdc = (Wfw + Wbp - Wdb)/(Vdc * c6)
        dpext = dpext0*(1. + f2*sin(2.*PI*frq*t) + f4*nsc2)
        Pdc = Ps + dpext
        Wbp = (Wfw * hfw - Wdb * hff - (Wfw - Wdb) * c5/c6)/(c5/c6 - hbp)
        dWdb = (((Wfw + Wbp) * (Wfw + Wbp) - Wdb * Wdb)/(Adc * ROdc) -...
                144. * gc * Adc * (Pdb - Pdc) - ...
                gc * Fw + Adc * g * Lbp * ROdc)/Lbp
        auxdb = (((Wfw + Wbp) * (Wfw + Wbp) - Wdb * Wdb)/(Adc * ROdc) +...
                144.*gc*Adc*Pdc - gc*Fw + Adc*g*Lbp*ROdc)/Lbp
        ROdc = Rf + alfdc * c6
        Fw = al8 * Lbp * Wdb * Wdb/ROdc
        Ldc = (1. - alfdc) * Lbp
        hbp = hs2

' equation for the secondary boiling liquid side '
        Qt = 2.*PI*Ro*N*hwb*(Twb - tsatt)/As

'    last node  '
        delb = Lb - z15
        Wb = Gb*As
        lstndl("b","n15")

'    node 15'
        z15 = 15*deltaz
        deln15 = z15 - z14
        genndl("n15","n14","b")

 **************************************************************
                                                             *
 " FOR REASON OF SPACE THE FORMAT FOR NODES 2 THROUGH 14     *
                                                             *
   IS GIVEN IN A GENERAL FORM "                              *
                                                             *
'    node i'                                                 *
        z_i = ( i )*deltaz                                   *
        deln_i = deltaz                                      *
        genndl("n_i","n_(i-1)","n_(i+1)")                    *
                                                             *
```

```
" FOR  2 =< i => 14 , E.G. i=13                          *
                                                          *
'    node 13'                                             *
      z13 = 13.*deltaz                                    *
      deln13 = deltaz                                     *
      genndl("n13","n12","n14")                           *
                                                          *
***********************************************************

'   first node '
      z1 = deltaz
      deln1 = z1
      Gdb = Wdb/As
      fstnl("n1","db","n2")
      pbb = pdb - kor*Gdb*Gdb/(2.*Rf)

' integration of state variables '

      tp1 = intvc(dtp1,tp10)
      tp2 = intvc(dtp2,tp20)
      tp3 = intvc(dtp3,tp30)
      tp4 = intvc(dtp4,tp40)
      tw1 = intvc(dtw1,tw10)
      tw2 = intvc(dtw2,tw20)
      tw3 = intvc(dtw3,tw30)
      tw4 = intvc(dtw4,tw40)
      Ps = intvc(dPs,Ps0)
      Ts1 = intvc(dTs1,Ts10)
      Ts2 = intvc(dTs2,Ts20)
      alfdc = intvc(dalfdc,alfdc0)
      Wdb = intvc(dWdb,Wdb0)
      Ws = intvc(dWs,Ws0)
      end
      termt(t.ge.tmax)
      end
end
```

APPENDIX B

The Lorenz System

Below are the differential equations for the Lorenz dynamical system [28], where the X, Y, and Z are the Lorenz variables.

$$\dot{X} = \sigma(Y - X) \tag{6.1}$$

$$\dot{Y} = X(R - Z) - Y \tag{6.2}$$

$$\dot{Z} = XY - bZ \tag{6.3}$$

The parameters σ, R, and b given below, sets the Lorenz system in a chaotic regime and are the values used in this dissertation. Other set of parameter values are found in reference [27].

$\sigma = 16.$
R = 45.92
b = 4.

The Rossler System

Below are the differential equations for the Rossler dynamical system [28], where the variables X, Y, and Z are the Rossler variables. The X variable was used throughout this work as a chaotic source.

$$\dot{X} = -(Y + Z) \tag{6.4}$$

$$\dot{Y} = X + aY \tag{6.5}$$

$$\dot{Z} = b + Z(X - c) \tag{6.6}$$

The parameters a, b, and c given below, set the Rossler system in a chaotic regime and are the values used in this dissertation. The interested reader may find other set of value, also in the chaotic regime, in references ([41],[27]).

$$\begin{aligned} a &= 0.15 \\ b &= 0.20 \\ c &= 10. \end{aligned}$$

VITA

Lamartine Nogueira Frutuoso Guimaraes, born in Resende, Brasil, on November 5th, 1959, the eldest son of Heitor Frutuoso Guimaraes and Zuleide Nogueira Guimaraes.

He attended the Universidade Federal do Rio de Janeiro, where he obtained the degree of Bachelor in Physics in December of 1981.

In January of 1982, he joint the Nuclear Engineering program of the Instituto Militar de Engenharia, where he obtained the degree of Master in Science in August of 1984.

He worked from September of 1984 to August of 1987 at the Centro Tecnico Aeroespacial, Instituto de Estudos Avancados, Divisao de Energia Nuclear located in Sao Jose dos Campos - SP, as a research assistant.

During the period that he lived in Sao Jose Dos Campos, he (fortunately) met and married Regina. He and Regina have been married for five years.

In September of 1987, he joined the PhD program at the Nuclear Engineering Department at the University of Tennessee, Knoxville - TN.